GAZİANTEP UNIVERSITY GRADUATE SCHOOL OF NATURAL & APPLIED SCIENCES

AN EXPERIMENTAL STUDY ON ABSORPTION REFRIGERATION SYSTEM DRIVEN BY ENGINE EXHAUST GAS FOR VEHICLES

Ph.D THESIS
IN
MECHANICAL ENGINEERING

BY
İSMAİL HİLALİ
JULY 2007

An Experimental Study on Absorption Refrigeration System Driven By Engine Exhaust Gas for Vehicles

PhD Thesis
in
Mechanical Engineering
University of Gaziantep

Supervisor
Prof. Dr. M. Sait SÖYLEMEZ

by
İsmail HİLALİ

July 2007

ABSTRACT

AN EXPERIMENTAL STUDY ON ABSORPTION REFRIGERATION SYSTEM DRIVEN BY ENGINE EXHAUST GAS FOR VEHICLES

HİLALİ, İsmail

PhD in Mechanical Engineering

Supervisor: Prof. Dr. M. Sait SÖYLEMEZ

July 2007, 144 pages

This thesis includes the analysis of a designed and constructed absorption refrigeration system. The system uses an aqua-Lithiumbromide solution with water as the refrigerant and Lithiumbromide as the absorbent. The system has a design cooling capacity of 2 kW.

A 1.3 liter internal combustion engine was also analyzed experimentally to determine whether it was capable of driving the experimental refrigeration system via its exhaust heat. This required a study of the power and heat distribution of the diesel engine under various speed and load conditions.

As far as the integrated system is concerned, the experiments were focused on the effect on the performance of the engine and effect on the performance of the absorption refrigeration system.

Introducing the refrigeration system into the exhaust system of the engine caused an increase on the engine back pressure and this caused higher fuel consumption and lower efficiency. The effect can be reduced by designing a generator with a minimum pressure drop. But more heat recovered from the exhaust gas of the IC engine the more heat transferred to the generator and hence this caused an increase on the cooling capacity of the experimental refrigeration system. This is due to the fact that, in the refrigeration system, the cooling capacity is directly proportional to the heat input to the generator

Keywords: Refrigeration, Absorption Refrigeration, Road Transport Refrigeration, Internal Combustion Engine

ÖZET

TAŞITLAR İÇİN MOTOR EGZOZ GAZI İLE ÇALIŞAN ABSORPSİYONLU SOĞUTMA SİSTEMİ ÜZERİNE DENEYSEL BİR ÇALIŞMA

HİLALİ, İsmail

Doktora Tezi, Makine Mühendisliği Bölümü

Tez Yöneticisi: Prof. Dr. M. Sait SÖYLEMEZ

Temmuz 2007, 144 sayfa

Bu çalışmada, tasarımı ve imalatı yapılmış bir absorpsiyonlu soğutma sisteminin analizi yapılmıştır. Soğutma sisteminde LiBr/Su akışkan çifti kullanılmıştır. Bu akışkan çiftlerinden su, soğutucu akışkan, LiBr ise emici olarak kullanılır. Soğutma sisteminin soğutma kapasitesi 2,5 kW' dır.

Ayrıca, 1.3 litrelik bir 4 silindirli motorda, imal edilen soğutma sistemi için gerekli ısıl enerjinin egzoz gazı ile elde edilebilirliği analiz edilmiştir. Analizler, değişik güç ve yük şartlarında yapılmıştır.

Yapılan deneyler, soğutma sistemi ile motor birlikte çalışırken, motor verimine ve soğutma sisteminin performansı üzerine yoğunlaşmıştır.

Yapılan deneylerde, soğutma sistemi, motor egzoz sistemi üzerine monte edildiği için motorda bir geri basınç artışı olduğu, dolayısıyla yakıt sarfiyatında bir miktar artış olduğu gözlenmiştir. Fakat egzozdan çekilen enerji artıkça soğutma sisteminin kapasitesinin arttığı görülmüştür.

Anahtar Kelimeler: Soğutma, Absorpsiyonlu Soğutma, Taşıt Soğutması, İçten yanmalı motor

ACKNOWLEDGEMENTS

My thanks and sincere appreciation goes to Prof. Dr. M. Sait SÖYLEMEZ for allowing me the opportunity to realize my goals. Without his wisdom, encouragement, and advice this work would not be complete. I am also very grateful for the guidance of Prof. Dr. Orhan BÜYÜKALACA and Assoc. Prof. Dr. Yaşar GÜNDOĞDU, who taught me the knowledge of experimental study.

I sincerely thank Assoc. Dr. Hüsamettin BULUT, Lecturer Müslüm AÇIKER, Lecturer Osman A. SERVİ and Assist. Prof. Dr. M. Azmi AKTACİR for you assisting me a lot. Special thanks also goes to the OLİMPİYAT OTOMASYON members – namely, Mikail KALKAN, Muhsin KALKAN and Mustafa KALKAN.

Lastly, I wish to offer my thanks to personal of the Mechanical Engineering Department, especially Ms. Elif AŞKIN, Mr. Mehmet TAŞDEMİR, Mr. İbrahim KORKMAZ, Mr. Engin ERTUĞRUL, Mr. Cengiz KÖNCÜ and Mehmet ÇETİNKAYA for their valuable help in the studying of Ph. D.

The financial support from the the TÜBİTAK-MAG (The Scientific and Technical Research Council of Turkey- Engineering Research Grant Committee.) has been essential so thanks TUBITAK.

Finally, I would like to express my gratitude to my family and friends for their encouragement.

CONTENTS

ABSTRACT…… iii

ÖZET…….. iv

ACKNOWLEDGEMENTS…….. v

CONTENTS……... vi

LIST OF TABLES…….

LIST OF FIGURES……...

LIST OF SYMBOLS…….

CHAPTER 1: INTRODUCTION …… 1

1.1 Research Objectives..... 5

1.2 Refrigeration System……. 6

1.2.1 Vapor Compression Refrigeration (VCR) System…… 7

1.2.2 Vapor Absorption Refrigeration (VAR) System..... 8

1.2.3 Comparison of Absorption and Compression Systems..... 17

CHAPTER 2: LITERATURE SURVEY …… 19

2.1 History Of Absorption Technology…….. 19

2.2 Research Emphases Of Current Absorption Technologies…….. 20

2.3 Theoretical and Experimental Works About Absorption Refrigeration Driven By Engine Exhaust Gas for Vehicles……. 21

CHAPTER 3: DESIGN OF THE EXPERIMENTAL SET-UP……. 33

3.1 Modeling and Simulation of Absorption Refrigeration System Proposed……. 33

3.1.1 Software Selection …… 33

3.1.2 Thermodynamic Analysis of the Designed Absorption Refrigeration System…….. 34

3.1.2.1 Energy analysis ……. 35

3.1.2.2 Exergy analysis ……..… 39

3.2 Construction of the Absorption Refrigeration System……... 42

3.2.1 Experimental Set-up Description……... 43

3.2.2 Measurement Methods and Instrumentation Used in the Set-up…….. 54

3.2.3 Control and Monitoring of the Absorption Refrigeration System…… 56
3.2.3.1 Control procedure of the set-up…… 58
3.2.3.2 Prevention of crystallization……. 59
3.3 Internal Combustion Engine's Set-up…….. 60
3.4 The Integration of the Absorption Refrigeration System In the Internal Combustion Engine…… 62
3.4.1 Generator Models…….. 62
3.4.2 Connection Of The Generator Models To The Internal Combustion Engine…… 65
3.4.3 Test Procedure……..... 65
3.5 Uncertainty Analysis Of Measurement System …… 66
CHAPTER 4: RESULTS AND DISCUSSION……. 69
4.1 Theoretical Results
4.2 Experimental Results
4.2.1 Experimental Results of Absorption Refrigeration System. 76
4.2.1.1 The effects of ambient air temperature…….. 76
4.2.1.2 The effects of generator temperature……. 80
4.2.2 The Experimental Results of Absorption Refrigeration System Integrated in Combustion Engine……. 83
4.2.2.1 The effects of the generator on performance of the combustion engine…….. 83
4.2.2.2 The effects of the generator on performance of the absorption refrigeration system…….. 87
4.3 General Discussion……... 89
CHAPTER 5: CONCLUSION……. 91
CHAPTER 6: SUGGESTIONS FOR FUTURE STUDIES ……..….... 94
APPENDICIES…….. 96
APPENDIX 1: CALIBRATION OF MEASUREMENT DEVICES…… 97
APPENDIX 2: THE COMPUTER CODES FOR THEORETICAL ANALYSIS ……..... 101
APPENDIX 3: THE THERMODYNAMIC AND TRANSPORT PROPERTIES OF LiBr/WATER SOLUTION..... 114
APPENDIX 4: THE DETAILS OF PARTS OF CONTROL UNIT..... 120

APPENDIX 5: TEST ENGINE SPECIFICATIONS..... 126
REFERENCES……..…….. 133
CURRICULUM VITAE..... 144

LIST OF FIGURES

Figure 1.1:	Refrigerated Automobile Air Conditioning System……..	3
Figure 1.2:	Ideal Vapor-Compression Refrigeration ……..	8
Figure 1.3:	Actual Vapor-Compression Cycle…….	8
Figure 1.4:	Methods of Transforming Low-pressure vapor into High-pressure Vapor in a Refrigeration System…….....	9
Figure 1.5:	(A) Absorption Process Occurs In Right Vessel Causing Cooling Effect in the Other; (B) Refrigerant Separation Process Occurs In the Right Vessel As A Result Of Additional Heat From Outside Heat Source……	11
Figure 1.6:	A Continuous Refrigeration Cycle Composes Of Two Processes Mentioned In the Earlier Figure…….	11
Figure 1.7:	P-T Chart of Absorption Cycle……..	12
Figure 1.8:	Diagram of Single-Effect Air-Cooled Absorption Cycle……..	14
Figure 1.9:	Double Effect Water/LiBr Absorption Cycle……	15
Figure 2.1:	Research Emphases of Absorption Technology…….	20
Figure 2.2:	Absorption Refrigeration System for Vehicle Application by Ghasemi……	22
Figure 2.3:	The Absorption Refrigeration System for Vehicle by Keating…	23
Figure 2.4:	Plan View of the Absorption Refrigeration System Designed by Mcnamara……	24
Figure 2.5:	Truck Absorption Refrigeration System Designed By Vincent At Al……..	26
Figure 2.6:	Generator Design by Vincent at Al. ……	26
Figure 2.7:	The Location of Absorption System on Truck By Vincent at Al……..	27
Figure 2.8:	Essential Components of the Air-Cooled Absorption Prototype for Transport Refrigeration……..……..	28
Figure 2.9:	Absorption Refrigeration System Used by Horuz……...	29

Figure 2.10: Two Different Heat Exchangers Details Used As Generator……. 29
Figure 2.11: Cooling capacity against engine speed …….……. 30
Figure 2.12: Typical average COP for proposed system by Alva…….. 31
Figure 3.1: Diagram of Single Effect Air-cooled Absorption Cooling System. 34
Figure 3.2: Availability Flow Balance for the Absorption Cycle……... 40
Figure 3.3: Saturation Temperature vs. Pressure at Different Solution Concentrations for LiBr/Water……... 42
Figure 3.4: Schematic Layout of Experimental Set-Up……... 44
Figure 3.5: Detailed Flow Diagram of Set-Up……. 45
Figure 3.6: Simple Generator Drawings…… 46
Figure 3.7: Photographs of Specially Constructed Generator…….. 47
Figure 3.8: Drawing of Air-Cooled Absorber …...…….. 48
Figure 3.9: Photograph of Air-Cooled Absorber……. 48
Figure 3.10: Drawing of Air-Cooled Condenser …...……..….. 49
Figure 3.11: Photograph of Air-Cooled Condenser……..…. 49
Figure 3.12: Photograph of Evaporator……..……..…….. 50
Figure 3.13: Special Constructed Insulated Metallic Housing For Evaporator.. 50
Figure 3.14: Photograph of Plate Type Solution Heat Exchanger……. 51
Figure 3.15: Specially Constructed Mixing Tank……. 52
Figure 3.16: Specially Constructed Condense Tank……. 52
Figure 3.17: Electronic Expansion Valve (EEV)…….. 53
Figure 3.18: Manuel Expansion Valve……..... 53
Figure 3.19: Circulation Pumps……....…… 53
Figure 3.20: Schematic Diagram for Instrumentation for Experimental Setup.. 54
Figure 3.21: Electromagnetic Flowmeter…….. 56
Figure 3.22: Turbine Type Flowmeter…….. 56
Figure 3.23: Absolute Pressure Transducer …….. 56
Figure 3.24: J Type Thermocouple with Immersion Bayonet…..……. 56
Figure 3.25: Block Diagram of Control System……...…. 57
Figure 3.26: Operation Panel……. 58
Figure 3.27: Decrystallization Line …….. 60
Figure 3.28: The Illustration of the Experimental Internal Combustion Engine Test Rig ……... 60

Figure 3.29: Complete Test Rig…… 61
Figure 3.30: First Type Generator Model ……..……...…… 64
Figure 3.31: The Second Type Generator Model …….. 64
Figure 3.32: Exhaust Pipe Line…….. 65
Figure 4.1: The Relationship of Different Generator Temperatures Versus COP and Q_a for a Given System ……... 73
Figure 4.2: The Relationship of Different Evaporator Temperatures Versus COP and Q_a for a Given System…….. 73
Figure 4.3: The Relationship of Different Absorber Temperatures Versus COP and Q_a for A Given System…….. 74
Figure 4.4: Variation of COP with Generator Temperatures……. 75
Figure 4.5: Comparison of COP Values with Condenser Temperatures..... 75
Figure 4.6: Comparison of COP Values with Absorber Temperatures..... 76
Figure 4.7: Variation of Cooling Capacity with Ambient Temperatures…... 78
Figure 4.8: Variation of COP with Ambient Temperatures……. 78
Figure 4.9: Variation of Heat Capacities with Ambient Temperatures…… 79
Figure 4.10: Variation of System Pressures with Ambient Temperatures……. 79
Figure 4.11: Variation of Evaporator Exit Temperature with Ambient Temperatures and Mass Flow Rate…… 80
Figure 4.12: Variation of COP with Generator Temperatures……... 81
Figure 4.13: Variation of Heat Capacities with Generator Temperatures……81
Figure 4.14: Variation of Condenser Temperature with Time……..... 82
Figure 4.15: Variation of Evaporator Temperature with Time……..... 82
Figure 4.16: Variation of Absorber Temperature with Time……..... 83
Figure 4.17: Fuel Consumption against Engine Speed …….……... 85
Figure 4.18: Engine Back Pressure against Engine Speed ……... 85
Figure 4.19: Power Loss against Engine Speed ……..…..……..... 86
Figure 4.20: Engine Efficiency against Speed ……..… 87
Figure 4.21: Cooling Capacity against Speed at Different Torques……..… 88
Figure 4.22: Heat recovered from exhaust gases against speed..... 88
Figure 4.22: COP against Speed at Different Torques……. 89

LIST OF TABLES

Table 2.1: Thermodynamic Properties of NH_3-Water Solution at Different Points of the Cycle…… 21
Table 2.2: Designed Conditions Chosen for Simulated System…… 31
Table 3.1: Test Engine Specifications…… 61
Table 3.2: Design details of exhaust heat exchangers …… 63
Table 4.1: State Points for the Single Effect Air-Cooled LiBr Absorption System at Design Condition…….. 71
Table 4.2: Heat Duty and UA of Each Component at Design Condition……. 72
Table 4.3: Exergy Difference for the Single Effect Air-Cooled LiBr Absorption System at Design Condition……. 72

LIST OF SYMBOLS

Abbreviations and Symbols

A	Cross sectional area
P	Pressure
T	Temperature
X	Concentration
$\dot{m}$	Mass flow rate
h	Enthalpy
COP	Coefficient of Performance
Q	Heat transfer rate
LMTD	Logarithmic mean temperature difference
U	Overall heat transfer coefficient
W	Power
S	Entropy
EV	Expansion valve
g	Gravity acceleration

Greek Symbols

ψ	Availability
ρ	Density

Subscripts

C	Condenser
e	Evaporator
a	Absorber
g	Generator
SHEX	Solution heat exchanger
Exh	exhaust
s	static
t	Total
1,2,3..	Measurement stations

CHAPTER 1

INTRODUCTION

The production of cold has applications in a considerable number of fields of human life, for example the food processing field, the air-conditioning sector, and the conservation of pharmaceutical products, etc. The conventional refrigeration cycles driven by traditional vapor compression in general contribute significantly in an opposite way to the concept of sustainable development. Two major problems have yet to be addressed:

- *The global increasing consumption of limited primary energy:* The traditional refrigeration cycles are driven by electricity or heat, which strongly increases the consumption of electricity and fossil energy. The International Institute of Refrigeration in Paris (IIF/ IIR) has estimated that approximately 15% of all the electricity produced in the whole world is employed for refrigeration and air-conditioning processes of various kinds, and the energy consumption for air-conditioning systems has recently been estimated to 45% of the whole households and commercial buildings. Moreover, peak electricity demand during summer is being re-enforced by the propagation of air conditioning appliances.
- *The refrigerants used cause serious environmental problems*: The traditional commercial, non-natural working fluids, like the chlorofluocarbures (CFCs), the hydrochlorofluorocarbures (HCFCs) and the hydrofluocarbures (HFCs) result in both ozone depletion and/or global warming. Since the protocol of Montreal in 1987, international agreements have been signed to reduce the emissions of these refrigerants. European Commission Regulation 2037/2000, which has been implemented on 1 October 2000, treats the whole spectrum of

control and phase-out schedule of all the ozone depleting substances. It is indicated that till 2015 all HCFCs will be banned for servicing and maintaining existing systems [1-2].

During recent years research aimed at the development of technologies that can offer reductions in energy consumption, peak electrical demand and energy costs without lowering the desired level of comfort conditions has intensified. By reason that absorption refrigeration technologies have the advantage of removing the majority of harmful effects of traditional refrigeration machines and that the peaks of requirements in cold coincide most of the time with the availability of the waste heat, the development of absorption refrigeration technologies became the worldwide focal point for concern again. Waste heat energy can be transformed either to electricity or to heat to power a refrigeration cycle. During the past decade, more interests have been paid to the waste heat-driven refrigeration technologies, especially absorption and adsorption systems.

Refrigeration systems can be defined as systems which remove heat at low temperatures and reject it at a higher temperature. The first refrigerated automobile air conditioning system is shown in Figure 1.1. The vapor compression refrigeration system utilizes a refrigerant compressor that is shaft or belt driven by the automobile engine. In the past 65 years, automobile air conditioning systems have undergone gradual and continual improvements in performance and efficiency as a result of improvements in the individual components, compressor efficiency and size/weight reduction, control (thermostatic expansion valves, electronic compressor clutch cycling, and variable displacement compressor), and size/weight reduction of evaporators and condensers. Despite these component advances, the core technology has not changed, and there are still problems in the state of the art system that is continually being addressed.

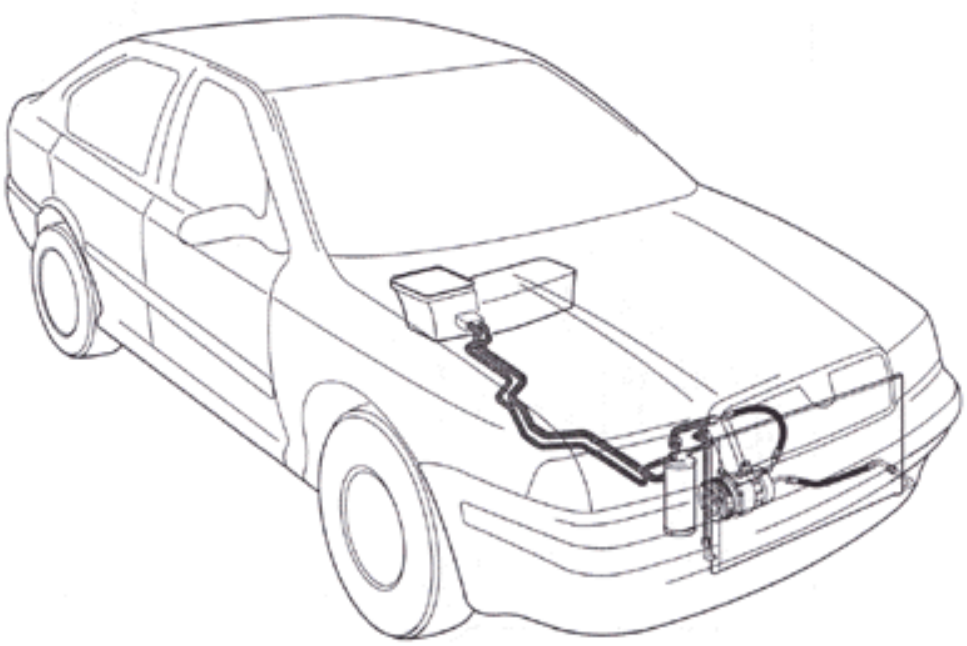

Figure 1.1 Refrigerated automobile air conditioning system

The most pressing issue for the automotive air conditioning industry throughout the last decade and continuing today is the search for environmentally-friendly refrigerants. As a result of the Montreal Protocol of 1987 (an agreement among 23 countries including the United States to limit production of ozone-depleting chemicals) the industry searched extensively for a non-CFC refrigerant with the performance characteristics of R-12. This search resulted in the acceptance of R-134a, which has recently been identified by the Kyoto Protocol of 1997 as a "greenhouse" or global warming gas. Recently tests have been performed using two natural refrigerants, butane/propane hydrocarbon (HC) and carbon dioxide (CO_2) refrigerant. Butane/propane hydrocarbon has similar refrigeration characteristics as R-134a, but can be explosive and will require a secondary coolant loop to keep the explosive refrigerant away from the passenger compartment. Carbon dioxide is neither toxic nor explosive, but requires system pressures 7 to 10 times higher than R-134a. Both will cost more than R-134a, and neither will run as efficiently, which could cause increased emissions. Consequently, much of the works to reduce the global warming impact of automobile refrigerants have shifted to increasing the efficiency and reducing leakage in R-134a systems. In addition to the concerns over the environmental impacts of automobile refrigerants, several mechanical issues are

associated with powering the refrigerant compressor with the automobile engine. The power required to drive the compressor is often a significant portion of the total engine power output during city driving conditions. Also, the compressor must deliver the required amount of refrigerant to match the cooling load regardless of engine speed, which varies from 500 to 6000 rpm. Although variable displacement compressors are available for high-end vehicles, the most common means of controlling refrigerant flow is cycling the compressor. At compressor engagement, accelerating the rotational mass of the compressor and the mass of refrigerant in the system can double the engine torque, resulting in annoying engine surge and even stalling of smaller engines at idle. Furthermore, during engagement, the clutch must dissipate a large amount of heat; therefore, care must be taken to limit the clutch cycling. Another problem is the constant competition between the air conditioning system and the engine cooling system. The air conditioning condenser is located ahead of the engine cooling radiator restricting airflow to the radiator and preheating the air entering the radiator, placing an additional burden on the engine cooling system. By locating the condenser behind the radiator a higher condenser pressure would result in decreased cooling capacity, increased compressor power, increased propensity of engine stalling, and premature failure of the compressor clutch or compressor.

Absorption-cycle refrigeration technology has the potential to eliminate the above concerns associated with conventional automotive air-conditioning technology. The absorption refrigeration cycle uses environmentally-friendly refrigerants and can be driven by waste heat from the vehicle engine rather than by siphoning valuable power from the engine.

The objective of this thesis is to study the performance and feasibility of using a waste heat driven absorption refrigeration system as an alternative to the conventional vapor compression system that has been used by the automobile industry for years. To achieve this objective, a mathematical model will be developed to simulate the performance of the absorption refrigeration system, and Absorption refrigeration system driven by engine exhaust gas for vehicles heat will be designed to obtain the performance and energy requirements of the absorption system under different operating conditions.

1.1 RESEARCH OBJECTIVES

1. Automobiles and trucks alone account for approximately 80 percent of all transportation energy expenditures. These internal combustion engines typically have a thermal efficiency 40 percent. The remaining energy is rejected to the atmosphere in the form of hot exhaust gases or as energy converted from the radiator and engine. Much work now in progress is directed to be improvement of the thermal efficiency by achieving better consumption of the fuel. Some effort has been devoted to the utilization of the vast amount of waste energy dissipated in the exhaust gases. But few have focused on using the waste heat for air-conditioning and refrigeration.
2. Besides energy usage for transport refrigeration wide-spread efforts are currently underway to develop replacement for the traditionally used halogenated hydrocarbon refrigerants which contribute to ozone depletion and greenhouse warming.
3. Most work on utilization of vehicle waste heat for cooling has been limited to schemes for air-conditioning of automobiles. Most of these schemes are inadequate if not completely inoperative from a thermodynamic or manufacturing point of view. Very few of the proposed designs have ever been built, even as prototypes [3-4].

   In according to the above inadequacies, industrial and economic benefits are:

   - Development of an absorption cooling system for vehicles (automobiles, buses, trucks etc.),
   - Reduction of fuel requirements for cooling by 100 % compared to compression cycle units,
   - Light weight,
   - High operational dependability.

This thesis aims to investigate the feasible use of Absorption Refrigeration Systems driven by engine exhaust gas for vehicles. The feasibility of vehicle air conditioning by exhaust gas operated absorption refrigeration system has been studied and it has been shown that the cooling potential in the exhaust gas is much

greater than the required for cooling of the vehicle interior space. It was demonstrated that an absorption refrigeration unit can be integrated with the engine and the operating coast was almost negligible. The feasibility of exhaust gas actuated absorption refrigeration system by using Lithium bromide-Water combination has been demonstrated and the system can be suitably installed and successfully operated.

1.2 REFRIGERATION SYSTEM

The refrigeration system is an enclosed, air-tight system of individual units and interconnecting pipe works so constructed as to allow a controlled quantity of refrigerant to flow between the units under definite and predetermined pressures. This allows thermal energy to be absorbed in a region of low pressure by means of liquid evaporation (in the evaporator unit), and rejected in a region of high pressure by means of condensation (in the condenser unit). The system is designed so that the refrigerant undergoes a cyclic series of processes.

Common usage differentiates between the two practical applications of such a device which can be associated with either the extraction of heat from the cold substance or the delivery of heat to the secondary substance or surroundings.

"Refrigerator or Refrigeration System" is the name applied to the cooling device; "Heat Pump" is the name given to the heating device. It is important to recognize that there is no fundamental difference between these devices. This distinction in terminology is arbitrary, because the heat pump and refrigerator are identical in principle. It is, in fact, possible to use the same device to fulfill the function of the heat pump and refrigerator simultaneously [16].

The most common types of refrigeration systems are as follows:

i) Vapor Compression Refrigeration (VCR) System

ii) Vapor Absorption Refrigeration (VAR) System

1.2.1 Vapor Compression Refrigeration (VCR) System

The vapor compression cycle is the most widely used refrigeration cycle in practice. As shown Figure 1.2, the processes constituting the standard ideal vapor compression cycle are:

1-2. Reversible and adiabatic compression from saturated vapor to the condenser pressure

1-3. Reversible rejection of heat at constant pressure, causing desuperheating and condensation of the refrigerant

3-4. Irreversible expansion at constant enthalpy from saturated liquid to evaporator pressure

4-1. Reversible addition of heat at constant pressure causing evaporation to saturated vapor

In an actual vapor-compression cycle, due to irreversibility and heat transfer to the compressor coolant, the compression process is neither reversible nor adiabatic. This process might approach either line 1-2a or line 1-2b in Figure 1.3, depending on whether frictional effect or heat-transfer effect dominates. In this figure, state 1 is shown slightly superheated and state 3 slightly sub-cooled. The superheating at state 1 is advisable to ensure complete vaporization at entrance to the compressor. The sub-cooling at state 3 is advisable, as it would result in increased refrigeration effect. The pressure differences between points 2 and 3 and between points 4 and 1 in Figure 1.3 are simply to indicate that there usually are pressure drops in the condenser and evaporator coils, in compressor suction and exhaust valves, and in pipelines [17].

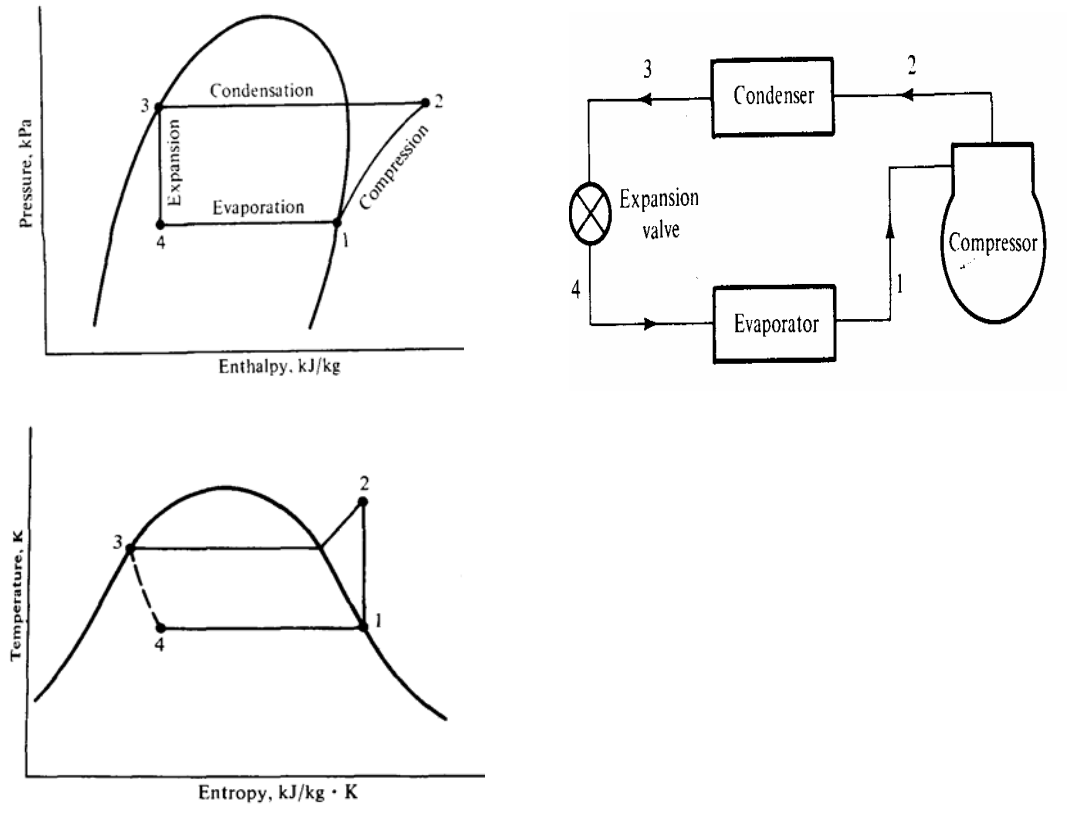

Figure 1.2 Ideal vapor-compression refrigeration cycle

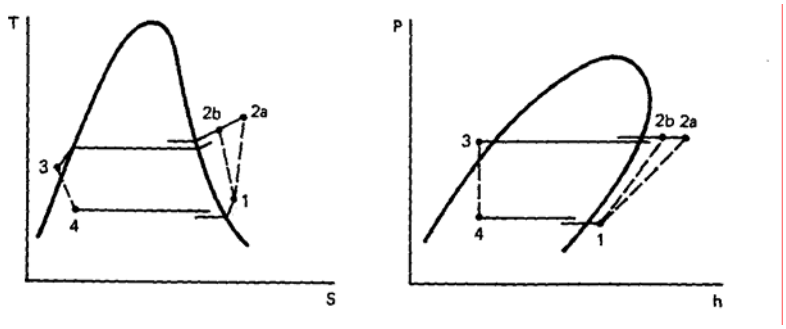

Figure 1.3 Actual vapor-compression cycle

1.2.2 Vapor Absorption Refrigeration (VAR) System

The absorption cycle is similar in certain respects to the vapor compression cycle. A refrigeration cycle will operate with the condenser, expansion valve, and evaporator shown in Figure 1.4. If the low-pressure vapor from the evaporator can be

transformed into high pressure vapor and delivered to the condenser. The vapor-compression system uses a compressor for this task. The absorption system first absorbs the low-pressure vapor in an appropriate absorbing liquid. Embodiment in the absorption process is the conversion of vapor into liquid; since the process is akin to condensation, heat must be rejected during the process. The next step is to increase the pressure of the liquid with a pump, and the final step releases the vapor from the absorbing liquid by adding heat.

The vapor-compression cycle is described as a work-operated cycle because the increase of pressure of the refrigerant is accomplished by a compressor that requires work. The absorption cycle, on the other hand, is referred to as a heat-operated cycle because most of operating cost is associated with providing the heat that drives off the vapor from the high-pressure liquid. Indeed there is a requirement for some work in the absorption cycle to drive the pump, but the amount of work for a given quantity of refrigeration is minor compared with that needed in the vapor compression cycle [18].

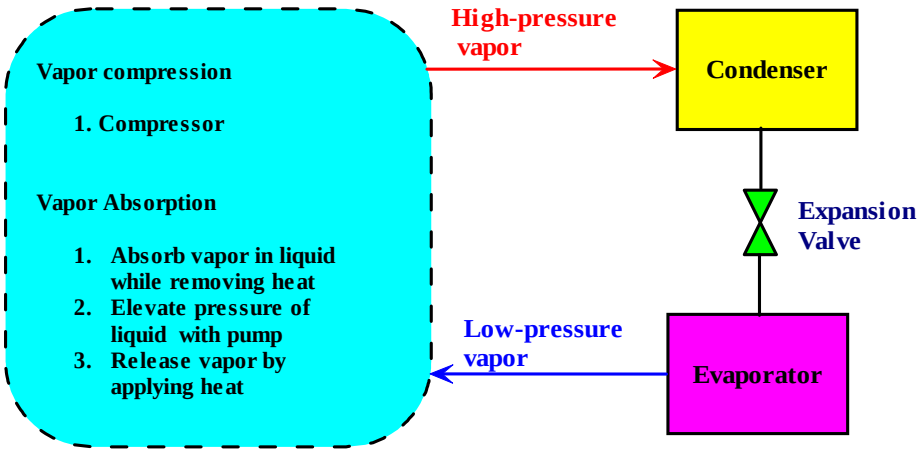

Figure 1.4 Methods of transforming low-pressure vapor into high pressure vapor in a refrigeration system

The working fluid in an absorption refrigeration system is a binary solution consisting of refrigerant and absorbent in Figure 1.5(a), two evacuated vessels are

connected to each other. The left vessel contains liquid refrigerant while the right vessel contains a binary solutions of absorbent/refrigerant. The solution in the right vessel absorb refrigerant vapor from the left vessel causing pressure to reduce. While the refrigerant vapor is being absorbed, the temperature of remaining refrigerant will reduce as a result of its vaporization. This causes a refrigeration effect to occur inside the left vessel. At the same time, solution inside the right vessel becomes more dilute because of higher content of refrigerant absorbed. This is called the "Absorption Process". Normally, the absorption process is an exothermic process; therefore, it must reject heat out to the surrounding in order to maintain its absorption capability.

Whenever the solution can not continue with the absorption process because of saturation of the refrigerant, the refrigerant must be separated out from the diluted solution. Heat is normally the key for this separation process. It is applied to the right vessel in order to dry the refrigerant from the solution as shown in Figure 1.5(b). The refrigerant vapor will be condensed by transferring heat to the surroundings. Whit this processes, the refrigeration effect can be produced by using heat energy. However, the cooling effect can not be produced continuously as the process can not be done simultaneously.

Therefore, an absorption refrigeration cycle is a combination of those processes as shown in Figure 1.6. As the separation process occurs at a higher pressure than the absorption process, a circulation pump is required to circulate the solution.

Coefficient of performance of an absorption refrigeration system is obtained from;

$$COP = \frac{\text{Cooling capacity obtained at evaporator}}{\text{Heat input for the generator + work input for the pump}} \qquad (1.1)$$

The work input for the pump is negligible relative to the heat input at the generator.

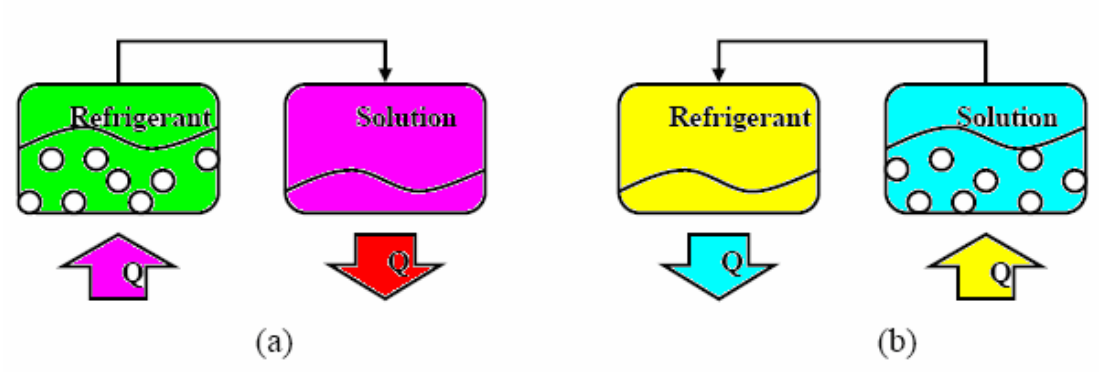

Figure 1.5 (a) Absorption process occurs in right vessel causing cooling effect in the other; (b) Refrigerant separation process occurs in the right vessel as a result of additional heat from outside heat source

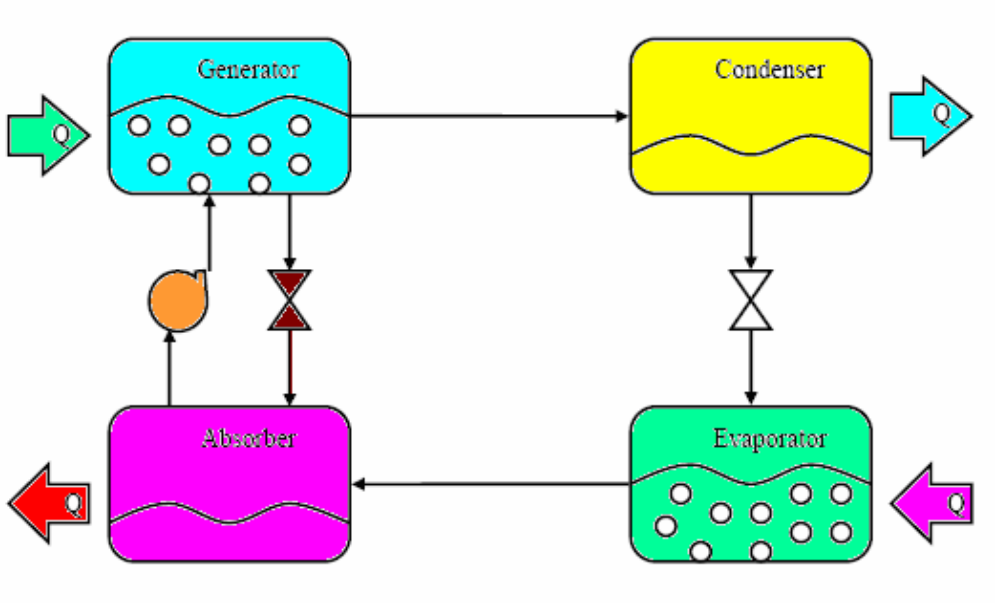

Figure 1.6 Continuous refrigeration cycle composes of two process mentioned in the earlier figure.

Usually the absorption cycle is plotted in a Dühring P-T chart, a pressure-temperature graph where the diagonal lines represent constant LiBr mass fraction, with the pure water line at the left and crystallization line at the right. A typical cycle and some state points are shown in Figure 1.7 [19].

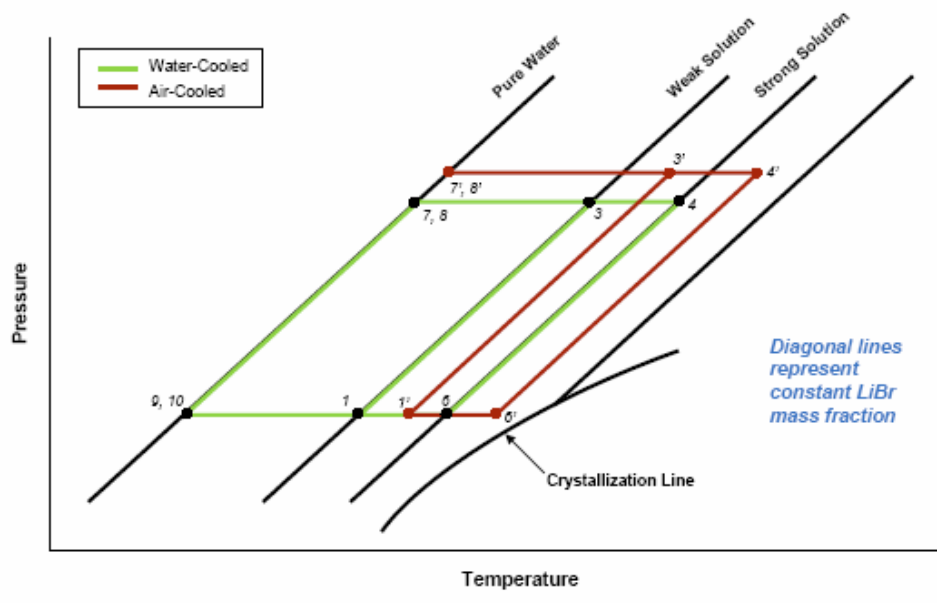

Figure 1.7 Dühring P-T chart of absorption cycle

Performance of an absorption refrigeration system is critically dependent on the chemical and thermodynamic properties of working fluid. Absorbent/refrigerant combination must have a margin of miscibility within the operating temperature range of cycle. The mixture should also be chemically stable, non-toxic and non-explosive. In addition to these requirements, the following are desirable:

- The elevation of boiling (The difference in boiling point between the pure refrigerant and the mixture at the same pressure) should be as large as possible.
- Refrigerant should have heat of vaporization and high concentration within the absorbent in order to maintain low circulation rate between the generator and the absorber per unit of cooling capacity.
- Transport properties that influence heat and mass transfer, e.g., viscosity, thermal conductivity, and diffusion coefficient should be favorable.
- Both refrigerant and absorbent should be non-corrosive, environmental friendly, and low-cost.

Many working fluids are suggested in literature. There are some 40 refrigerant compounds and 200 absorbent compounds available. However, the most

common working fluids are water/NH_3 and LiBr/Water. Both NH_3 (refrigerant) and water (absorbent) are highly stable for a wide range of operating temperature and pressure. NH_3 has a high latent heat of vaporization, which is necessary for efficient performance of the system. It can be used for low temperature applications, as the freezing point of NH_3 is –77 ^oC. Since NH_3 and water are volatile, the cycle requires a rectifier to strip away water that normally evaporates with NH_3 without a rectifier; the water would accumulate in the evaporator and offset the system performance. The other disadvantages are high pressure, toxicity and corrosive action to copper and copper alloy. However, water/NH_3 is low-cost.

The use of LiBr/Water for absorption refrigeration systems began around 1930. Two outstanding features of LiBr/water are non-volatile as an absorbent of LiBr (The need of rectifier is eliminated) and extremely high heat of vaporization of as a refrigerant of water. However, using water as a refrigerant limits the low temperature application to that above 0 ^oC. The system must be operated under vacuum conditions. It is also corrosive to some metal and expensive. At high concentrations, the solution is prone to crystallization. Some additive may be added to LiBr/Water as a corrosion inhibitor or to improve heat-mass transfer performance.

At high concentration such as at high temperatures, the solution is prone to crystallization. It was found that the addition of a second salt as in a ternary mixture such as LiBr-$ZnBr_2$ /water can be improving the solubility of the solution.

There are various designs of Absorption Refrigeration Cycles. A single-effect absorption refrigeration system is the simplest and most commonly used design. There are two design configurations depending on the working fluids used [20-25].

Figure 1.8 shows a single effect system using non-volatile absorbent such as LiBr/water. The main components of an absorption system include the absorber, generator, condenser, evaporator, and solution heat exchanger. In Figure 1.8, the dashed lines stand for the solution loop and solid lines for the refrigerant loop. Firstly, the LiBr-H_2O solution in the absorber, at point (1), gets pumped through the solution heat exchanger (2) into the generator (3). Heat input (11) to the generator allows the water to boil off from the solution into vapor (7). For the refrigerant loop,

the water vapor is condensed in the condenser by ambient air (15). The water (8) then passes an expansion valve and continues to the evaporator (9) where it evaporates and provides the desirable cooling effect. The water vapor (10) then gets reabsorbed into the solution in the absorber with the help of the external coolant – ambient air (13) again. For the solution loop, the remaining solution in the generator (4) passes through the solution heat exchanger (5) before re-entering the absorber (6). The heat exchanger allows the solution from the absorber to be preheated before entering the generator by using the heat from the hot solution leaving the generator. Therefore, COP is improved as the heat input at the generator is reduced. Experimental studies show that COP can be increased up to 60% when a solution heat exchanger is used. When volatile absorbent such as NH_3/water is used the system requires an extra component called "a rectifier" which will purify the refrigerant before entering the condenser.

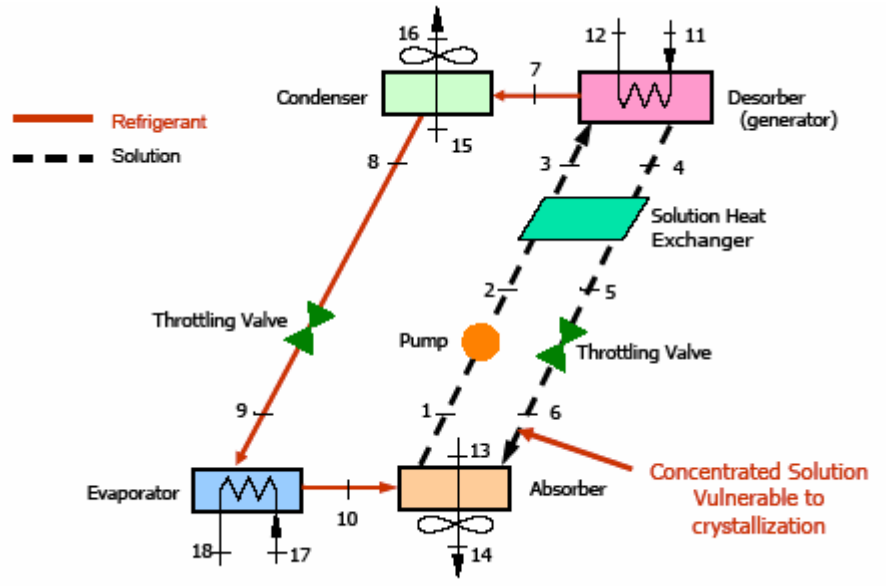

Figure 1.8 Diagram of single-effect air-cooled absorption cycle

The main objective of higher effect cycle is to increase system performance when high temperature heat source is available. By the term "multi-effect", the cycle has to be configured in a way that heat rejected from a high-temperature stage is used as a heat input in a low temperature stage for generation of additional cooling effect in the low temperature stage. Figure 1.9 shows a double effect system using LiBr/water. High temperature heat from an external source supplies to the first effect

generator. The vapor refrigerant generated is condensed at high pressure in the second effect generator. The heat rejected is used to produce addition refrigerant vapor from the solution coming from the first effect generator. This system configuration is considered as series flow double effect absorption system. According the analysis, a double effect absorption system has a COP of 0.96 when the corresponding single effect system has a COP of 0.6.

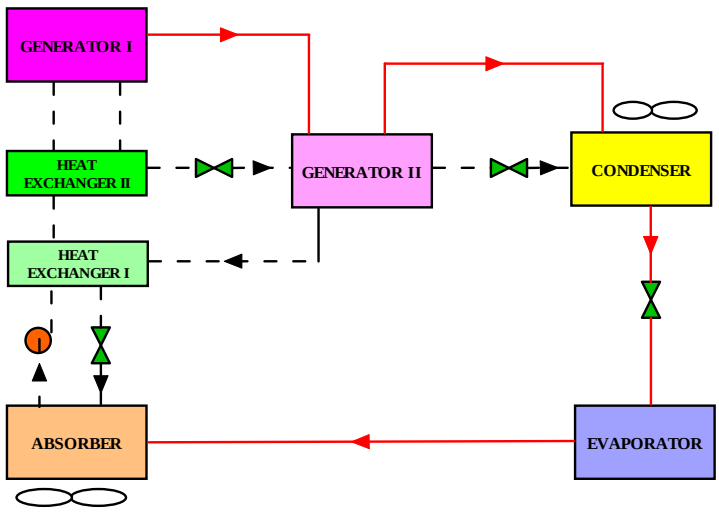

Figure 1.9 Double effect water/LiBr absorption cycle

In absorption systems, if the solution concentration is too high or the solution temperature is reduced too low, crystallization may occur and interrupt machine operation. The vulnerable location is also decided by the mechanical structure of pipes and fittings; this is most likely to occur in the strong solution entering the absorber; that is the point 6 in Figure 1.8, the concentrated solution at the lowest temperature. Crystallization must be avoided because the formation of slush in the piping network over time could form a solid and block the flow. If this occurs, the concentrated solution temperature needs to be raised above its saturation point so that the salt crystals will return to the solution, freeing the machine. The big difference between water-cooled and air-cooled LiBr-water absorption cycles is the temperature of the absorber. With air-cooling, one cannot achieve a temperature of the solution in the absorber sufficiently low to maintain the evaporator pressure. The only way to compensate for the high absorber temperature is to increase the concentration of LiBr in the solution, but that brings it closer to crystallization [26-31]. One of the

following five causes or a combination of those causes may trigger crystallization of air-cooled absorption cycles, and the associated precautions are also suggested as well:

1. Higher ambient temperature (it is higher condenser cooling water temperature for the water-cooled machine): The air-cooled absorbers tend to run hotter than water-cooled units due to the relatively poor heat transfer characteristics of air.

2. Air leak into the machine or non-absorbable gases produced during corrosion: Both deteriorate the UA and cause higher system pressure, decreased capacity and COP, and higher crystallization probability. A direct method for keeping the required pressure is to evacuate the vapor space periodically with a vacuum pump. This situation can be simulated by assuming a decreased UA, which will cause X_6, the concentration of point 6, to move closer to the crystallization line limit. As a precaution to this issue, the system should be evacuated routinely.

3. Too much heat input to the generator: either the exhaust temperature or the flow rate is too high, which results in increased solution concentrations to the point where crystallization may occur. As a precaution to this issue, the exhaust temperature or flow rate into the generator should be maintained within a specific range.

4. Failed dilution after shutdown: During normal shutdown, the machine undergoes an automatic dilution cycle, which lowers the concentration of the solution throughout the machine. In such a case, the machine may cool to ambient temperature without crystallization occurring in the solutions. Crystallization is most likely to occur when the machine is stopped due to power outage while operating at full load, when highly concentrated solutions are present in the solution heat exchanger [13].

1.2.3 Comparison of Absorption and Compression Systems

1. The pump or pumps in an absorption system require less electrical power than a compressor in a compression system.

2. If a steam or hot water boiler is to be kept in operation for other purposes, it may be more economical to use this heat supply for the generator of an absorption system than to use electrical power for a compression refrigeration system. The use of an absorption system may be more economical if waste or exhaust steam is available. A critical factor is the simultaneous availability of waste heat and the requirement for cooling.

3. Slugs of liquid carried over from the evaporator do no damage in the absorption system whereas liquid carryover will damage a compressor.

4. The absorption system requires more space than the compression system.

5. Cooling water requirements are larger for an absorption system than for a compression system.

The second chapter of this thesis presents the history of Absorption Refrigeration and literature review on the relevant studies.

The third chapter presents preliminary design results for components and system configurations. The refrigeration system designed is modeled and simulated by EES (Engineering Equation Solver) program. A simple steady-state simulation model has been developed and implemented in a computer program using EES. The model equations are formulated from species, mass and energy balances. State equations used for the LiBr-H_2O equilibrium and thermodynamic properties are taken from EES subroutines. Input data required by the model are the evaporation, absorption, condensation and generation temperatures, refrigeration capacity and temperature differences in the heat exchangers. Detailed designs for each component are presented in this chapter. They are based on the results of the simulation model. The measurement devices and control units used in the set-up and calibrations are

outlined in this chapter. Two generator models designed and constructed are coupled on internal combustion engine.

In the fourth chapter, the theoretical and experimental results are presented by measured and evaluated data and the results are discussed. The conclusions are given in fifth chapter. In the final chapter, suggestions for complementary works are given.

The experimental study presented in this thesis was financially supported by the TÜBİTAK-MAG (The Scientific and Technical Research Council of Turkey-Engineering Research Grant Committee.) under the project number: **104M422**.

CHAPTER 2

LITERATURE SURVEY

In this chapter, a summary of the studies relevant to the present study are presented.

2.1 HISTORY OF ABSORPTION TECHNOLOGY

Edmond Carré developed the first absorption machine in 1850, using water and sulfuric acid. His brother, Ferdinand Carré, demonstrated an ammonia/water refrigeration machine in 1859, and in 1860 Ferdinand received the first U.S. patent for a commercial absorption unit. Servel was founded in 1902 as the Hercules Buggy Works, and became a manufacturer of electric refrigerators (the name is short for "Serve Electrically"). In 1925, Servel purchased US rights to a new AB Electrolux gas heat-driven absorption refrigerator invented by Swedish engineering students, Carl G. Munters and Baltzar von Platen. The new Electrolux-Servel absorption refrigerator entered the US market in 1926 and brought absorption refrigerators to millions of homes until production was stopped in the 1950s [5].

American companies manufactured 100% of $LiBr/H_2O$ absorption chillers worldwide, in the late 1960's, using the standard single-effect absorption cycle. Trane Company introduced the first mass-produced steam-fired double-effect $LiBr/H_2O$ absorption chiller in 1970.

Several factors have influenced absorption chiller sales natural gas prices, as well as, fuel availability concerns and governmental policies caused U.S. absorption

chiller sales to decline in the mid-1970s and throughout the 1980s. Since the early 1990s, absorption chiller sales have increased modestly in the USA. Absorption chiller use in countries like Japan, China and Korea has grown exponentially since the mid-1970s. The general underlying reasons for the disparate growth phenomena in Asia are complex, but it is clear that the economics of delivered energy are being evaluated differently between historical America and modern Asia when it comes to commercial water chiller technology.

2.2 RESEARCH EMPHASES OF CURRENT ABSORPTION TECHNOLOGIES

More than 150 papers associated with absorption technologies have been reviewed to classify the current research emphases. Figure 2.1 shows ten categories of research areas. A small percentage of the literature is about the air-cooled absorption machines alone (2%).

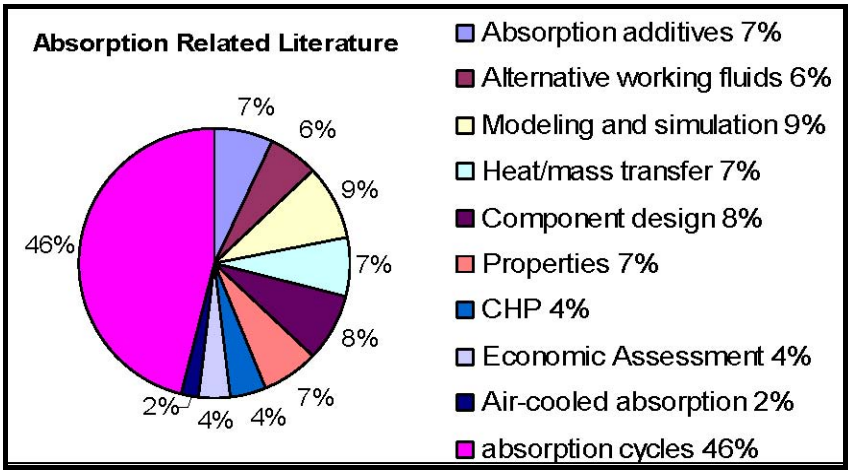

Figure 2.1 Research emphases of absorption technology

However, there is little literature on air-cooled absorption refrigeration system, mainly due to the unavailability of a commercialized product, and most is restricted to purely theoretical simulation.

2.3 THEORETICAL AND EXPERIMENTAL WORKS ABOUT ABSORPTION REFRIGERATION DRIVEN BY ENGINE EXHAUST GAS FOR VEHICLES

Ghassemi [90] examined theoretically the absorption refrigeration system for vehicle application. He introduced an NH_3-Water absorption refrigeration system utilizing the energy which is given to environment through the vehicle radiator for the inside cooling of the vehicle. Ghasemi pointed out that, this energy was about 1/3 of the total fuel energy at 80 ^oC. In his design, shown in Figure 2.2, the hot water from the engine was passed, by the engine water pump through a heat exchanger installed in the generator to evaporate ammonia. In the experimental model, the air cooled condenser was placed on the roof of the driver cabin, while the evaporator was placed inside the cabinet. Thermodynamic properties of NH_3-Water solution at different points of the cycle are tabulated in Table 2.1.

Table 2.1 Thermodynamic properties of NH_3-Water solution at different points of the cycle

Points	P (Bar)	T (^oC)	$\dot{m}$ (kg/s)	X (%)	h (kJ/kg)
1	11.6	30.5	0.453	0.996	141.5
2	11.5	-----	0.453	0.996	-190.5
3	2.4	-12.2	0.453	0.996	1192.4
4	2.3	24.9	0.453	0.996	1152.9
5	2.3	25.5	1.87	0.523	143.8
6	11.8	-----	1.87	0.523	-142.2
7	11.7	65.4	1.87	0.523	5.8
8	11.7	76.4	1.41	0.456	92.8
9	11.7	71.0	0.465	0.986	1422.1
10	11.7	54.4	0.012	0.611	25.5
11	11.7	54.4	0.453	0.996	1359

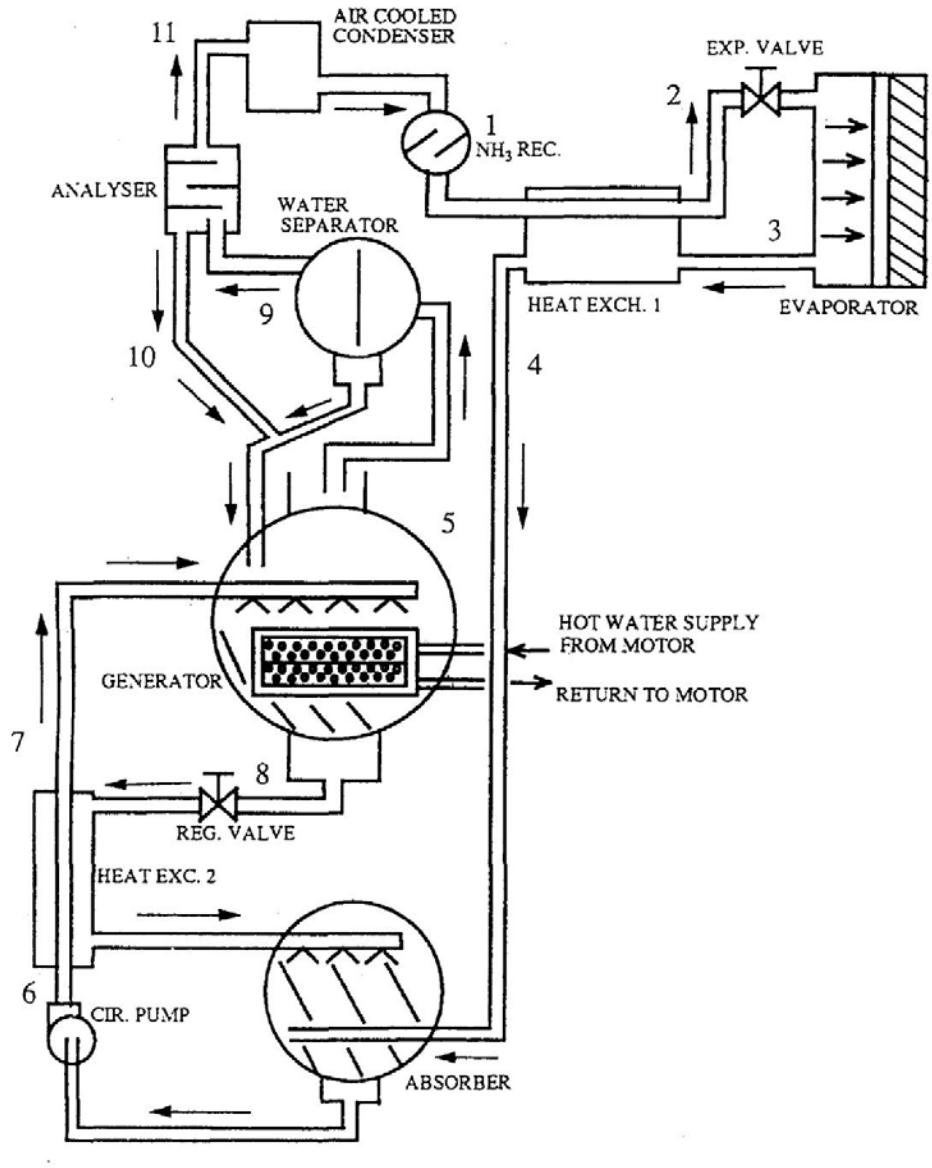

Figure 2.2 Absorption refrigeration system for vehicle application by Ghasemi

Ghasemi concluded that, there was a possibility of using the absorption systems for cooling the vehicles cabinet and by doing so, fuel cost and capital cost on the system would be decreased. Overall cycle COP are around 0,29 [90].

Keating [6] invented an absorption refrigeration system for mobile application and had a patent for it in 1954. His invention was specially designed and constructed for mobile application on vehicles, boats, railway cars utilizing the heat of the exhaust gases from the IC engine. Keating claimed that he designed the system

to provide a portable absorption refrigeration system which is designed for application in a vehicle, using either the heat of exhaust gases from the vehicle' s engine. Figure 2.3 shows the absorption refrigeration system designed by Keating [6].

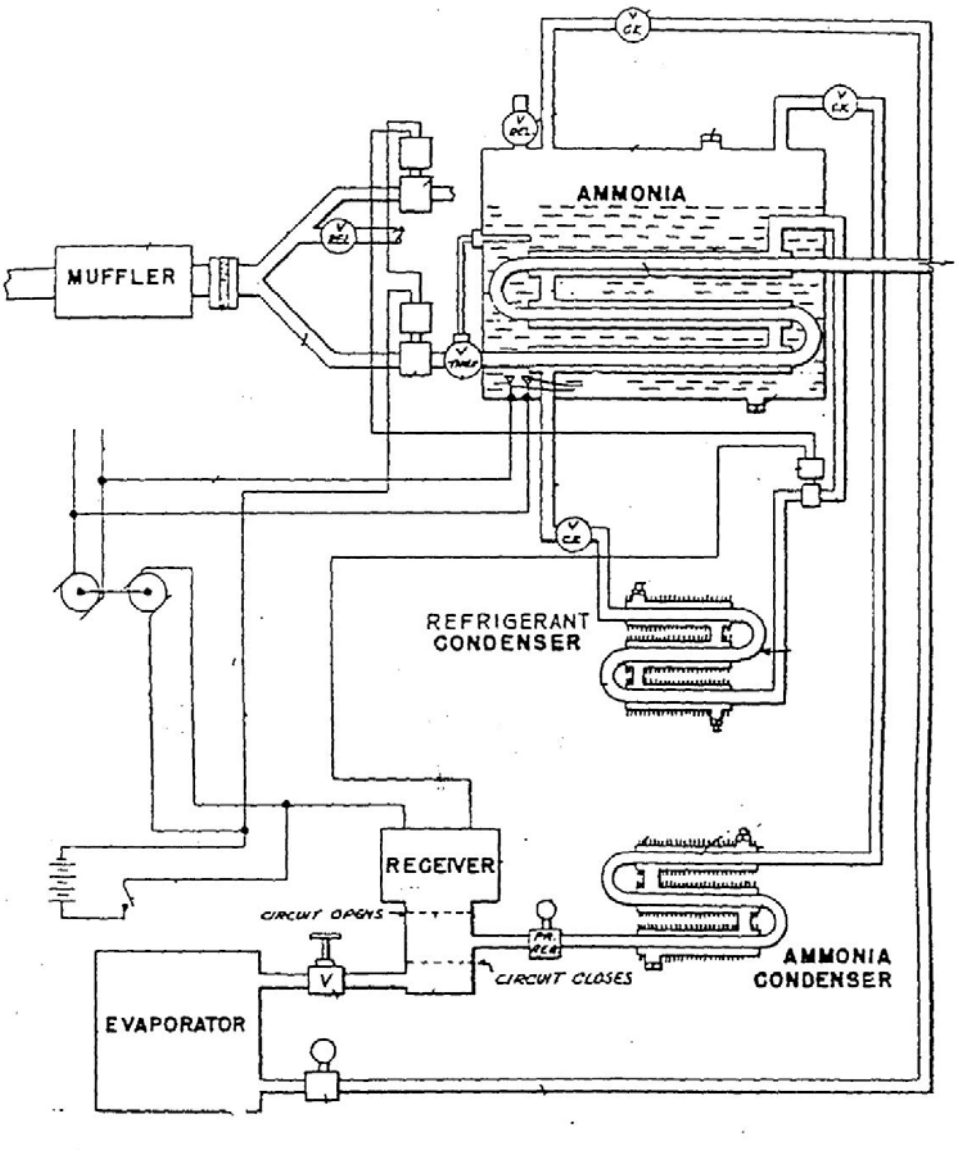

Figure 2.3 Absorption refrigeration system for vehicle by Keating [6]

McNamara [7] designed a mobile absorption refrigeration and air conditioning system utilizing the exhaust heat from the engine, which might be either diesel, steam, IC or a turbine and he had a patent for it in 1972. Figure 2.4 shows the

plan view of the absorption refrigeration system designed by McNamara. His system was using a mixture of water and ammonia and helium to maintain a constant vapor pressure. The purpose of this system was to provide a simple, low cost, easily installed absorption refrigeration system for vehicles which utilizes the waste heat from the exhaust gases without reducing the efficiency of the vehicle engine [7].

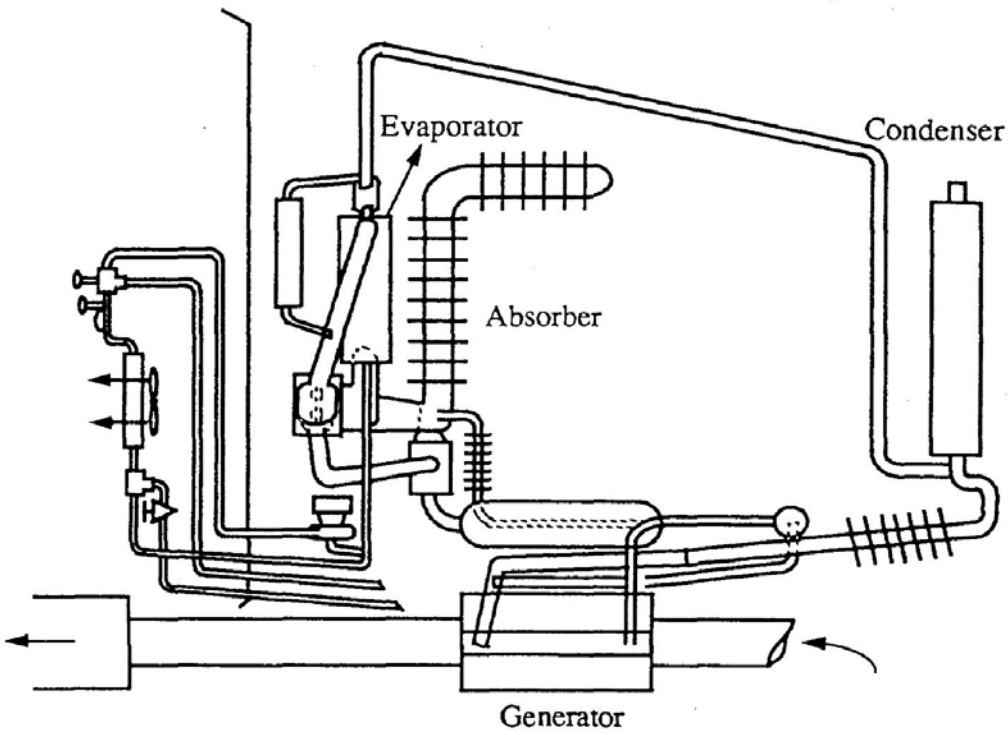

Figure 2.4 Plan view of the absorption refrigeration system designed by McNamara

Keating and McNamara's inventions are similar to the present research, since all aim is to utilize the waste heat in the exhaust gases of the vehicle. However, the way of utilizing heat of these two designs may cause some trouble in practice. The Keating's one may provide very high back pressure which would affect the engine efficiency, because the coils in the generator chamber could cause large pressure drops. On the other hand, it is doubtful to have enough heat transfer in McNamara's generator because of smaller heat transfer area [5].

Akerman [8] investigated the suitability of absorption refrigeration cycles for use in the air conditioning of automobile vehicles. He examined an automotive

absorption air conditioning system using engine-rejected heat as its energy source. He outlined the basic principles of absorption refrigeration systems and discussed the general arrangement for adapting them for automotive air conditioning and the functioning of the component parts. Akerman selected two different absorption cycles with different refrigerant pairs and studied details of both [8].

Vincent et al. [9] studied a truck absorption refrigeration system utilizing the waste heat in the exhaust gas of the main propulsion unit of the truck as power source. The feature of their research was the idea of utilizing exhaust heat from trucks and automobiles for refrigeration. For that reason, the cooling potential of exhaust gases from an automobile and truck was analyzed and a special heat exchanger was designed for waste heat without excessive pressure drops in the exhaust system. Additionally, they incorporated an eutectic plate storage system to moderate fluctuations of cooling potential due to variable vehicle speed and to be used as an evaporator coil with a large heat exchange surface when necessary. Figure 2.5 illustrates the truck absorption refrigeration system proposed by Vincent et al. Figure 2.6 shows the generator-analyzer designed by them and Figure 2.7 illustrates the arrangement of the system on truck [9].

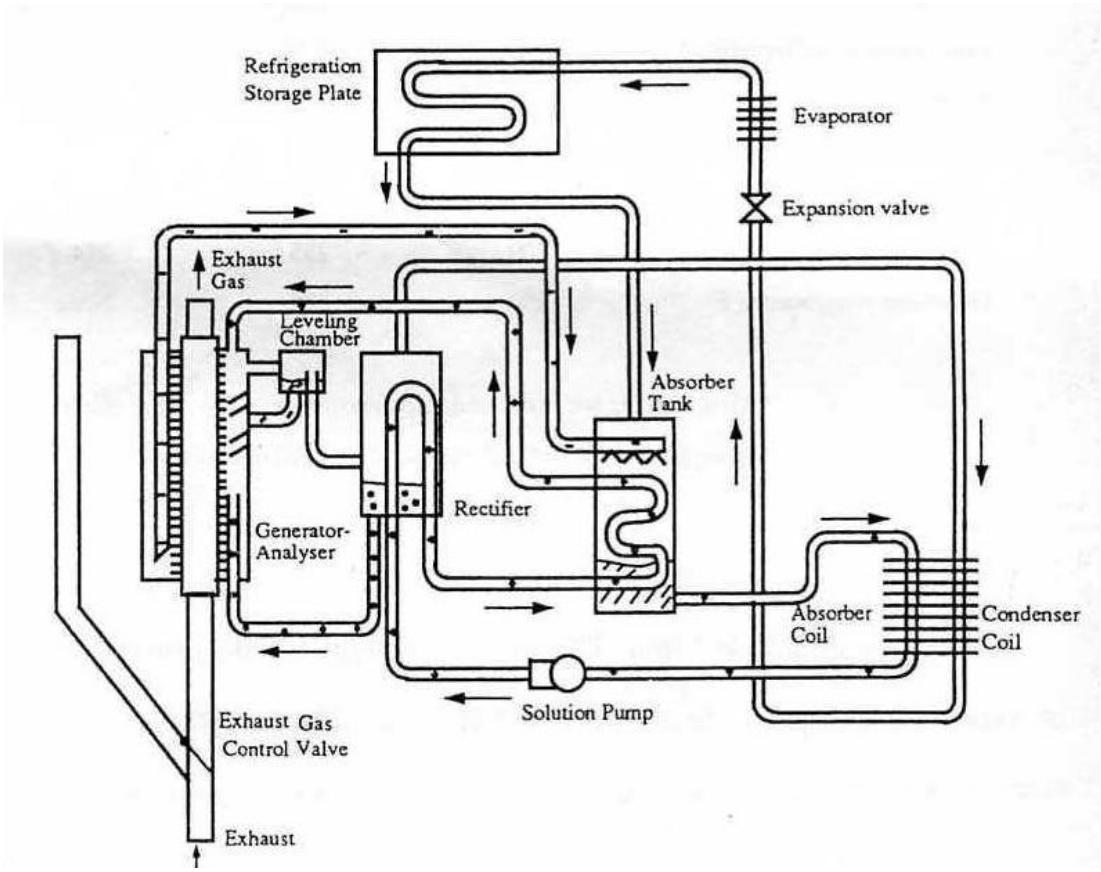

Figure 2.5 Truck absorption refrigeration system designed by Vincent et al.[9]

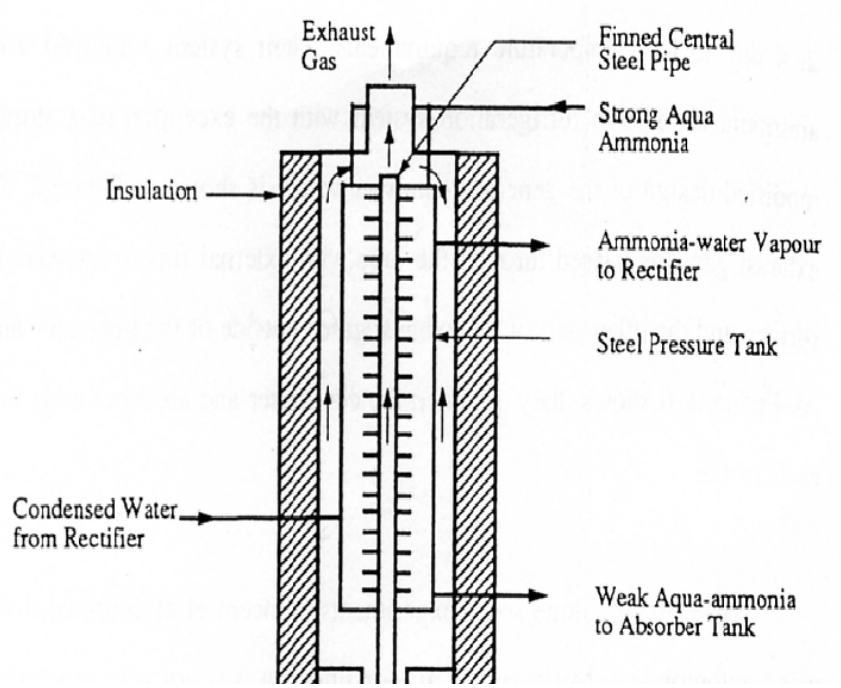

Figure 2.6 Generator design by Vincent et al. [9]

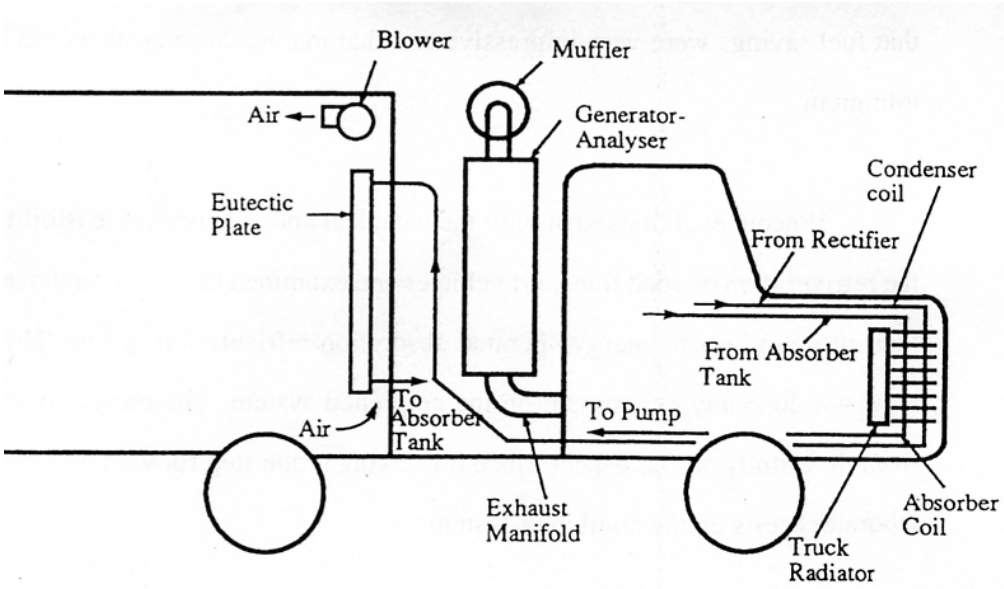

Figure 2.7 Location of absorption system on truck by Vincent et al.

Vincent et al. looked at only the technical and economical feasibility aspects of the refrigeration on road transport vehicles and examined the merits and demerits of their proposed waste energy operated absorption refrigeration system. However, they have not carried out any experiment on the combined system.

Koehler et al. [10] designed, built and tested a breadboard prototype of an absorption system for truck refrigeration using heat from the exhaust gases. Figure 2.8 shows the absorption refrigeration system designed by Koehler et al. Measured COP values of unoptimized single-stage ammonia-water absorption cycle varied between 23 % and 30 %, but system modeling shows that this can be improved to values considerably over 30%. Computer simulation for the system included cycle analysis as well as component modeling, using a detailed two-fluid model for flow of the ammonia-water mixture in the condenser and absorber. In addition, the recoverable energy of the exhaust gases was analyzed for representative truck-driving conditions for city traffic, mountain roads and flat roads. The results show that the system is promising for the long distance driving on flat roads [10].

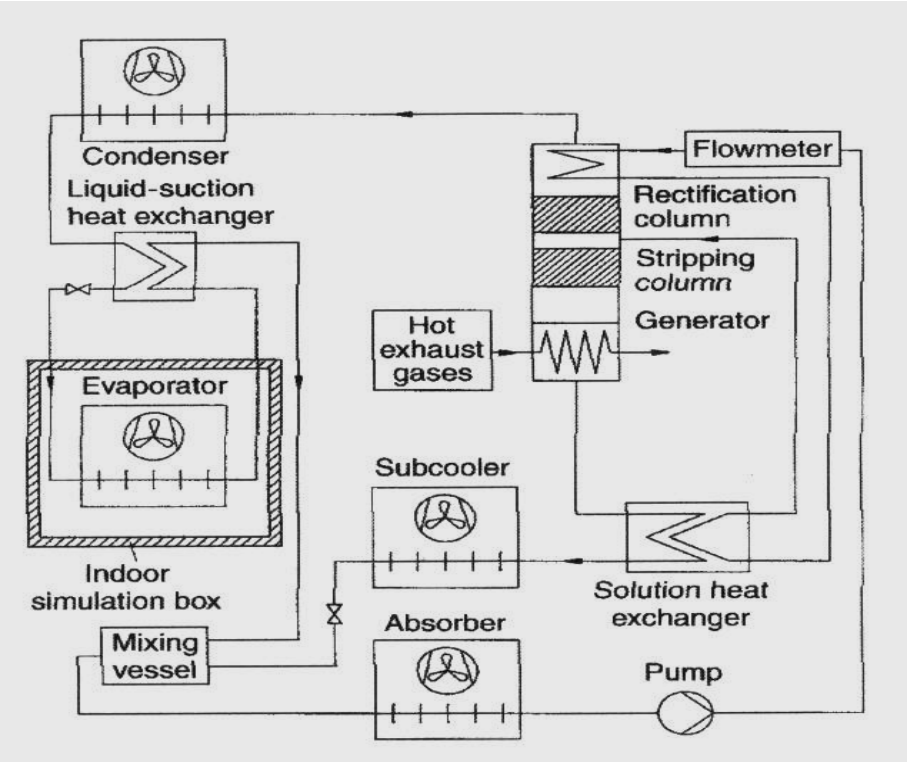

Figure 2.8 Essential components of the air-cooled absorption prototype for transport refrigeration

Horuz' s study [3-5] included an experimental investigation into use of vapour absorption refrigeration (VAR) systems for road transport vehicles using the waste heat in the exhaust gases of the main propulsion unit as the energy source. In the study, the performance of a VAR system fired by natural gas is compared with that of same system driven by engine exhaust gases. This showed that the exhaust gas driven system produced the same performance characteristics as the gas fired system. A comparison of the capital and running costs of conventional and proposed alternative system was made. Suggestions are also made regarding operation of the VAR system during off-road/slow running conditions. Figure 2.9 shows the absorption refrigeration system used by Horuz. Figure 2.10 shows the two generators designed and constructed by Horuz [3-5]. Experimental results proved that the 6-litre turbo diesel engine used was capable of providing enough energy to drive the VAR system via its waste exhaust heat. Figure 2.11 indicates that the higher the engine power, the greater the cooling capacity of the VAR system.

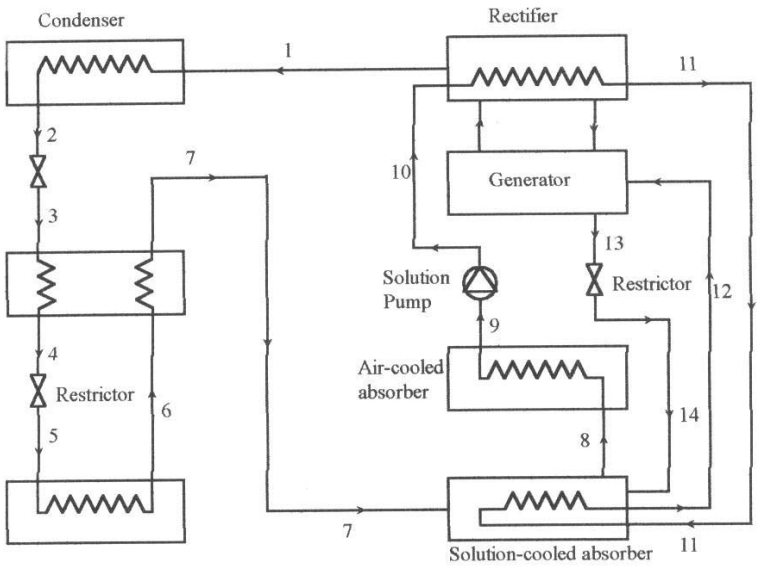

Figure 2.9 Absorption refrigeration system used by Horuz [3-5]

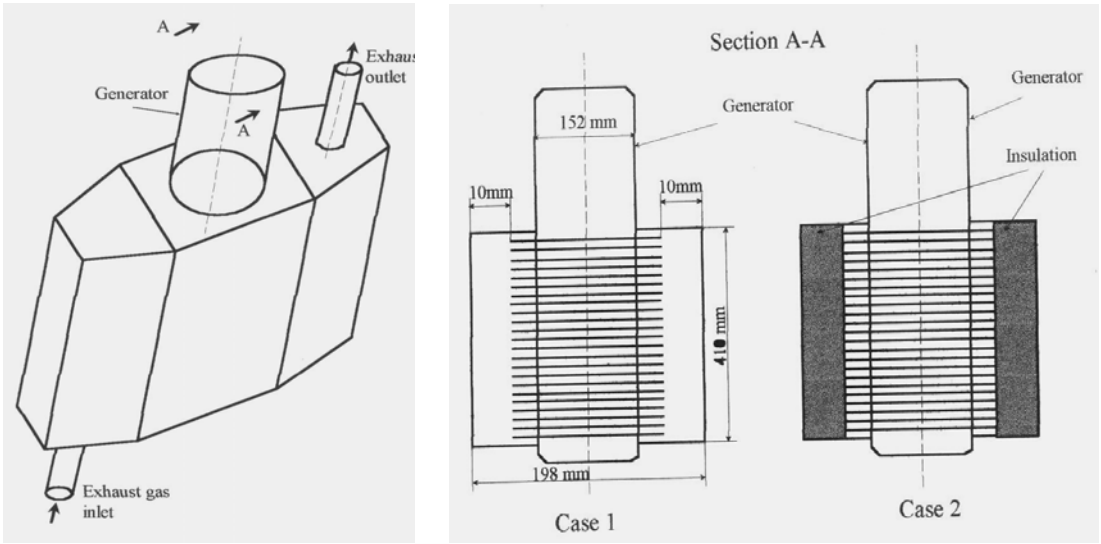

Figure 2.10 Two different heat exchangers details used as generator

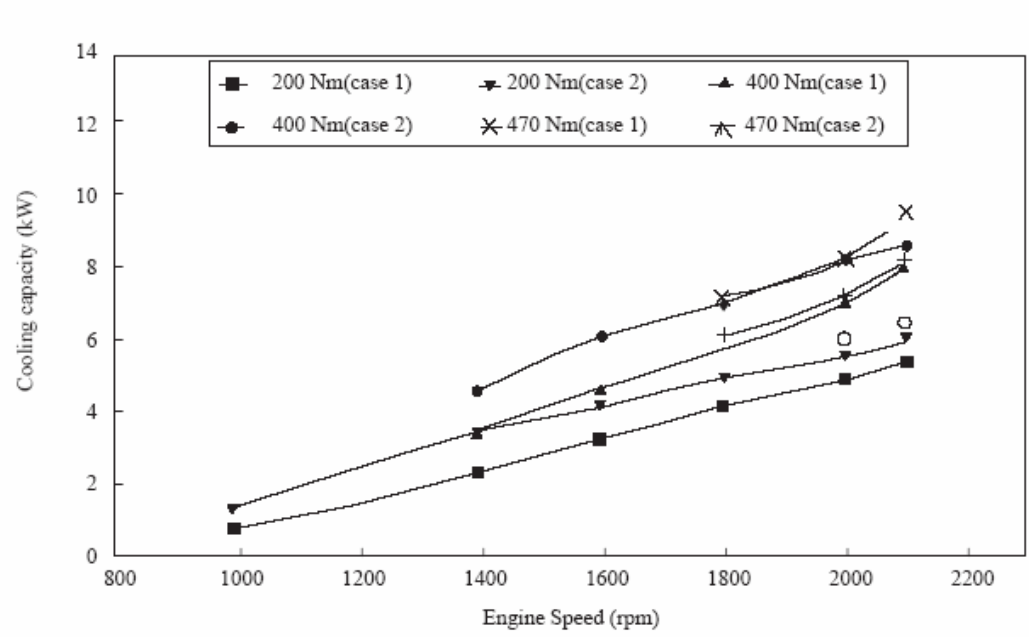

Figure 2.11 Cooling capacities against engine speed [3-5]

Salim, M. [11] simulated an automotive LiBr absorption air-conditioner system with 7 kW cooling capacity by ABSIM software (ABsorption SIMulation). Based on the steady-state thermodynamic modeling and simulation of a single-effect air-cooled absorption chiller, together with the experience of running water-cooled absorption chillers, the authors propose the crystallization control guideline, which is applicable for either air-cooled or water-cooled absorption chillers. The experiments based on steady-state operation conditions prove both the modeling and the crystallization control strategy. However no experimental validation is supplied [11].

An interesting phenomenon is that most papers of this category are associated with solar applications. For example, Alva, L. [12] simulated a proposed air-cooled solar-assisted absorption system with the cooling loads in the range of 10.5, 14 and 17.5 kW. A typical coefficient of performance (COP) variation is shown in Figure 2.11. Again, no experimental validation is conducted [12].

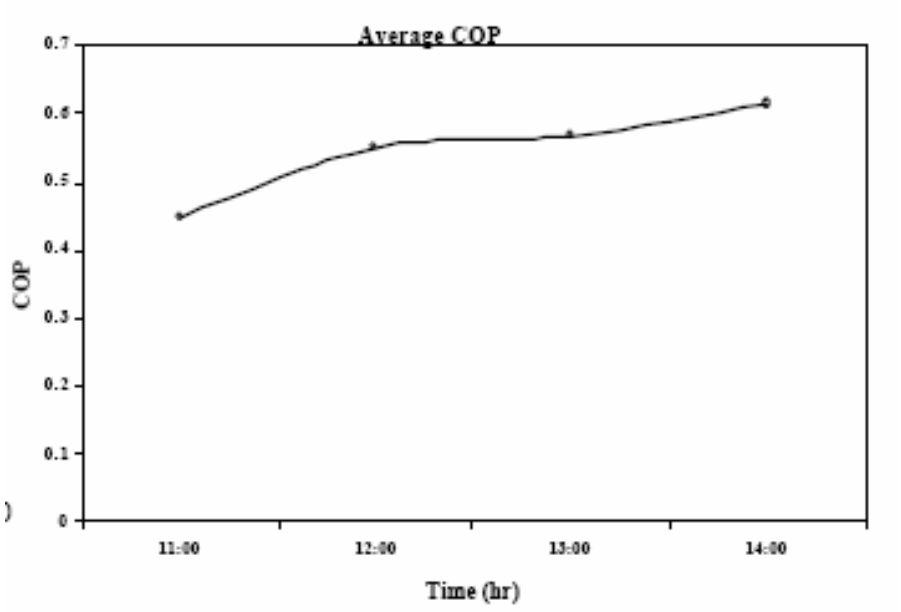

Figure 2.12 Typical average COP for proposed system by Alva [12]

Florides, G. [13] mentioned several causes of crystallization occurring in a water-cooled LiBr absorption machine, which include: 1) Air leakage into the machine, which results in increased pressure in the evaporator; 2) Excessively cold condenser water, coupled with a high load condition; 3) electric power failure. To investigate the accuracy of the theoretical procedure described above for the design of the various heat exchangers, a 1 kW model was designed and constructed. The designed conditions chosen are indicated in Table 2.2. A summary of the experimental results is presented in Table 2.3 [13].

Table 2.2 Designed conditions chosen for simulated system

Description	**Symbol**	**kW**
Capacity (evaporator output power)	Q_e	1.0
Absorber heat, rejected to the environment	Q_a	1.28
Heat input to the generator	Q_g	1.35
Condenser heat, rejected to the environment	Q_c	1.07
Coefficient of performance	COP	0.74

Table 2.3 A summary of the experimental results

Heat exchanger	Cooling/heating water temperature (^oC)		Overall heat transfer coefficient, U ($W/m^2 K$)	
	Entering	Leaving	Theoretically estimated	Actual value
Generator	92	88	1600-7500	2300
Condenser	27	28,5	2980	3265
Evaporator	13	11	-	195
Absorber	30	31	625	400
Solution heat exch.	-	-	130	≈130

Garrabrant, M.A. [14] designed, built and tested an air-liquid exhaust gas heat exchanger and hydronically heated ammonia generator that could be mounted permanently on a large transport truck in the exhaust gases in an absorption refrigeration system. The prototype heat exchanger performed as expected, with a very low flue gas side pressure loss. Generator performance was approximately 20% low. Overall cycle COPs at the required evaporator temperatures were within the range required for the application (COP=0.43) [14].

Izquierdo, M. [15] calculated the operating parameters of a single-effect and a double-effect LiBr air-cooled absorption system driven by solar energy with the objective of crystallization prevention. The cooling capacity of the systems is small, less that 7 kW. Some conclusions included: 1) The double-effect absorption cycle still might work without crystallization problems for the condensation temperature up to 53°C; for the single-effect the limit is 40~45°C. 2) For higher condensation temperature, the generation temperature required is very high and crystallization occurs. 3) Single-stage cycles can not operate for condensation temperatures higher than 40–45 ^oC using heat from flat plate collectors. For higher condensation temperatures the generation temperatures required are very high and crystallization occurs. 4) Calculation process shows that about 80 ^oC of generation temperature are required in the double-stage absorption machine when condensation temperature reaches 50 ^oC, obtaining a COP equal to 0.38 in the theoretical cycle [15].

CHAPTER 3

DESIGN OF THE EXPERIMENTAL SET-UP

3.1 MODELLING AND SIMULATION OF THE ABSORPTION SYSTEM PROPOSED

This chapter presents preliminary design results for components and system configurations. The designed refrigeration system is modeled and simulated by EES (Engineering Equation Solver) program [32]. A simple steady-state simulation model has been developed and implemented in a computer program using EES. The model equations are formulated from species, mass and energy balances. State equations used for the LiBr-H_2O equilibrium and thermodynamic properties are taken from EES subroutines. Input data required by the model are the evaporation, absorption condensation and generation temperatures, refrigeration capacity, temperature differences in the heat exchangers.

3.1.1 Software Selection

The EES is commonly used to simulate the operation of absorption chillers. The basic function provided by EES is the numerical solution of a set of algebraic equations. EES can also be used to solve differential and integral equations, conduct optimization, provide uncertainty analyses and linear and non-linear regression, build a simple interface and generate plots. There are two major differences between EES and other equation solving programs or software. First, EES allows equations to be entered in any order with unknown variables placed anywhere in the equations; EES

automatically reorders the equations for efficient solution. Second, EES provides many built-in mathematical and thermo-physical property functions of working fluids useful for engineering calculations.

3.1.2 Thermodynamic Analysis of The Absorption Refrigeration System Designed

The thermodynamic analysis of the system which is shown schematically in Figure 3.1 is given below. The mass balance and the first and second laws of thermodynamics are used to analyze the absorption refrigeration system. Each component can be considered as an inlet and outlet control volume with steady flow for its contribution to the overall system. The mass balance of the system is the sum of the mass balance of each component [33-37].

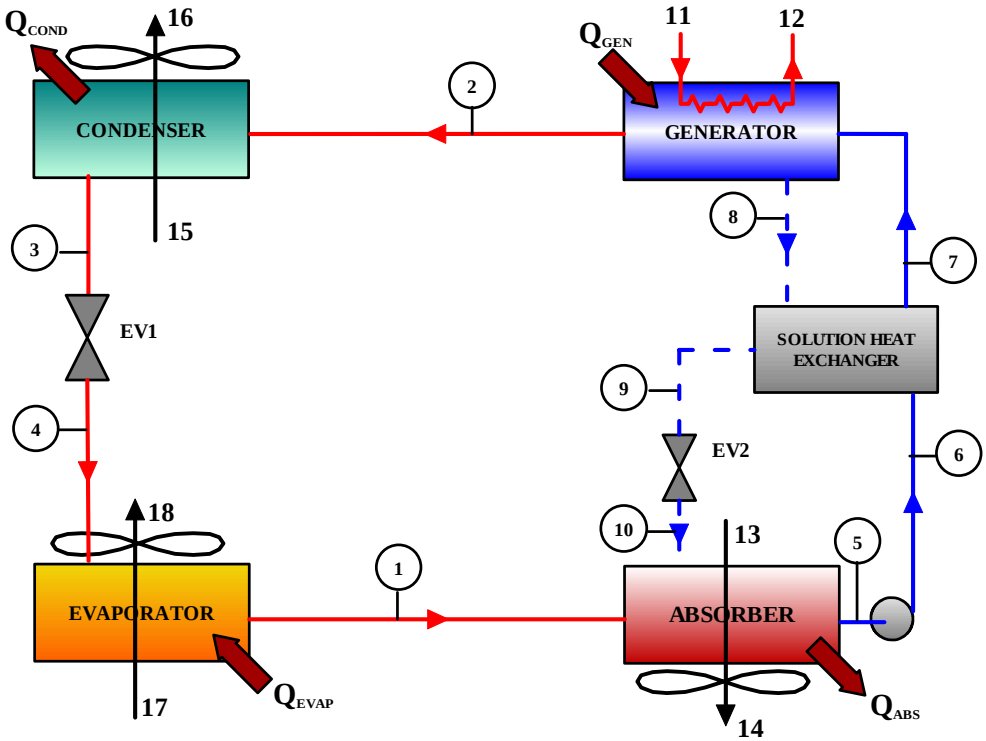

Figure 3.1 Diagram of single-effect air-cooled absorption cooling system

The following assumptions and the thermodynamic status of each state point are used in the modeling of single-effect absorption system designed;

- The system is operating in a steady state;
- There are 2 pressures (P_{high} and P_{low}) in the system: the pressure in the generator and condenser is at P_{high}, while the pressure in the evaporator and absorber is at P_{low}, and there is no pressure drop or heat transfer in the piping network;
- The throttling device is isenthalpic;
- The solution pump is adiabatic, and it is used to maintain the constant solution level in the generator;
- 1st point is saturated water vapor;
- 2nd point is superheated water vapor;
- 3rd point is saturated liquid water;
- 4th point is vapor-liquid water state;
- 5th point is saturated liquid solution;
- 6th point is sub-cooled liquid solution(at P_{low});
- 7th point is sub-cooled liquid solution(at P_{high});
- 8th point is saturated liquid solution;
- 9th point is sub-cooled liquid solution;
- 10th point is vapor-liquid solution state.

3.1.2.1 Energy analysis

The simulation model introduced in this section was specially developed for the thermodynamic design of absorption cycles.

In the following sections, all numeric references of state points are based on the schematic cycle diagrams shown in Figure 3.1.

All transfer processes in a system were assumed heat transfer-dominated, i.e. mass transfer resistance is neglected, and simplified so that they could be modeled by the ***UA-LMTD*** method [38].

In this investigation, the UA-LMTD method is used. That is, the overall heat transfer coefficient (UA) of each heat exchanger is known and can be considered constant after the absorption refrigeration set-up is built. LMTD is the temperature difference at one end of the heat exchanger minus the temperature difference at the other end of the heat exchanger, divided by the natural logarithm of the ratio of these two temperature differences. The UA-LMTD method involves two important assumptions: (1) the fluid specific heats do not vary significantly with temperature, and (2) the convection heat transfer coefficients are relatively constant throughout the heat exchanger.

All component models are introduced step by step in the following section [39-40].

Generator / Desorber

The energy balances on the solution side and heat source are:

$$Q_{GEN} = \dot{m}_2 .h_2 + \dot{m}_8 .h_8 - \dot{m}_7 .h_7 \tag{3.1}$$

$$Q_{GEN} = \dot{m}_{11} .(h_{11} - h_{12}) \tag{3.2}$$

The heat transfer rate is calculated by

$$Q_{GEN} = U.A_{GEN}.LMTD_{GEN} \tag{3.3}$$

$$LMTD_{GEN} = \frac{(T_{11} - T_8) - (T_{12} - T_2)}{\ln \frac{(T_{11} - T_8)}{(T_{12} - T_2)}} \tag{3.4}$$

The mass and salt should balance to satisfy the conservation law:

$$\dot{m}_7 = \dot{m}_2 + \dot{m}_8 \tag{3.5}$$

$$\dot{m}_7 . x_7 = \dot{m}_8 . x_8 \tag{3.6}$$

Condenser

The energy balances on the solution side and cooling air are:

$$Q_{CON} = \dot{m}_2 .(h_2 - h_3) \tag{3.7}$$

$$Q_{CON} = \dot{m}_{15} .(h_{16} - h_{15}) \tag{3.8}$$

The heat transfer rate is calculated by

$$Q_{CON} = U.A_{CON} .LMTD_{CON} \tag{3.9}$$

$$LMTD_{CON} = \frac{(T_3 - T_2)}{\ln \frac{(T_3 - T_{15})}{(T_3 - T_{16})}} \tag{3.10}$$

Evaporator

The energy balances on the solution side and chilled water are:

$$Q_{EVAP} = \dot{m}_4 .(h_1 - h_4) \tag{3.11}$$

$$Q_{EVAP} = \dot{m}_{17} .(h_{17} - h_{18}) \tag{3.12}$$

The heat transfer rate is calculated by

$$Q_{EVAP} = U.A_{EVAP}.LMTD_{EVAP} \quad (3.13)$$

$$LMTD_{EVAP} = \frac{(T_{18} - T_{17})}{\ln \frac{(T_{17} - T_1)}{(T_{18} - T_1)}} \quad (3.14)$$

Absorber

The energy balances on the solution side and cooling air are:

$$Q_{ABS} = \dot{m}_{10}.h_{10} + \dot{m}_1.h_1 - \dot{m}_5.h_5 \quad (3.15)$$

$$Q_{ABS} = \dot{m}_{13}.(h_{14} - h_{13}) \quad (3.16)$$

The heat transfer rate is calculated by

$$Q_{ABS} = U.A_{ABS}.LMTD_{ABS} \quad (3.17)$$

$$LMTD_{ABS} = \frac{(T_{10} - T_{14}) - (T_5 - T_{13})}{\ln \frac{(T_{10} - T_{14})}{(T_5 - T_{13})}} \quad (3.18)$$

Solution Heat Exchanger

The energy balances on the cold and hot solution side are:

$$Q_{SHEX} = \dot{m}_5.(h_7 - h_6) \quad (3.19)$$

$$Q_{SHEX} = \dot{m}_8.(h_8 - h_9) \quad (3.20)$$

The heat transfer rate is calculated by,

$$Q_{SHEX} = U.A_{SHEX}.LMTD_{SHEX} \quad (3.21)$$

$$LMTD_{SHEX} = \frac{(T_8 - T_7) - (T_9 - T_6)}{\ln \frac{(T_8 - T_7)}{(T_9 - T_6)}} \quad (3.22)$$

The energy balance equation of the absorption system is

$$Q_{ABS}+Q_{CON}-Q_{GEN}-Q_{EVAP}-W_{pump}=0 \quad (3.23)$$

It is assumed that W_{pump} is negligible compared with other quantities, then Eq 3.23 becomes

$$Q_{ABS}+Q_{CON}= Q_{GEN}-Q_{EVAP} \quad (3.24)$$

$$COP = \frac{Q_{EVAP}}{Q_{GEN}} \quad (3.25)$$

3.1.2.2 Exergy analysis

A schematic diagram of the system the equivalent availability flow balance is shown in Figure 3.2 [41-44].

Generator

$$\Delta\psi_{G,ht} = Q_G\left(1-\frac{T_o}{T_G}\right) - \dot{m}_{12}(\psi_{12} - \psi_{11}) \quad (3.26)$$

$$\Delta\psi_{G,in} = \dot{m}_8\psi_8 + \dot{m}_2\psi_2 - \dot{m}_7\psi_7 - Q_G\left(1-\frac{T_o}{T_G}\right) \quad (3.27)$$

$$\Delta\psi_{G,hi} = \dot{m}_{12}(\psi_{12} - \psi_{11}) \quad (3.28)$$

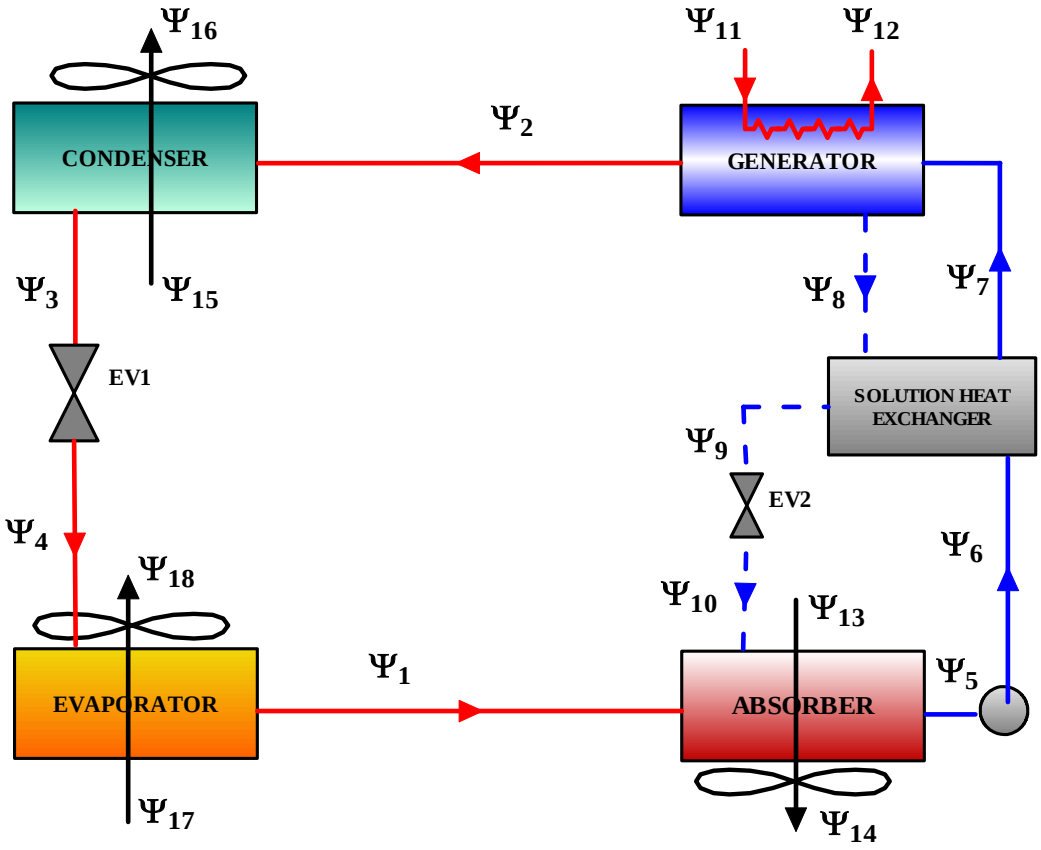

Figure 3.2 Availability flow balance for the absorption cycle

Condenser

$$\Delta\psi_{C,ho} = \dot{m}_{16}(\psi_{16} - \psi_{15}) \tag{3.29}$$

$$\Delta\psi_{C,ht} = Q_C\left(1 - \frac{T_o}{T_C}\right) - \dot{m}_{16}(\psi_{16} - \psi_{15}) \tag{3.30}$$

$$\Delta\psi_{C,in} = \dot{m}_2(\psi_2 - \psi_3) - Q_C\left(1 - \frac{T_o}{T_C}\right) \tag{3.31}$$

Refrigerant Expansion Valve

$$\Delta\psi_{vl} = \dot{m}_3(\psi_3 - \psi_4) \tag{3.32}$$

Evaporator

$$\Delta\psi_{E,ho} = \dot{m}_{17}(\psi_{17} - \psi_{18}) \tag{3.33}$$

$$\Delta\psi_{E,ht} = Q_E\left(1 - \frac{T_o}{T_E}\right) - \dot{m}_{17}(\psi_{17} - \psi_{18}) \tag{3.34}$$

$$\Delta\psi_{E,in} = \dot{m}_1(\psi_1 - \psi_4) - Q_E\left(1 - \frac{T_o}{T_E}\right) \tag{3.35}$$

Solution Expansion valve

$$\Delta\psi_{v2} = \dot{m}_{10}(\psi_{10} - \psi_9) \tag{3.36}$$

Absorber

$$\Delta\psi_{A,ho} = \dot{m}_{13}(\psi_{13} - \psi_{14}) \tag{3.37}$$

$$\Delta\psi_{A,ht} = Q_A\left(1 - \frac{T_o}{T_A}\right) - \dot{m}_{13}(\psi_{13} - \psi_{14}) \tag{3.38}$$

$$\Delta\psi_{A,in} = \dot{m}_1\psi_1 + \dot{m}_{10}\psi_{10} - \dot{m}_5\psi_5 - Q_A\left(1 - \frac{T_o}{T_A}\right) \tag{3.39}$$

Solution Heat Exchanger

$$\Delta\psi_{SHE,ht} = \dot{m}_8\psi_8 + \dot{m}_6\psi_6 - \dot{m}_7\psi_7 - \dot{m}_9\psi_9 \tag{3.40}$$

Solution Pump

$$\Delta\psi_{Pump} = \frac{\dot{m}_5(P_5 - P_6)}{P_6} \tag{3.41}$$

3.2 CONSTRUCTION OF THE ABSORPTION REFRIGERATION SYSTEM

There may be many choices of physical designs to realize a absorption system with the chosen cycle. But there are some common subjects in the design of H_2O/LiBr system. Some of them are briefly introduced below.

The chosen cycle has two different sub-atmospheric pressures. They are typically, 5.63 kPa for generator and condenser, 1 kPa for absorber and evaporator. Under these low pressures, a saturation temperature can dramatically change due to a small pressure difference. An example is given in Figure 3.3.

As is natural, the influence of pressure on saturation temperature is stronger at low pressure. At around 1kPa, saturation temperature increases by 10 K for 1 kPa increase in pressure. This means a flooded component, where an accumulated liquid exerts hydraulic pressure on transfer surface, is not an option. Pressure drop in vapor flow should be minimized from the same reason. Because the huge specific volume of vapor makes the flow difficult to handle with minimum pressure drop, long and narrow passages for vapor should be absolutely avoided.

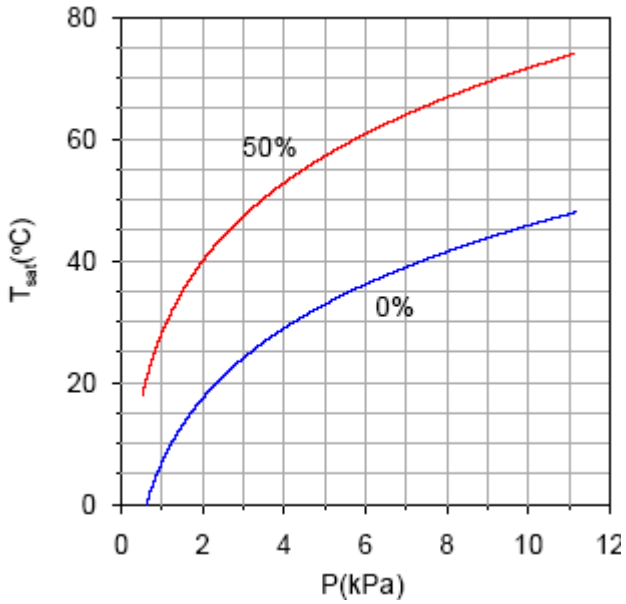

Figure 3.3 Saturation temperature vs. pressure at different solution concentrations for LiBr/Water

Since the system works in vacuum environment, the existence of inert gas inside the system significantly deteriorates the system performance. The inert gas acts as a barrier for mass transfer between transfer surfaces. The major source of inert gas is the corrosion of construction materials. It is especially serious when there are mechanical or welded joints of different metals immersed in high-temperature solutions. They become galvanic cells that produce hydrogen. Although the maximum temperature of the proposed cycle is relatively low, enough care should be given to selection of construction materials and manufacturing methods. In this study, aluminum and stainless steel were chosen for all transfer surfaces and tanks because of their low corrosion rates in H_2O/LiBr environment.

The set-up has to be small and compact because the system is intended to be used in a vehicle, but, compactness does not necessarily mean large pressure drops. Components should be arranged in such a way as one can easily access any component whenever it is necessary. Since all components should be developed simultaneously, it is decided that all components should be easily separable so that they can be replaced or modified with the minimum of time and effort.

3.2.1 Experimental Set-up Description

Figure 3.4 shows the layout of experimental set-up. It was designed for continuous operation; the mixing tank receives concentrated solution and refrigerant vapor. The resultant dilute solution is pumped upward to plate heat exchanger by gear pump, and then flows to generator where it is again separated into concentrated solution and water vapor. This vapor is led to air-cooled condenser where it loses its latent heat to cooling air. The vapor changes back to liquid state and collects in condense tank. The condensed liquid drops through an electronic expansion valve into the evaporator below. While concentrated solution returns straight to the mixing tank from generator, it passes across the plate type heat exchanger where it gets the desired degree of sub-cooling before entering once again the mixing tank.

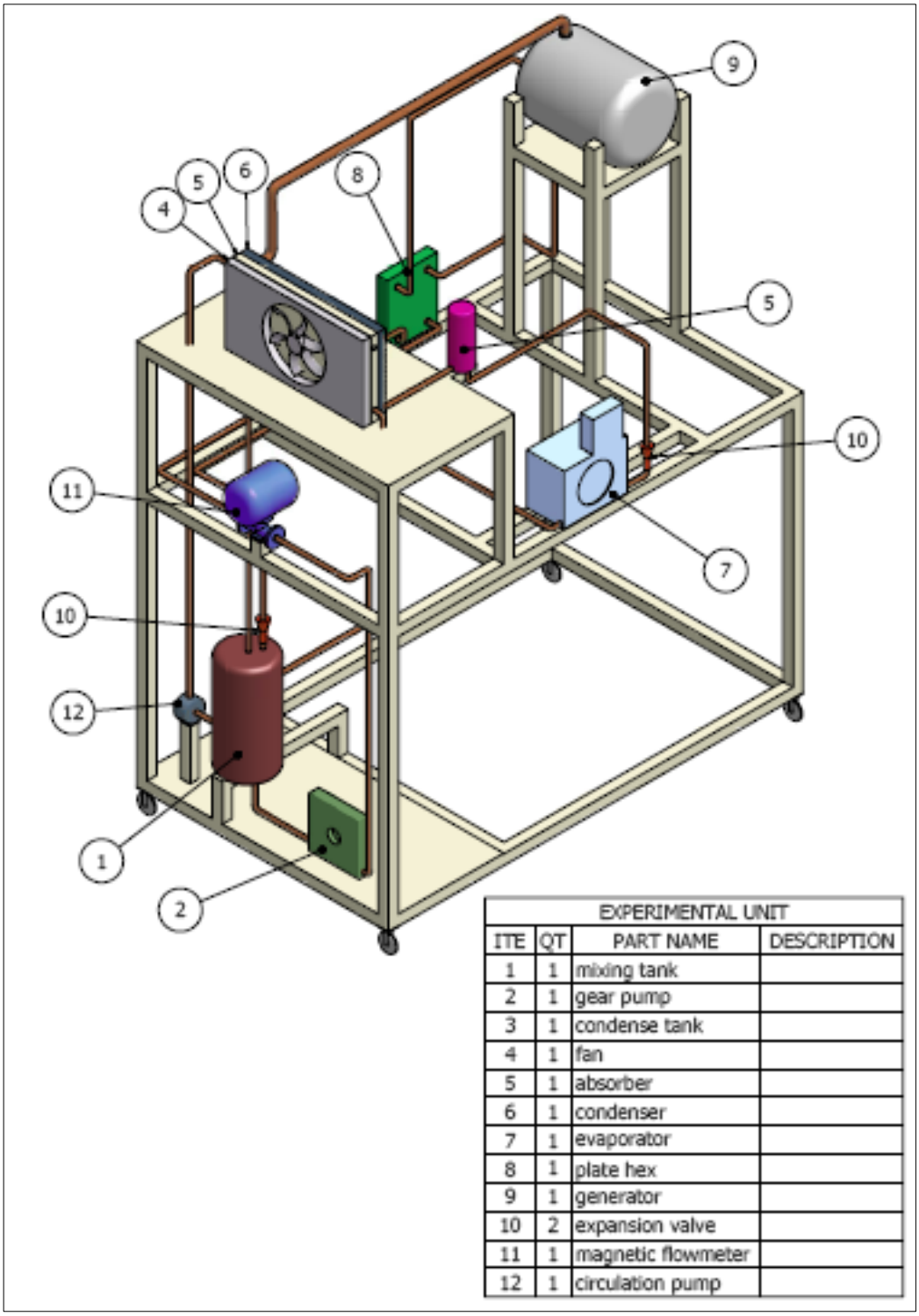

EXPERIMENTAL UNIT			
ITE	QT	PART NAME	DESCRIPTION
1	1	mixing tank	
2	1	gear pump	
3	1	condense tank	
4	1	fan	
5	1	absorber	
6	1	condenser	
7	1	evaporator	
8	1	plate hex	
9	1	generator	
10	2	expansion valve	
11	1	magnetic flowmeter	
12	1	circulation pump	

Figure 3.4 Schematic layout of experimental set-up

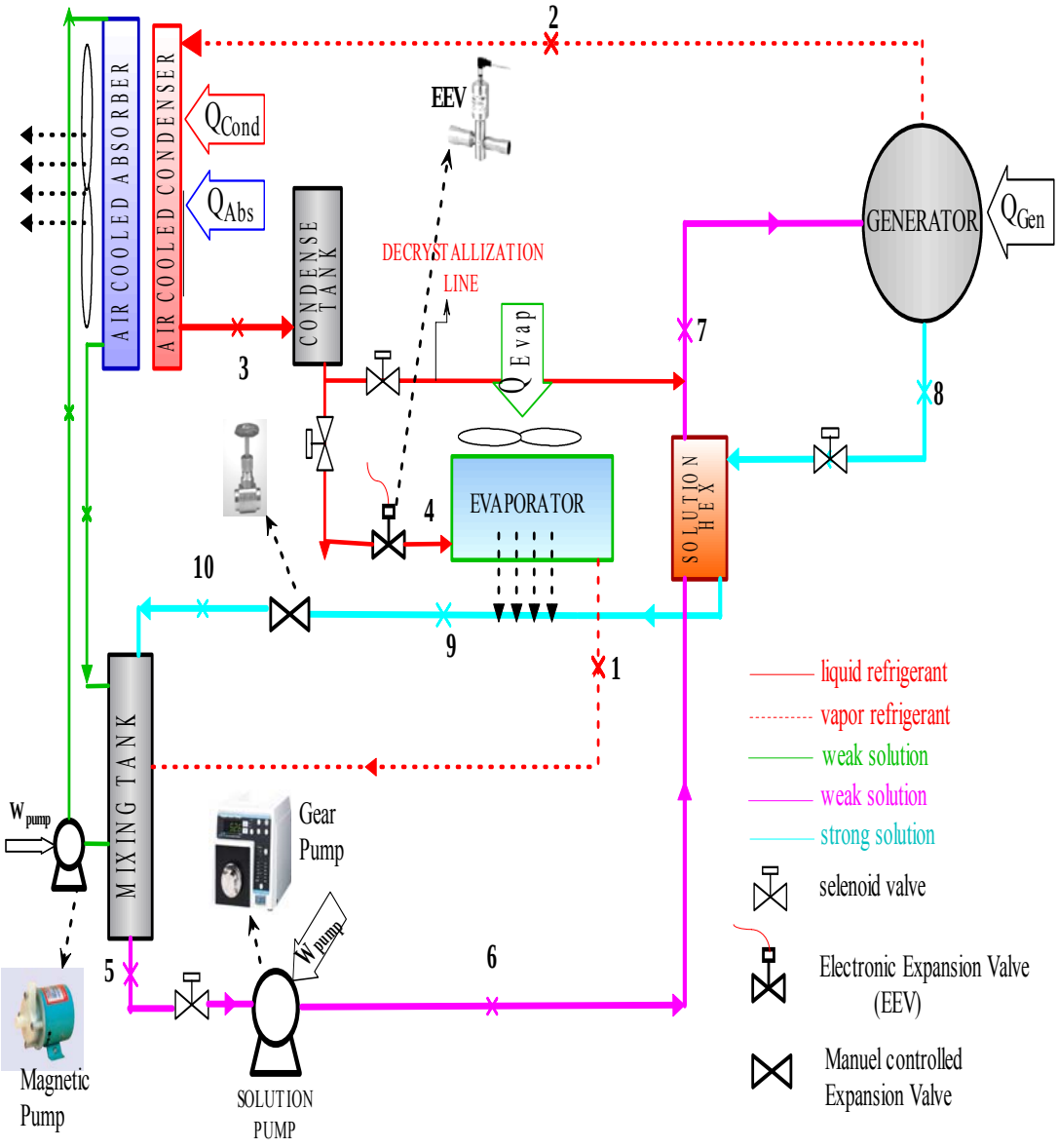

Figure 3.5 Detailed flow diagram of set-up

The generator is a shell-and-tube type heat exchanger and all the other components are air-cooled finned pipe type except the solution-heat exchanger. This set-up has a heat transfer loop with a circulation pump between mixing tank and air-cooled absorber. The heat of absorption in mixing tank should be transferred to surrounding so that the absorber pressure is as low as possible. If the absorber temperature increases, the absorber pressure increases. Consequently, the evaporation temperature increases. The heat should be transferred directly through the fan of air-cooled absorber. So, air-cooled absorber should play the roles of

partitioning and transferring heat at the same time. This idea is shown in Figure 3.5 [45-51].

The process of construction of the absorption refrigeration system has been detailed below according to the parts of the set-up. The required sizes for all components are calculated in terms of heat transfer correlations. Heat transfer correlations used are given in Appendix 2.

- **Construction of the generator**

At the beginning of the study, the generator was designed as a simple tank, which is heated by an electrical heater. At the second design, it will be constructed as shell and tube heat exchanger driven by exhaust gas. As seen in Figure 3.6 and Figure 3.7, generator was built from stainless steel sheet.

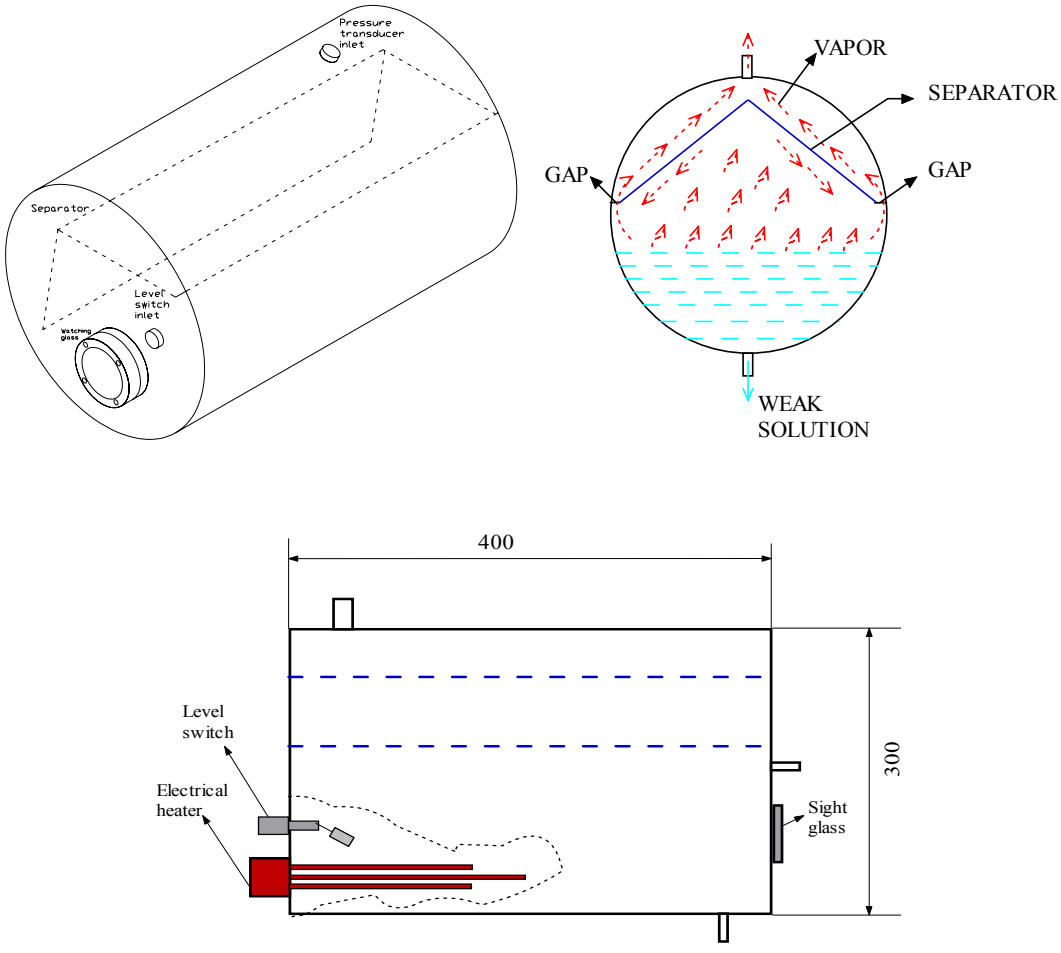

Figure 3.6 Simple generator drawings

The generator consists of a small watching window, level switch with electrical output and electrical heater (4 kW) controlled by control unit. The separator was welded to generator's inner surface. Separator restricts LiBr contaminants in refrigerant vapor, while the refrigerant vapor passes through out an upper exhaust pipe. The tank had a maximum capacity of 28 l.

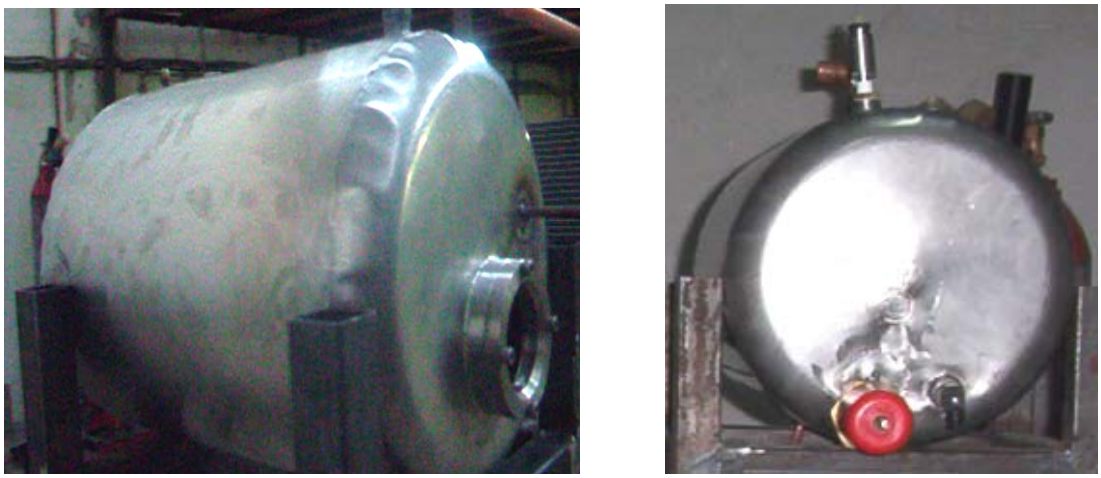

Figure 3.7 Photographs of specially constructed generator

- **Construction of the air-cooled absorber**

A typical radiator used in cars was used in the experimental set-up as air cooled absorber. The radiator's function is to get rid of the heat from the hot LiBr solution circulating in the system. The hot solution enters the left tank in the radiator, filters down through the core fins of the radiator and cools. The absorber consisted of aluminum tubes and aluminum fins. Size calculations were given in Appendix 2 [59-61]. As seen in Figures 3.8 and 3.9, the absorber is a finned exchanger with horizontal elliptical tubes, a frontal area of 396×600 mm and a thickness of 36 mm. This unit is placed next to the condenser.

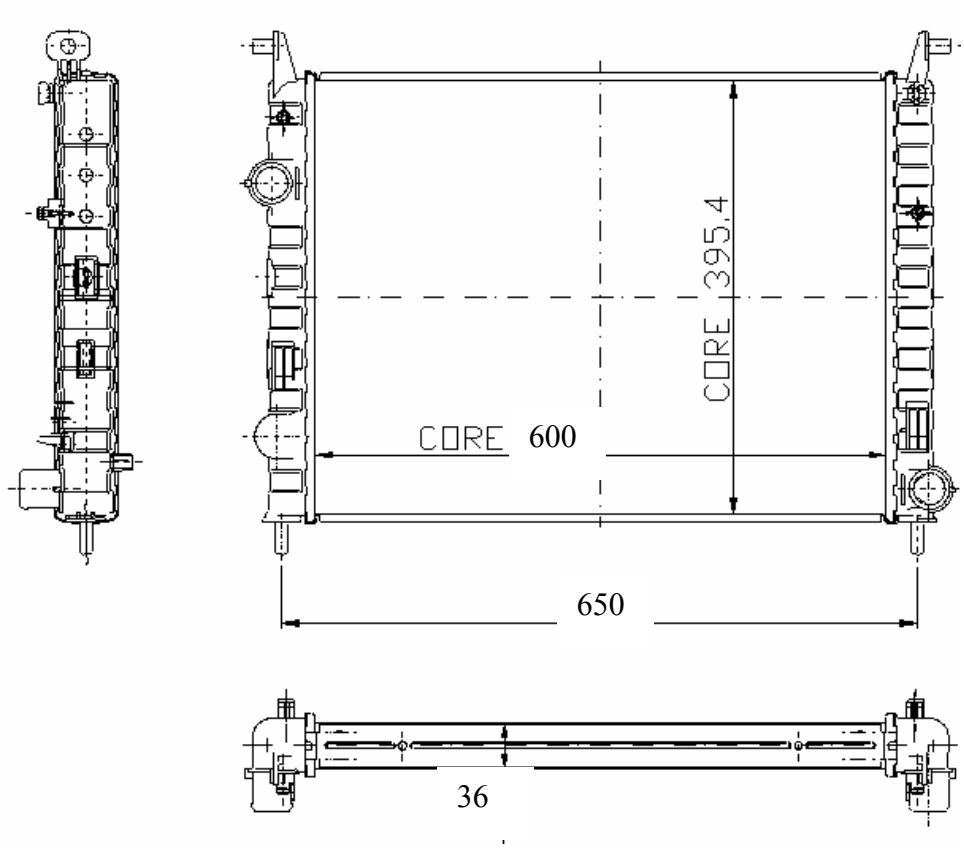

Figure 3.8 Air-cooled absorber drawing

Figure 3.9 Photograph of air-cooled absorber

- **Construction of the air-cooled condenser**

A typical condenser used in the air-conditioning system of cars was used in the experimental set-up as air cooled condenser. Size calculations were given in Appendix 2. The condenser is also a finned exchanger, consisting of horizontal elliptical tubes. The condenser consisted of aluminum tubes and aluminum fins. As seen in Figures 3.10 and 3.11, the frontal area is 468×352 mm and the thickness is 17 mm. It was placed on the front side of the absorber.

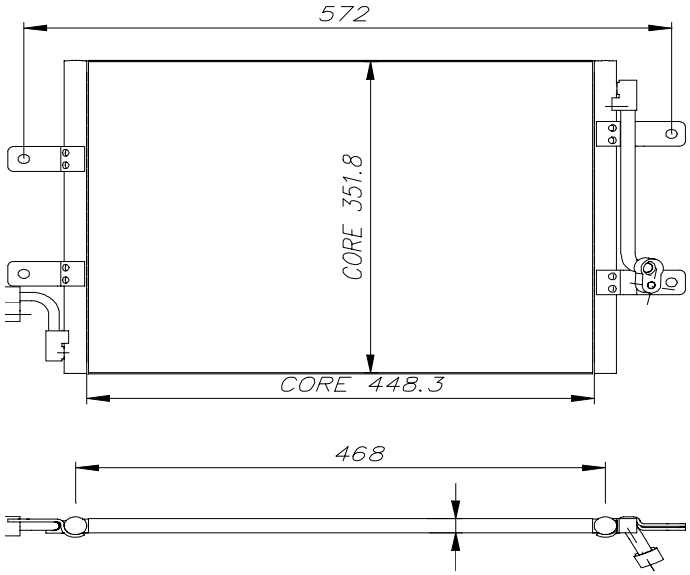

Figure 3.10 Drawing of air-cooled condenser

Figure 3.11 Photograph of air-cooled condenser

5.3.1 Construction of the evaporator

A typical evaporator used in the air-conditioning system of cars was used in the experimental set-up as evaporator. Size calculations were reported in Appendix 2. The evaporator is also a finned exchanger, consisting of horizontal elliptical tubes. As seen in Figures 3.12 and 3.13, the evaporator consisted of aluminum tubes and aluminum fins. The frontal area is 235×170 mm and the thickness is 65 mm. It was placed in specially constructed insulated metal housing that is below the condense tank.

Figure 3.12 Photograph of evaporator

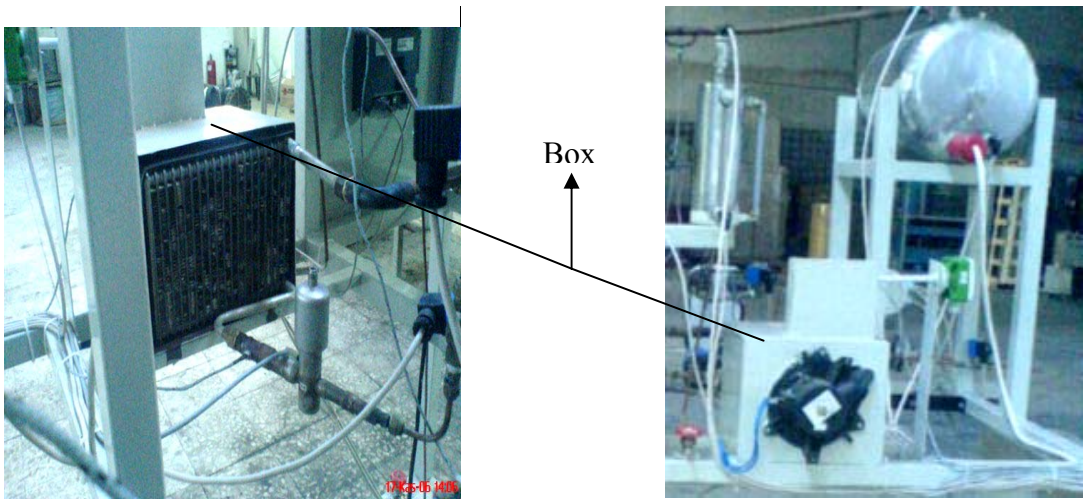

Figure 3.13 Special constructed insulated metallic housing for evaporator

- **Selection of commercial solution heat exchanger**

As seen in Figure 3.14, brazed plate heat exchanger was used as solution heat exchanger. Compact gasket-free brazed plate heat exchanger consists of corrugated pressed stainless steel plates, which are brazed together with copper in a special vacuum process. The heat exchanger will be employed to transfer heat between the strong solution entering and weak solution leaves generator. Size calculations were done by manufacturer with respect to system's conditions. Specifications:

- Heat transfer area : 0.46 m^2
- Height, Width, Length : 278, 124, 21 mm
- Number of plates : 6

Figure 3.14 Photograph of plate type solution heat exchanger

- **Construction of the tanks**

The tanks were built from stainless steel. They consist of a glass liquid level indicators and electrical level switches. As seen in Figure 3.15 and 3.16, the mixing tank had a maximum capacity of 12 l and the condense tank had a maximum capacity of 1.5 l, respectively.

Figure 3.15 Specially constructed mixing tank

Figure 3.16 Specially constructed condense tank

- **Valves**

In the experimental set-up, an electronic expansion and a manuel controlled expansion valves were used to reduce the pressure. As shown Figure 3.17, the gate type electronic valve is specifically designed for linear flow characteristics in order to provide a wide range of capacity with a linear relation between flow and positioning of the valve (capacity vs. number of steps). Manuel expansion valve was used as a restriction valve between solution heat exchanger and mixing tank. As seen in Figure 3.18, it was built from fully copper materials.

Figure 3.17 Electronic expansion valve

Figure 3.18 Manuel expansion valve

- **Circulation Pumps**

As seen in Figure 3.19, a small gear pump and a centrifugal pump which are controlled by electronic pump drives were used as circulation pump. The console drive controls the speed of gear pump heads to provide flow rates from 1 to 8210 ml/min. The console drive controls the speed of centrifugal pump heads to provide flow rates from 1 to 4010 ml/min.

Figure 3.19 Circulation pumps

- Cupper nickels tubes of 1/4” of outer diameter were used in experimental setup
- Ball valves for isolating the circuit parts were used in experimental set-up

3.2.2 Measurement Methods and Instrumentation Used in the Set-Up

As shown in Figure 3.20, instrumentation of the experimental set-up is composed of J type thermocouples, electromagnetic flowmeters, turbine type flowmeter, a hot wire anemometer and pressure transducers.

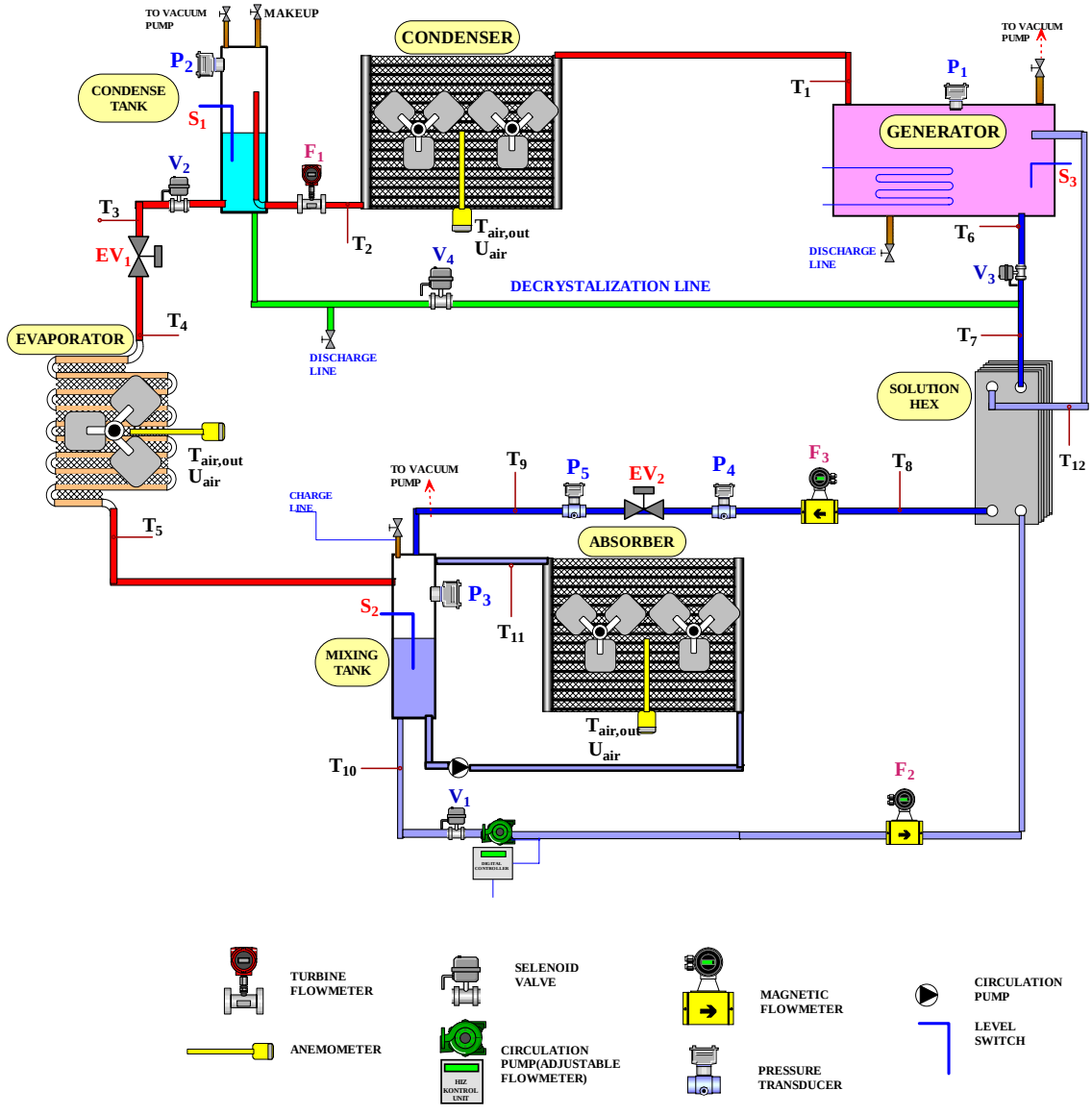

Figure 3.20 Schematic diagram for instrumentation of the experimental set-up

- As seen in Figure 3.21, two electromagnetic flowmeters were mounted at two points in the experimental set-up for flow rate measurement of the concentrated solution. Accuracy: ±0.15% of rate

- As seen in Figure 3.22, turbine type flowmeter was mounted at condense tank exit for measurement of liquid refrigerant flow rate. Accuracy: ±3% of full scale including linearity.

- As seen in Figure 3.23, the transducers were mounted at five points in experimental set-up. As seen figure 3.24, the transducer is a resistive type absolute pressure transducer. Accuracy: ±0.4% of full scale.

- Two L-shaped copper pitot tubes of 2.2 mm outer diameter and 1.1 mm inner diameter together with a wall static pressure tappings drilled on the pipes wall at the line of the tip of pitot tubes were used to measure the average velocity at the reference station on the exhaust pipe lines of condenser-absorber and evaporator. The reference station of condenser-absorber was placed at the section that had the distance of 110 cm from the outlet of the fan. The reference station of evaporator was placed at the section that had the distance of 260 cm from the outlet of the fan. The pitot tubes were traversed across the pipe cross-section with an accuracy of 0.025 mm by means of the traverse mechanisms that had capable of traverse in the radial direction of the pipes. The static pressures on the walls of the pipes were measured by using the wall static pressure tapings. Only one tapping was used to measure the static pressure at the reference station in order to regulate the mass flow rate in the set-up, because of the static pressure distribution across the pipe was constant.

- As seen figure 3.24, immersion J type thermocouples with bayonet fittings were mounted at 14 points in the experimental set-up for temperature measurement.

Figure 3.21 Electromagnetic flowmeter

Figure 3.22 Turbine type flowmeter

Figure 3.23 Pressure transducer

Figure 3.24 Thermocouple with Immersion bayonet

3.2.3 Control and Monitoring of the Absorption Refrigeration System

As seen Figure 3.25, the controller is an intelligent digital controller for refrigeration system control functions and management. The controller operates on a network, allowing connectivity with other devices and systems which comply with the programme developed by OLIMPIYAT Inc.

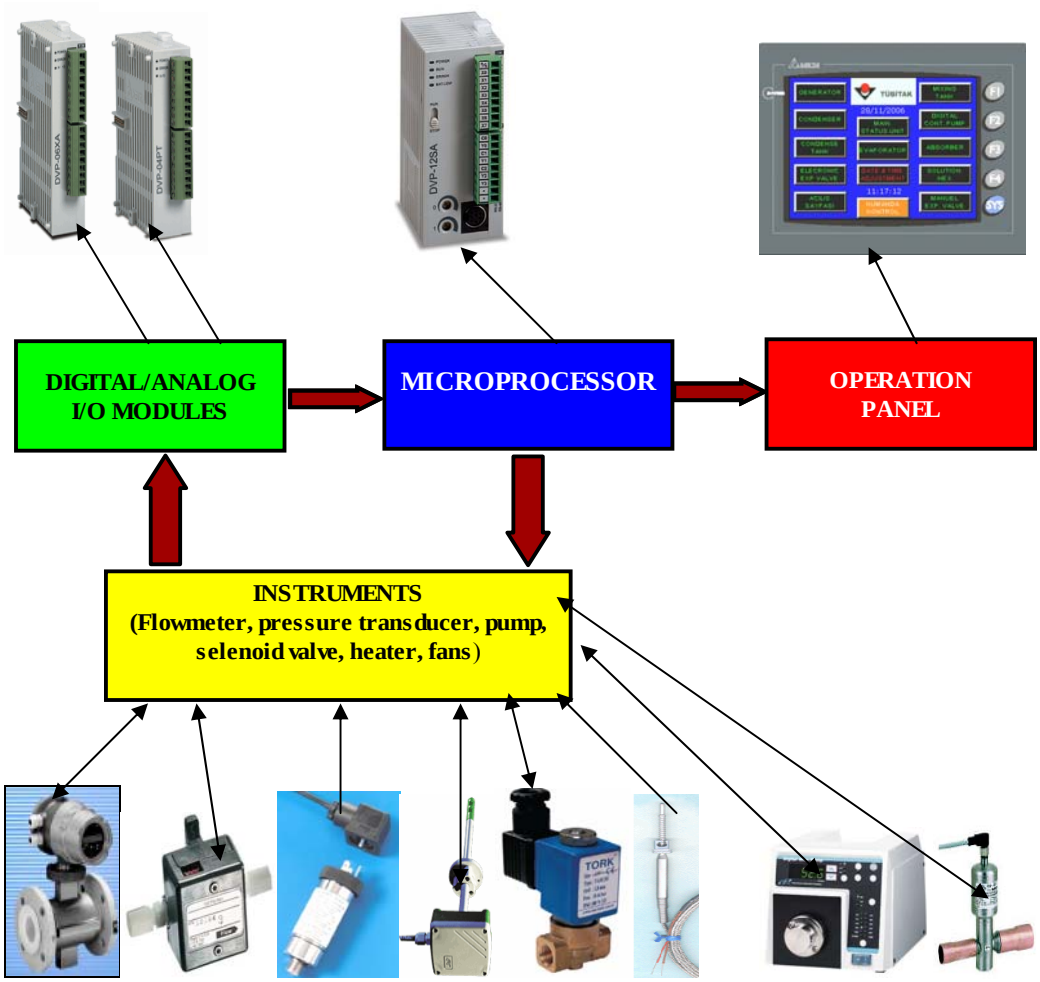

Figure 3.25 Block diagram of the control system

As seen Figure 3.26, the operation panel allows monitoring of data, access to reports via the touch sensitive screen and color LCD display. The touch-screen operation panel is easily used by operators. All actions like manual control parameters, contact timing limits and definable temperature limits are menu driven. Operators can rapidly configure certain functions. Screen displays allow the operator to determine optimum running states correctly. The required configurations are done by panel's compiler. The details of parts of control unit were given in Appendix 4.

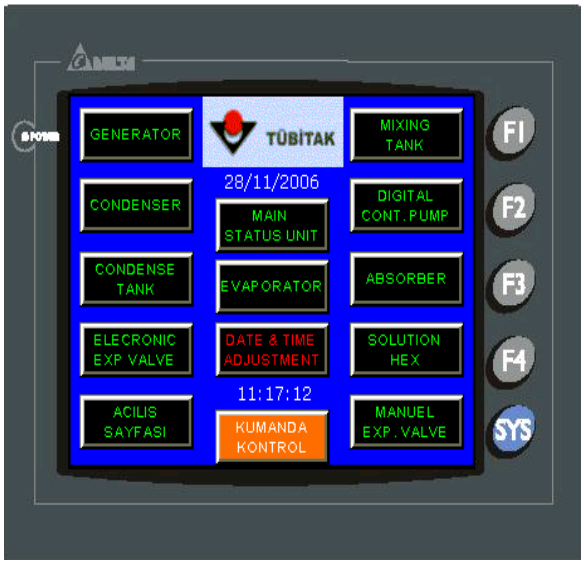

Figure 3.26 Operation panel

3.2.3.1 Control procedure of the set-up

The control of set-up was designed and programmed with respect to two alternative states. The first state is manual control. According to this state, the system's entire points can be controlled as manual. For example, the valves can be open, turn on or off pumps and heater and fan, EEV can be adjusted to set pressure drop. The second sate is automatic control. In this state, the system runs automatic with respect to default parameter.

Start-up and Shutdown

- When the level switch 1 is on, open the valve 1 and turn on the gear pump.
- When the level switch 2 is on, wait for some time (10-20 seconds) and turn on the heater and open the valve 3 and turn on the centrifugal pump and condenser's fan
- When the T_6 reaches to set value, turn off the heater
- When the P_2 reaches to set value and level switch is on, wait for some time (10-20 second) and open valve 2.
- If the T_6 less then set value, close valve 2 and open valve 4

- When the system is stop, turn off heater and gear pump, close valve 2, open valve 3 and valve 4. Wait for some time(30-40 second)

Solution flow rates to the generator and absorbers are most important parameters in determining the capacity and COP of the set-up., those flow rates would have been controllable parameters for our designed system. Once a certain amount of solution was charged into the set-up, the flow rate from the generator is determined by the sum of the pressure differentials and the hydraulic head between generator and mixing tank. For the control of the flow rate from the generator, electric valves may be used. For example, wide range of solenoid-driven metering valves is available in the market. But we used manual controlled globe vane. For the control of the flow rate from the mixing tank to generator, a small gear pump which is controlled by electronic pump drives was used as circulation pump. The console drive controls the speed of gear pump heads to provide flow rates from 1 to 4210 ml/min.

3.2.3.2 Prevention of crystallization

Crystallization ordinarily commences when the solution temperature falls below the normal crystallization temperature for a particular salt concentration. This can occur unless special precautions are taken when the system is shutdown. Even though the operating points of the system are far from the crystallization limit of LiBr, monitoring of the working condition is necessary for the potential risk. Since crystallization limit is defined by the concentration and temperature of a solution, a control system should constantly monitor both parameters and give warning or take necessary measures. But because a measuring device of concentration or density is not cheap, the system's working condition was set to over crystallization limit curve. In the present work, as shown Figures 3.20 and 3.27, decrystallization line was added on the return line from generator. Therefore, crystallization problem can be avoided by diluting the solution throughout the system prior to shutdown.

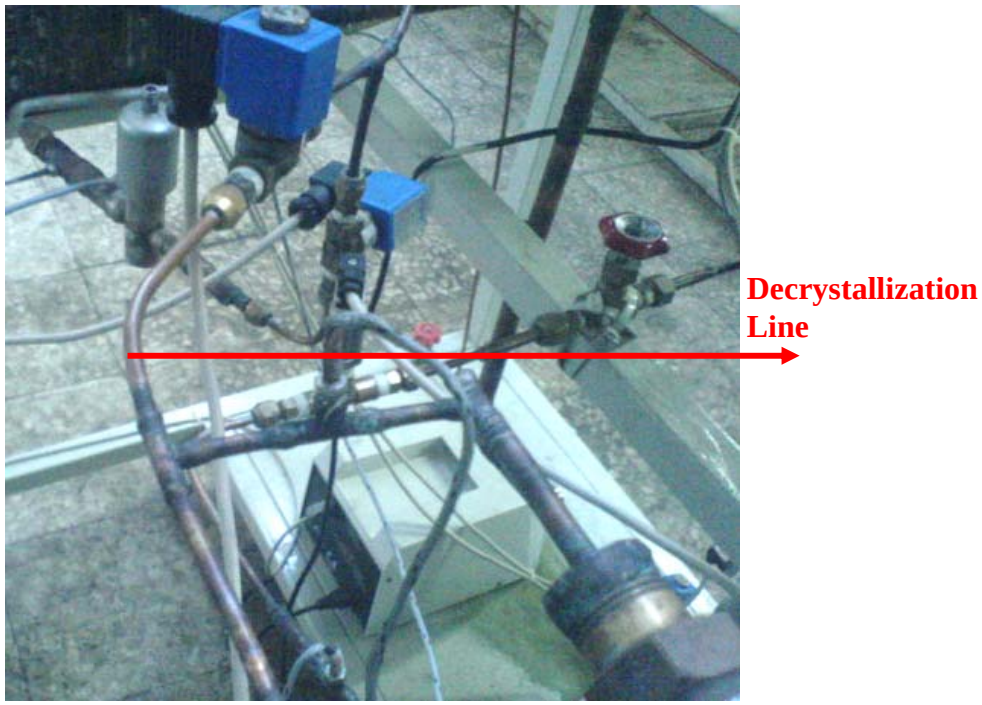

Figure 3.27 Decrystallization line

3.3 INTERNAL COMBUSTION ENGINE'S SET-UP

The experimental internal combustion engine test rig, which is illustrated in Figure 3.28, consists of three main components which are the internal combustion engine, a hydraulic dynamometer and dynamometer control unit. The complete system was shown in Figure 3.29 [57-58].

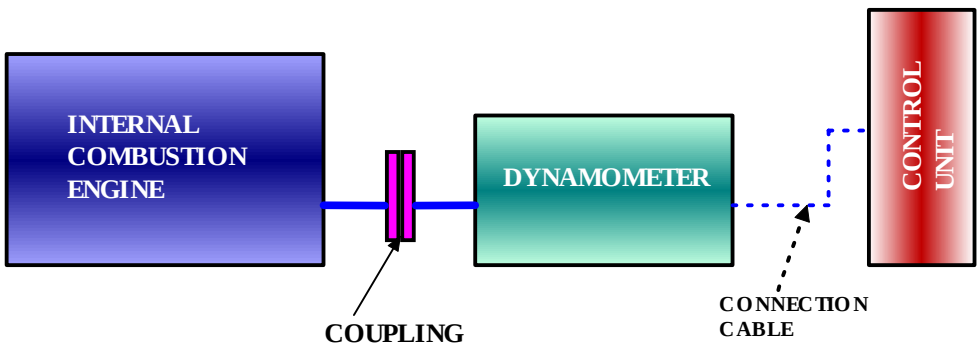

Figure 3.28 Illustration of the experimental internal combustion engine test rig

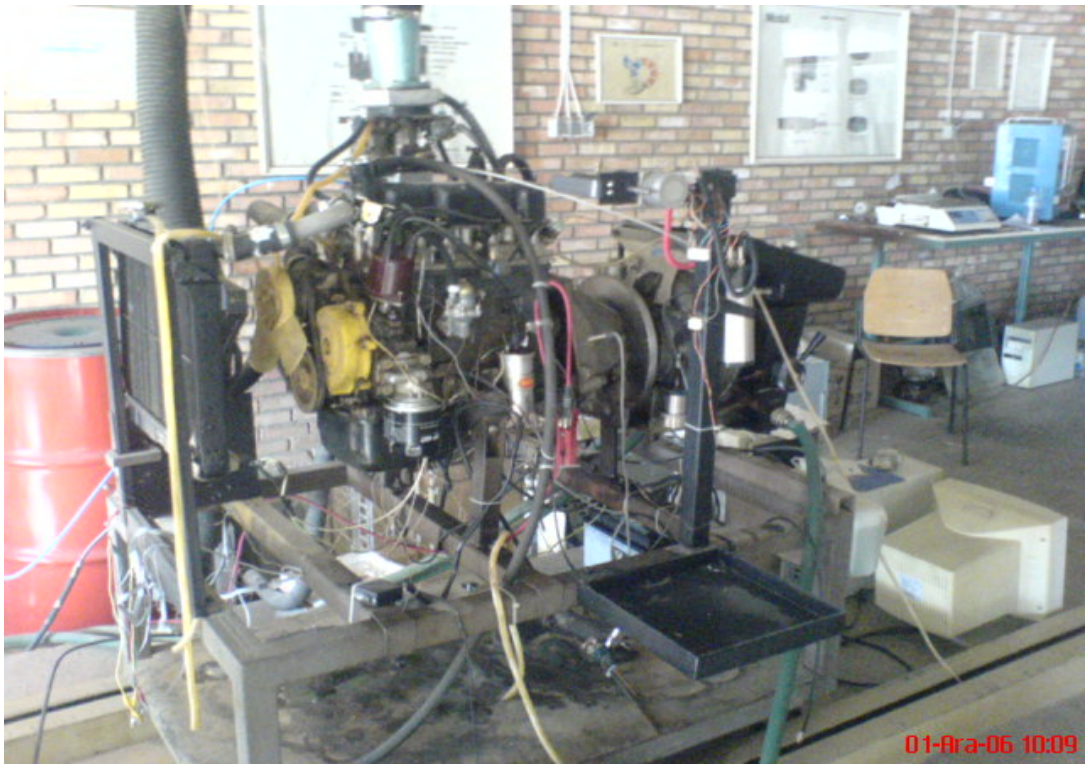

Figure 3.29 Complete test rig

The engine chosen as a test engine for the refrigeration system was a spark ignition engine as shown in Figure 3.29. It has an overhead valve design and is water cooled. Details of measurement devices of engine were given in Appendix 2. The specifications of the engine were listed in Table 3.1.

Table 3.1: Test engine specifications

Engine Type	**4 cycle, spark ignition**
No. of Cylinders	4
Bore (mm)	76
Stroke (mm)	71.5
Swept Volume (cm^3)	1297
Compression Ratio	7.8
Firing Order	1,3,4,2
Rated Power	49 kW@5200 rpm
Maximum Torque	102 Nm@3000 rpm
Coolant	Water

The test engine was loaded with the help of dynamometer. The dynamometer is a hydraulic brake retarder. The rotating torque of the engine is converted to a stationary torque that will be measured. The turbulent action of the water absorbs the power of the engine. The load is controlled by the water inlet. The power is converted into heat which is carried away by the continually flowing water.

3.4 THE INTEGRATION OF THE AIR-COOLED ABSORPTION SYSTEM IN INTERNAL COMBUSTION ENGINE

The aim of this study is to investigate the utilization of exhaust gases from an internal combustion engine to drive an air-cooled absorption system for refrigeration purposes. The experimental air-cooled absorption system used was a unique unit designed to be driven by electrical heater. To integrate air-cooled absorption system to engine, two generator models that we designed and constructed were coupled to the internal combustion engine.

3.4.1 Generator Models

The generator must be designed with proper geometrical and functional characteristics. In fact, the most important problem is related to poor space availability and to the shape constraints. Another problem is related to total weight and cost. As a consequence, the generators modeled in this study consist of two different shell-and-tube heat exchangers. The objective of the study is the examination of the thermodynamic performance of this component of absorption cycle. Details of the proposed heat exchangers are shown in Figures 3.30 and 3.31.

Using the EES computer program, two generator models were designed. The calculations showed that the designed heat exchangers could be utilized to run the system using the exhaust gases from the existing internal combustion engine. According to the calculation results, two models were constructed. All calculations are given in Appendix 2.

As shown in Figure 3.30, the first design utilizes finned copper-nickel tube, with a low fin pitch to prevent deposit accumulation from the sooty exhaust gas. The tube is double wrapped inside a 155 mm shell Exhaust gas enters at the left (or right) and flows over the inside of the finned tube, while the solution flows outside the tube from top to bottom. The design details, given in Table 10.1, were obtained with the use of a design model constructed in EES. The model was run with a wide variety of standard tube-fin dimensions. The resulting design represents the best compromise between heat exchanger size, cost, and pressure losses.

As seen Figure 3.31, the second generator is a shell and tube-type helical-coil exchanger. To be able to transfer heat well, the tube material was selected copper-nickel. Because heat is transferred from a hot to a cold side through the tubes, there is a temperature difference through the width of the tubes. This exhaust gas heat exchanger is constructed with copper-nickel tubes, cast iron shell and cast iron end covers.

Table 3.2 Design details of exhaust heat exchangers

	1st Type Exhaust HEX	**2nd Type Exhaust HEX**
Outer shell diameter (mm)	155	155
Number of tubes	1	14
Total tube length(mm)	500	500
Height of HEX(mm)	550	700
Outer diameter, fin (mm)	100	-
Root diameter, tube (mm)	54	-
Tube wall thickness (mm)	4.5	3
Fin pitch (fins/cm)	2	-
Material	copper-nickel tubes, copper-nickel fins, cast iron shell and cast iron end covers	copper-nickel tubes, cast iron shell and cast iron end covers

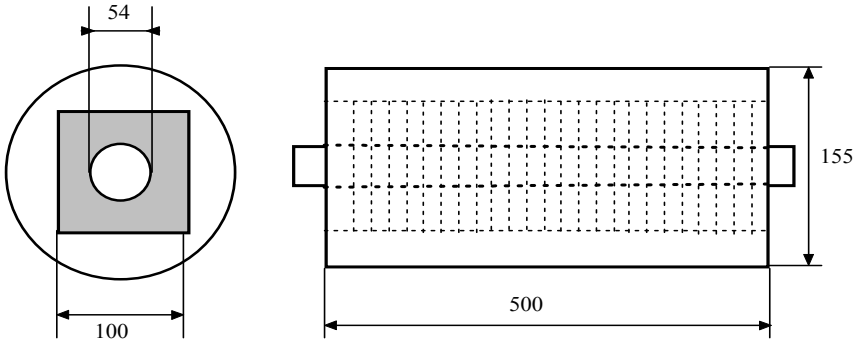

Figure 3.30 First type generator model

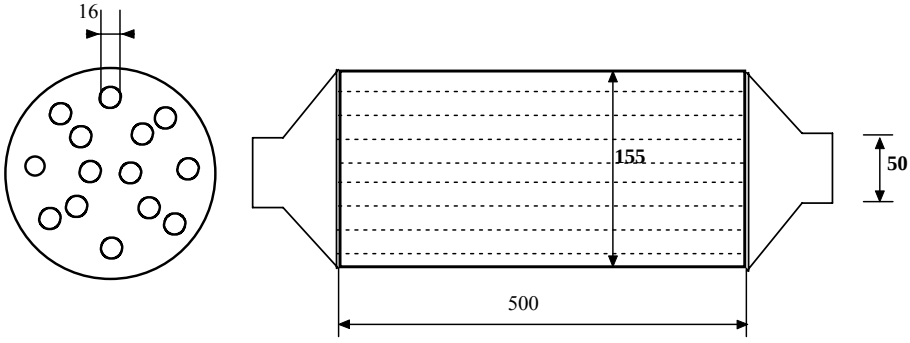

Figure 3.31 Second type generator model

3.4.2 Connection Of The Generator Models To The Internal Combustion Engine

The exhaust pipe line is illustrated in Figure 3.32. As figure 3.32 shows, thermocouple probes and pressure transducers were connected convenient points to determine pressure drops and the amount of heat transferred. The generator is placed to the engine exit and connected with flexible metal hose.

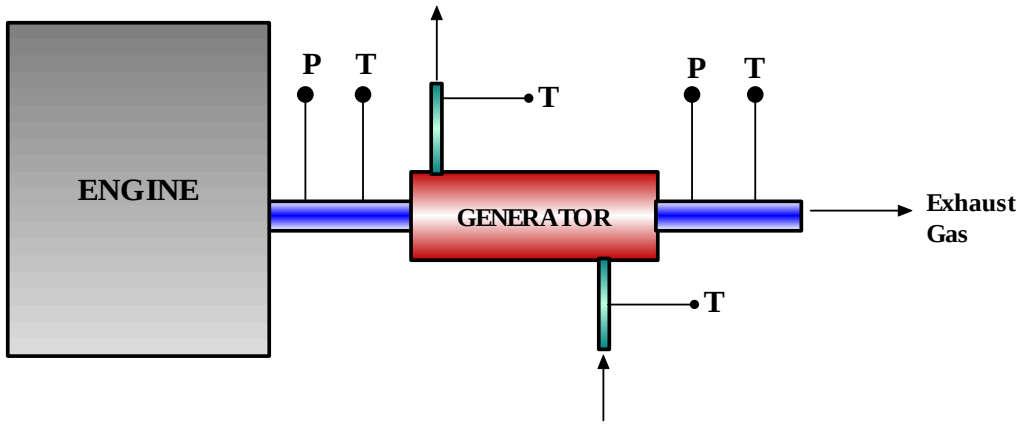

Figure 3.32 Exhaust pipe line

3.4.3 Test Procedure

The test procedures for generator: The engine was set to run under certain speed and torque. A variable speed-variable load test is performed on spark ignition engine. The aim of this analysis is to obtain the variation of basic engine characteristics during the loading of the engine by the dynamometer while the engine speed is changing with load. A constant speed-variable load test is performed on a spark ignition engine. The aim of this experiment is to observe the variation of basic engine characteristics during the gradual loading of the engine by the dynamometer while the engine speed is kept as constant. For steady state condition, the engine was run for at least five minutes. After steady conditions were confirmed, all the experimental data were recorded.

3.5 UNCERTAINTY ANALYSIS OF MEASUREMENT SYSTEM

All instruments and measurements have certain general characteristics. An understanding of these common qualities is the first step towards accurate measurements. Errors and uncertainties are inherent in both the instrument and the process of making the measurement. Final accuracy depends on a sound program and on correct methods for taking readings on proper instruments. Errors and uncertainties in the experiments can arise from instrument selection, instrument condition, instrument calibration, environment, observation, and reading [54].

The R is to be a result estimating data as a function of primary measured variables as the independent variables, x_1, x_2, …x_n . Thus,

$$R=f(x_i),\ i=1, 2,\ldots n \tag{3.42}$$

Let w_r be the uncertainty in the result and w_i be the uncertainties in the independent variables, and the uncertainty of desired result may be estimated by

$$w_R = \left[\sum_{i=1}^{n} \left(w_{x_i} \frac{\partial R}{\partial x_i} \right)^2 \right]^{1/2} \tag{3.43}$$

$$W_R = \left[\left(\frac{\partial R}{\partial x_1} w_1 \right)^2 + \left(\frac{\partial R}{\partial x_2} w_2 \right)^2 + \ldots\ldots\ldots + \left(\frac{\partial R}{\partial x_n} w_n \right)^2 \right]^{1/2} \tag{3.44}$$

Table 3.3 shows instrumentation with the associated error for each sensor. It should be noted that all data collected by the data acquisition systems used in this experimental study was subjected to small errors. These error were in order of 0.02% for 12 bit system and 0.001% for 16 bit system and were considered negligibly small when compared to the other sources of error

Air flow velocities are calculated by using the pressure values measured by the manometers and their uncertainty are estimated as,

$$P_T - P_S = P_{dyn} = \frac{\rho}{2} U^2 \tag{3.45}$$

$$U^2 = 2g \frac{\rho_{al}}{\rho} \frac{h}{1000.C} \tag{3.46}$$

$$\dot{m} = \rho A U \tag{3.47}$$

The partial derivatives of each independent measurement in the parameters were calculated using the uncertainty propagation function in the *Engineering Equation Solver* and applied within the program to the root mean square outcome. So, the uncertainty of the air mass flow rates is estimated as ±1.2%.

Engine torque was measured with a dynamometer. Water brake dynamometer was used to measure engine torque at different speeds; by changing the water level in the dynamometer. Inlet air flow rate was determined by measuring the pressure drop across a calibrated venture nozzle attached to a large surge tank. Fuel flow rate measurement has the potential to be substantial source of error.

In our case W_R is the COP and variables w_{xi} are $\dot{m}_{evap}$, $\dot{m}_{Gen}$, ΔT_{evap}, ΔT_{Gen}.

$$COP = \frac{\dot{m}_{evap}.C_p.\Delta T_{evap}}{\dot{m}_{gen}.C_p.\Delta T_{gen}} \tag{3.48}$$

Consider $\Delta \dot{m}$ (the error obtained measuring each flow rate, respectively) equal to 0.01 $\dot{m}$ and ΔT (the error obtained measuring each temperature, respectively) equal to 0.002 T, we can value ΔCOP equal to 0.05 (absolute error). The relative error on COP is equal to 9%.

Table 3.3 Instrumentation and sensor errors

Measurement	Sensor	Error
Strong solution flow rate	ABB magnetic flowmeter	±0.5% of rate
Weak solution flow rate	ABB magnetic flowmeter	±0.5% of rate
Liquid Refrigerant flow rate	Flosensor turbine flowmeter	±3% of full scale
Inlet-outlet temperatures	J type thermocouple	±0.6° C or ±0.075% (0 to 750° C)
Air flow rate for condenser-absorber and evaporator	Pitot tube	±1,2%
Absorption system power consumption	KAAN electronic electricity meters	±1%
Pressure Measurement	Cole-parmer transducer	±0.4%
Air flow rate	İnclined manometer	±1%
Fuel flow rate	Scaled bottle	±1%
Torque	Bourdon type gage	±3%
Speed	Tachometer	±1 %
Pressure Measurement	Cole-parmer transducer	±0.4%
Load	Water brake dynamometer	±0.25%

CHAPTER 4

RESULTS AND DISCUSSION

4.1 THEORETICAL RESULTS

The output list of the computer program is presented in Tables 4.1-4.3. The cycle collects the free energy from the exhaust engine and the ambient air, and channels it through the condenser to the users. The condenser and evaporator loads are approximately 25% less than the corresponding generator and absorber loads. This difference is largely due to heat of mixing effects in the solution, which are not present in the pure fluid. It has been shown that higher efficiencies of the absorption system can be obtained at lower generator temperatures and small temperature difference between exhaust heat and solution in the generator. As a check, the sum of the heat input at the generator and at the evaporator is equal to the heat rejected at the condenser and at the absorber. This means the temperature drop at each of the expansion valves occurs because the vapour has a higher internal energy than the liquid. Thus, some energy must be extracted from the liquid to drive the phase change. The load in the condenser is slightly higher than that in the evaporator. This is primarily due to superheat the inlet vapour to the condenser. The pump work is quite small as compared to the heat transfer rates associated with the other components. Figure 4.1 shows the relationship of different generator temperatures versus COP and Q_{abs} for a given system. When the generator temperature changed from 70°C to 90°C and cooling air inlet temperature is fixed at 20°C, the COP value changed from 0.36 to 0.76 and Q_{abs} increased from 3.12 kW to 6.90 kW. The higher

waste energy inlet temperature had a better COP value. The evaluation of different evaporator temperatures for a given system is shown in Figure 4.2. The high COP values are obtained at high evaporator temperatures. Figure 4.3 shows the relationship of different absorber temperatures versus COP and Q_a for a given system. When the absorber temperature changed from 30°C to 40°C and generator temperature is fixed at 80°C, the COP value decreased from 0.80 to 0.55 and Q_a increased from 3.0 kW to 4.40 kW.

The exergy analysis emphasizes that both losses and irreversibility have an impact on system performance. In states 13, 15 and 17, the exergy flow from the ambient environment is equal to zero, because the temperature of the considered system is equal to the ambient temperature. In terms of availability, the principle of conservation does not exit. In this case, the inlet and outlet exergy do not match. The difference is the amount of availability consumed in the process. Table 4.3 ranks the order of the components of the system based on the significance of their contribution in the exergy losses. The generator has the highest exergy loss of 50%, basically due to the temperature difference between the generator and the exhaust gas. This can be reduced by increasing the surface area of the generator, consequently, increasing the cost of the generator. In order to improve the performance of the cycle, special attention must be made to reduce the irreversibilities that exist in this component in the overall design. Due to the temperature difference between the absorber and the surrounding, the next largest exergy loss occurred in the absorber. This can be reduced by increasing the surface area of the absorber; consequently, increasing the cost of the absorber. The exergy loss in the evaporator results mainly from the temperature difference between the environment and the evaporating refrigerant. The individual irreversibility values must be non-negative, as is shown Table 4.1.

Table 4.1 State points for the single effect air-cooled LiBr absorption system at design condition

State point	P (kPa)	T (^{o}C)	X (%)	$\dot{m}$ (kg/s)	h (kJ/kg)	S (kJ/kg.K)	Ψ (kJ/kg)
1	1.00	7	0.0	0.001056	2513.0	8.97	1254
2	5.63	85	0.0	0.001056	2659.0	8.64	1499
3	5.63	35	0.0	0.001056	146.60	0.50	1370
4	1.00	7	0.0	0.001056	146.60	0.50	1370
5	1.00	37	55.6	0.008970	89.450	0.26	1384
6	5.63	37	55.6	0.008970	89.450	0.26	1384
7	5.63	59.2	55.6	0.008970	135.00	0.40	1389
8	5.63	85	63.0	0.007914	215.90	0.50	1441
9	5.63	57	63.0	0.007914	164.30	0.38	1424
10	1.00	57	63.0	0.007914	164.30	0.38	1424
11	101.2	500	-	0.042000	594.80	0.99	1675
12	101.2	300	-	0.042000	515.70	1.10	1565
13	101.2	22	-	1.566000	295.50	5.69	0.01
14	101.2	24	-	1.566000	297.60	5.69	0.03
15	101.2	20	-	1.318000	293.50	5.68	0.00
16	101.2	22	-	1.318000	295.50	5.69	0.01
17	101.2	20	-	0.276000	293.50	5.68	0.00
18	101.2	11	-	0.276000	284.50	5.65	0.14

Table 4.2 Heat duty and UA of each component at design condition

COMPONENT	HEAT DUTY (Kw)	UA (kW/K)	LMTD (K)
Generator	3.31	0.011	304.10
Absorber	3.16	0.14	22.83
Evaporator	2.50	0.33	7.64
Condenser	2.65	0.19	13.98
Solution HEX	0.41	0.41	22.78
COP=0.75			

Table 4.3 Exergy difference for the single effect air-cooled LiBr absorption system at design condition

COMPONENT	EXERGY (kW)		EXERGY DIFFERENCE (Δψ)	CONTRUBITION (%)
	Input	Output		
Generator	12.98	12.46	0.5242	49.65
Absorber	12.59	12.42	0.1762	16.69
Evaporator	1.447	1.325	0.1221	11.56
Condenser	1.583	1.447	0.1362	12.90
Solution HEX	23.82	23.73	0.08975	8.5
Exp. Valve I	1.447	1.447	0	0.0
Exp. Valve II	11.27	11.27	0	0.0
Solution pump	1384	1383.99	0.0074	0.7
Entire System	1449.14	1448.1	1.0556	100

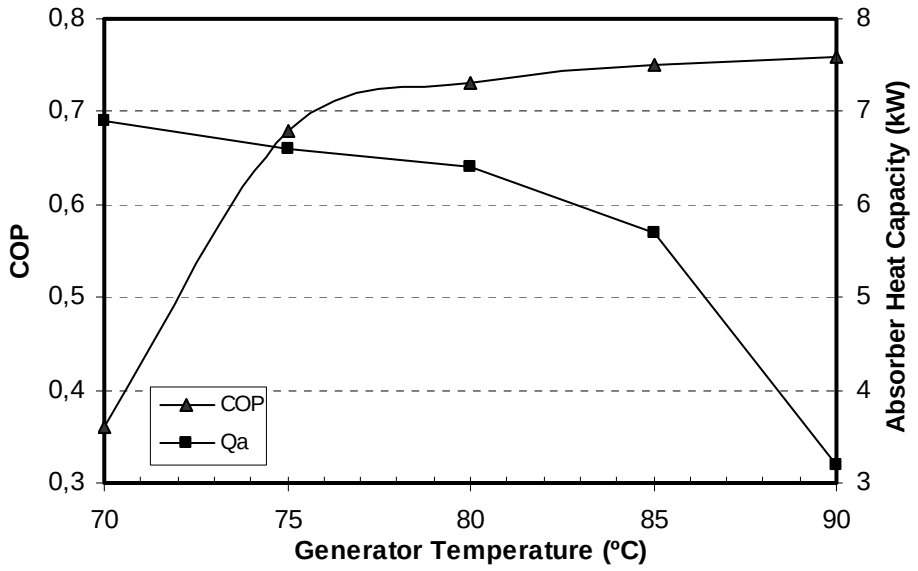

Figure 4.1 Relationship of different generator temperatures versus COP and Q_a for a given system.

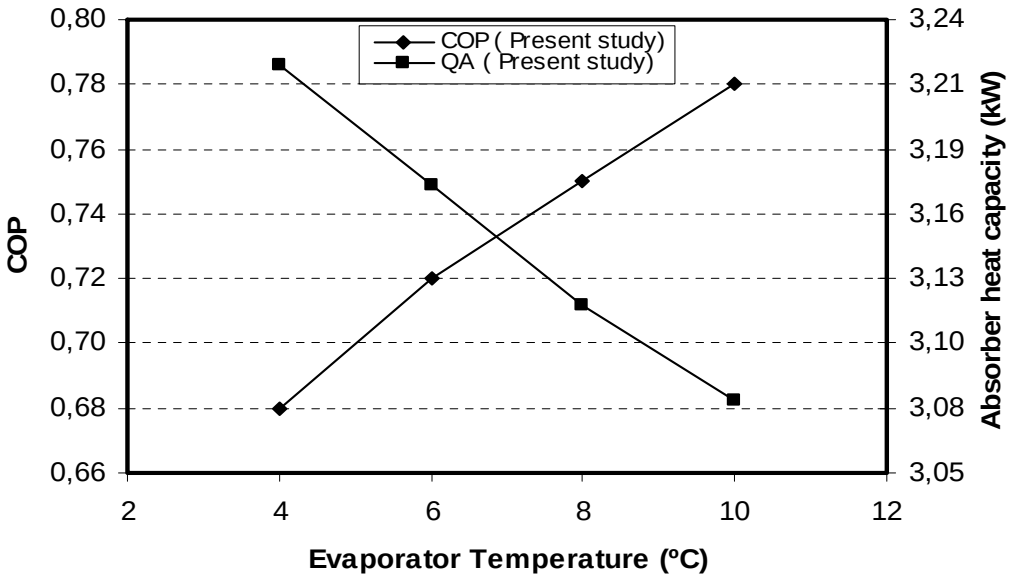

Figure 4.2 Relationship of different evaporator temperatures versus COP and Q_a for a given system

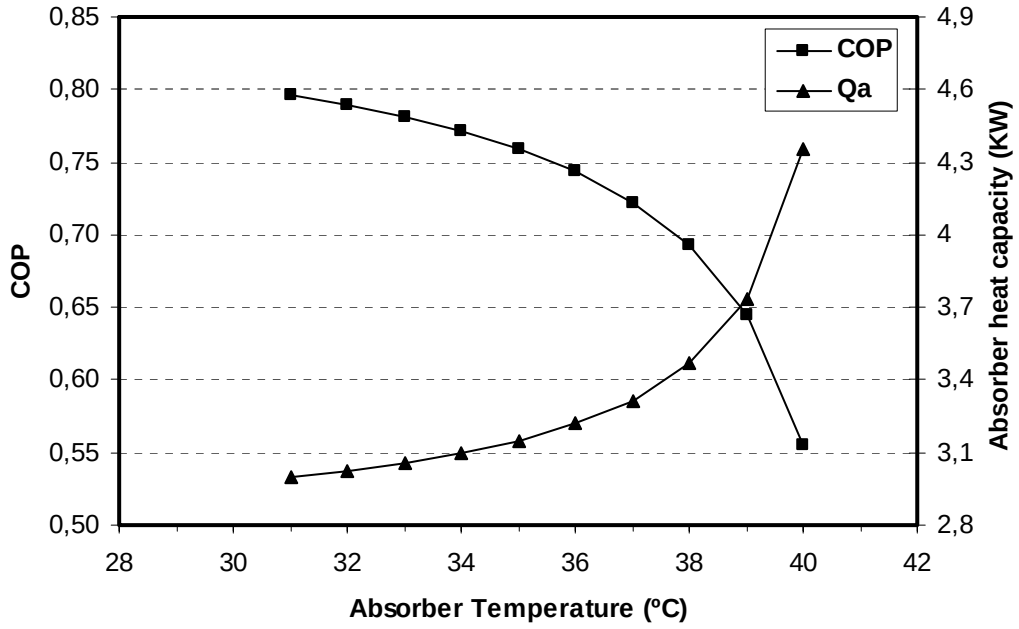

Figure 4.3 Relationship of different absorber temperatures versus COP and Q_a for a given system

In order to validate the present model, the simulation results have been compared with the available numerical data in the literature. The comparative variation of the COP value with generator temperature is given in Figure 4.4. In this simulation, the following values have been used: T_e=6 ^oC, T_c= T_a= 25 ^oC. It can be seen that, as expected, the COP value increases with increasing generator temperature, and the result obtained from the present simulation are in good agreement with results of Kaynakli et al. [28]. Furthermore, at different operating conditions (T_e=6 ^oC, T_c= T_a= 40 ^oC), the variations of the COP values with condenser temperatures and the variations of the COP values with absorber temperatures are given Figure 4.5 and 4.6. The results obtained from the present model are also in good agreement with the results of Kaynakli et al. [28].

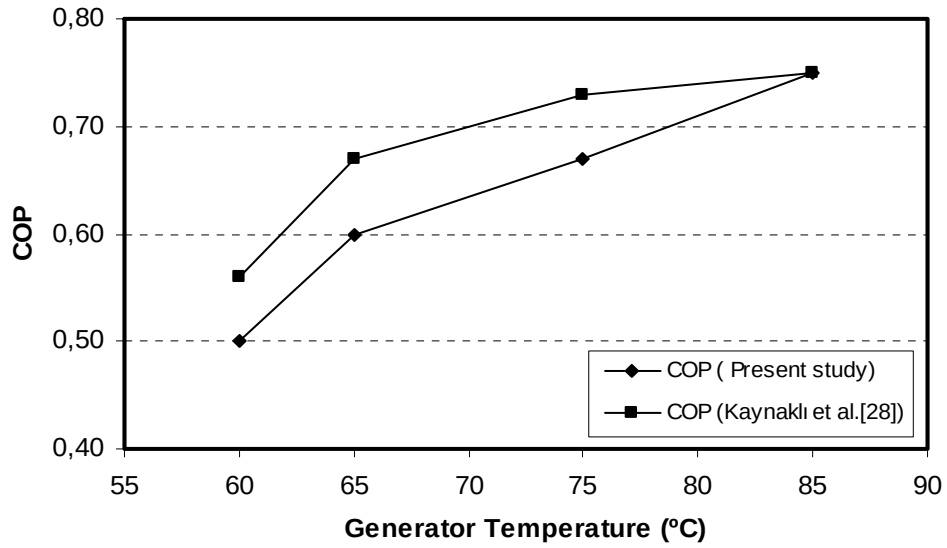

Figure 4.4 Variation of COP (T_e=6 ^oC, T_c= T_a= 25 ^oC) with generator temperatures

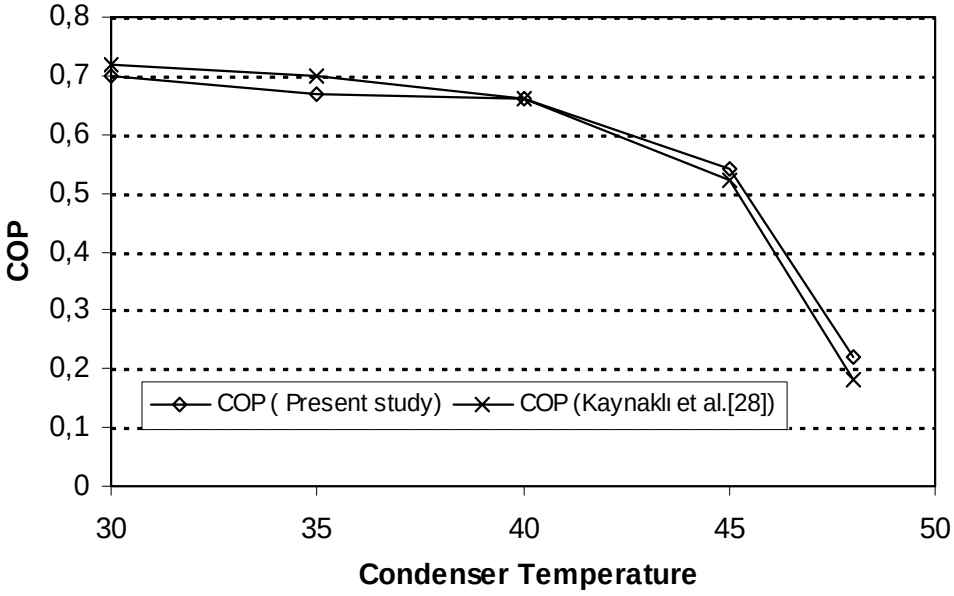

Figure 4.5 Comparison of COP values (T_e=6 ^oC, T_a= 40 ^oC, T_g= 90 ^oC) with condenser temperatures

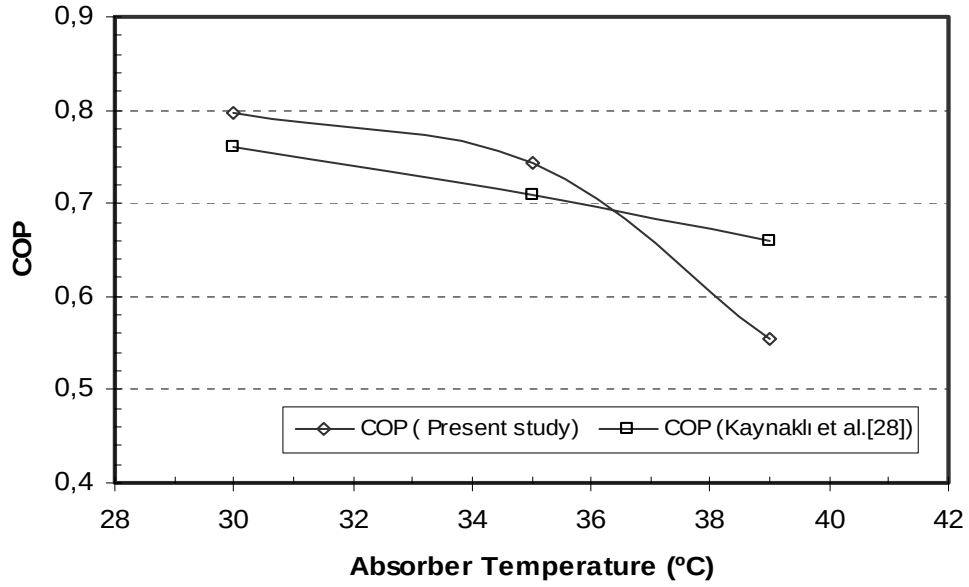

Figure 4.6 Comparison of COP values (T_e=6 ^oC, T_c= 40 ^oC, T_g= 90 ^oC) with absorber temperatures

4.2 EXPERIMENTAL RESULTS

4.2.1 The Experimental Results Of Absorption Refrigeration System

The effects of the generator, evaporator, condenser and absorber temperatures on the thermal loads of the components are shown in figures 4.7-15.

4.2.1.1 The effects of ambient air temperature

The experiments were performed with different ambient temperatures. To obtain different temperatures, electrical air heater (10 kW) was mounted into air supply channel of refrigeration unit. The channel was directly connected to absorber, condenser and evaporator. T_g=70^oC, $m_{air,c}$ =0,42 kg/s are the common parameters while $m_{air,e}$ is varied as 0.10 kg/s, 0.22 kg/s and 0.31 kg/s. During the experiments,

condensation of water was not deserved in outer surface of the evaporator due to air flow through the evaporator. Because the evaporator air exit temperatures was greater than the dew point of the evaporator surface temperature. During the experiments, the ambient temperature was varied between 24-48 ^{o}C. The evaporator capacity was determined using equation 3.11 or 3.12. As seen Figure 4.7, when the T_{amb} was increased, the evaporator capacity decreased due to the increase in evaporating temperature. The COP was determined using equation 3.25. The details of calculations of heat capacity were explained in chapter 3. It is seen from Figure 4.8, COP values decrease with increasing condenser and absorber temperatures according as ambient temperature. When the temperatures of the condenser and absorber increase, the thermal load of the generator rises, and the performance of the system gets worse. This also caused a decrease on COP (Figure 4.8). Also, the air-cooled absorber and air-cooled condenser capacity were affected by ambient temperature. As seen Figure 4.9, an increase of ambient temperature causes a decrease on the condenser capacity and an increase in absorber capacity. The high pressure of the system increases and the concentration of the strong solution decreases when the condenser temperature increases. With decreasing strong solution concentration, the thermal loads of both the generator and absorber increase (Figure 4.9). The enthalpy of the saturated liquid (h_3) leaving the condenser increases with increasing condenser temperature. Thus, it causes a small amount of decrease in the condenser and evaporator thermal loads. By increasing the absorber temperature, the concentration of the weak solution approaches the concentration of the strong solution. Therefore, the thermal load of the absorber increases (Figure 4.9). An increase in condenser pressure was also observed (Figure 4.10).

The variation of evaporator air exit temperature was given for different ambient temperatures and air mass flow rates in Figure 4.11.

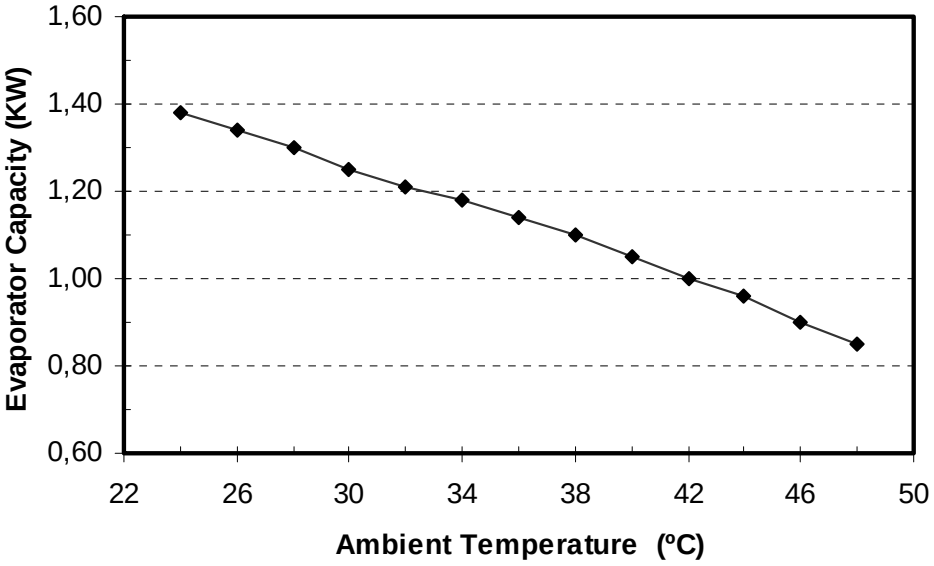

Figure 4.7 Variation of cooling capacity with the ambient temperature (T_g= 75^{o}C, T_e=12 ^{o}C, Q_g=2.5 kW)

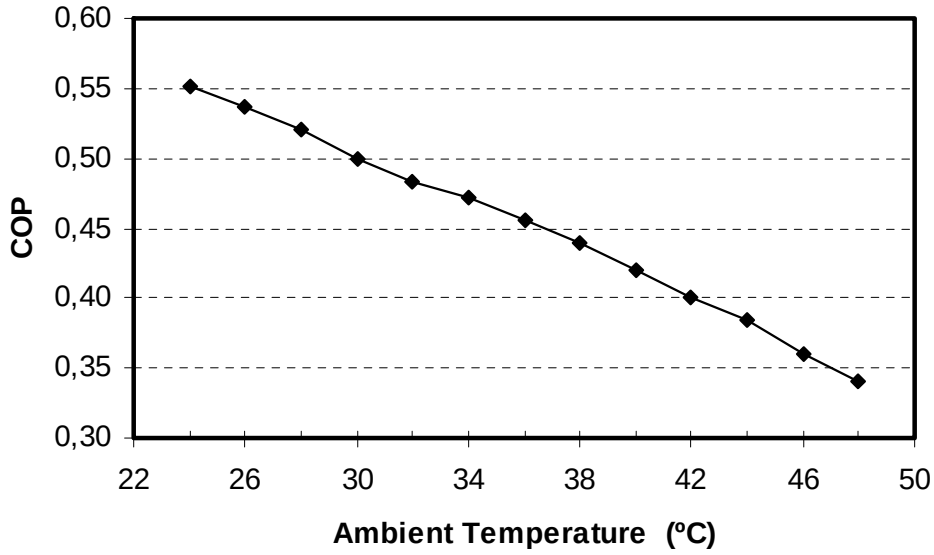

Figure 4.8 Variation of COP with the ambient temperature (T_g= 75^{o}C, T_e=12 ^{o}C, Q_g=2.5 kW)

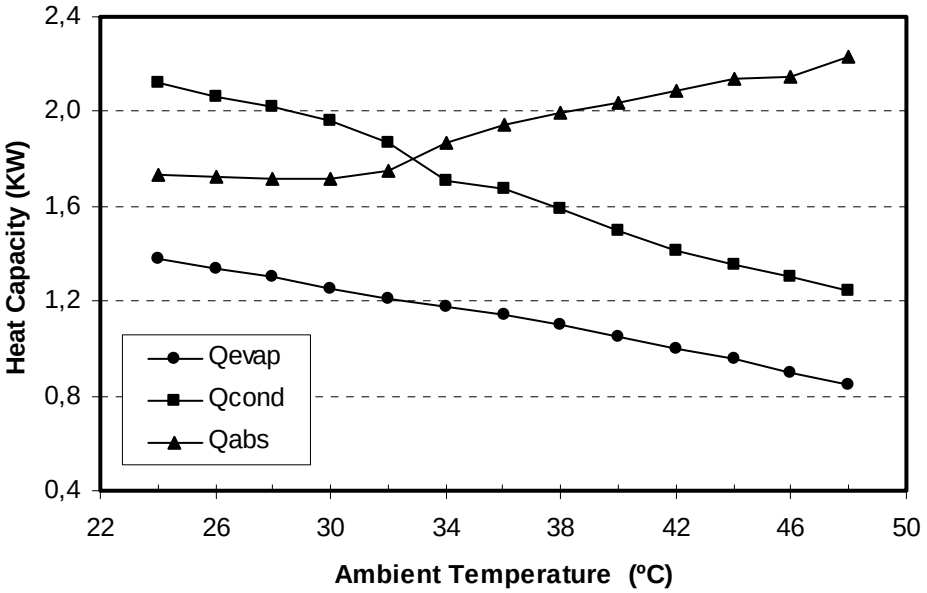

Figure 4.9 Variation of heat capacities with the ambient temperature
(T_e=12 ^oC, $Q_{g=}$2.5 kW, $m_{air,evap}$=0,1 kg/s, $m_{air,cond}$ =0,42 kg/s)

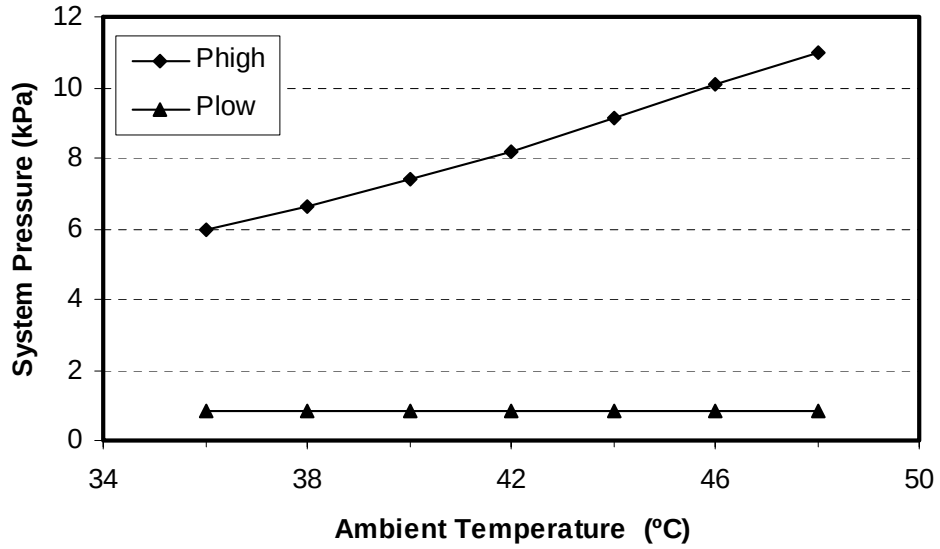

Figure 4.10 Variation of system pressures with the ambient temperature
(Tg= 75^oC, T_e=12 ^oC, $Q_{g=}$2.5 kW)

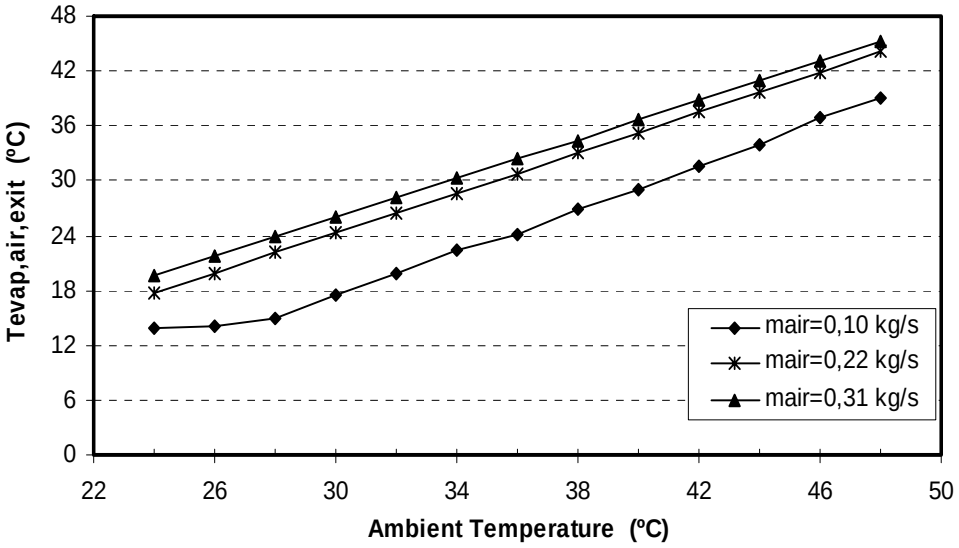

Figure 4.11 Variation of evaporator air exit temperature with the ambient temperature and mass flow rate (T_g= 75^{o}C, T_e=12 ^{o}C, Q_g=2,5 kW)

4.2.1.2 The Effects of Generator Temperature

Figure 4.12 shows the variation of COP with T_g. The COP increases with T_g. As it can be seen from Figure 4.13, when the generator temperature increases, the generator and absorber thermal loads (Q_g and Q_a) decrease. If the generator temperature gets higher, the concentration of the solution leaving the generator increases. Moreover, the weak solution temperature and, hence, the enthalpy (h_{10}) is increased by the strong solution in the solution heat exchanger. The generator thermal load is decreased both by increasing h_{10}. The enthalpy of the superheated water vapor (h_2) leaving the generator increases with increasing generator temperature. The thermal load of condenser (Q_C) is rising. The evaporator thermal load does not change with generator temperature and remains constant. The evaporator temperature affects the low pressure of the system. If the evaporator temperature rises, the concentration of the weak solution decreases. It causes a decrease in the absorber thermal load; on the other hand, decrease of the concentration of the weak solution decreases the generator thermal load (Figure 4.15). A small increase in condenser outlet enthalpy (h_1) also causes a small amount of increase in the condenser thermal load. The time required to reach steady state for

typical operating conditions is given in Figure 4.14, 4.15 and 4.16 through variations of condenser, evaporator and absorber temperatures with respect to time.

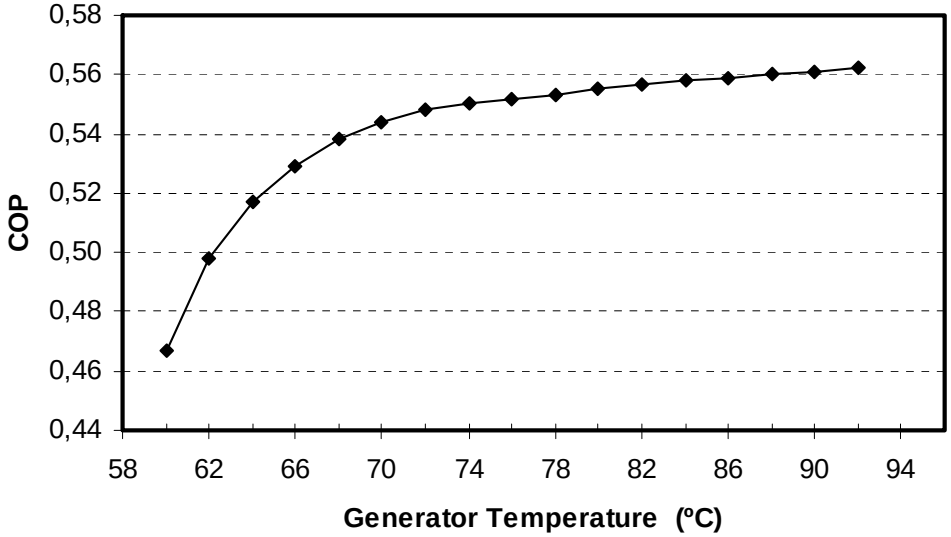

Figure 4.12 Variation of COP with the generator temperature (T_{amb}= 24^{o}C,T_e=12 ^{o}C)

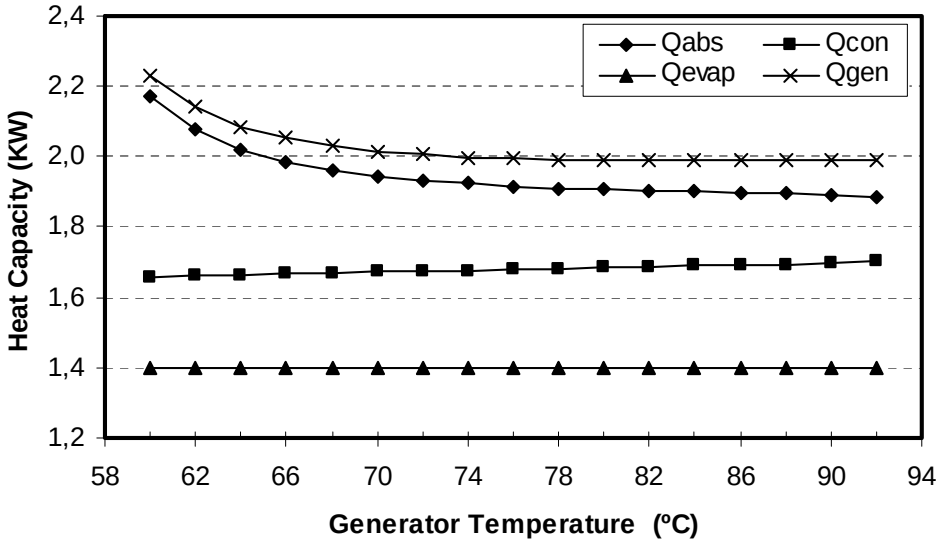

Figure 4.13 Variation of heat capacities with the generator temperature (T_{amb}= 24^{o}C, T_e=12 ^{o}C)

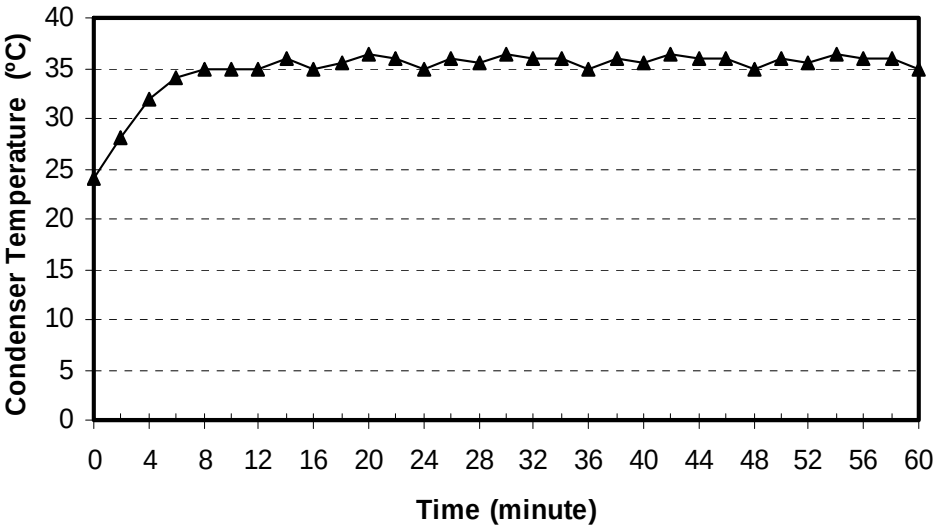

Figure 4.14 Variation of condenser temperature with time

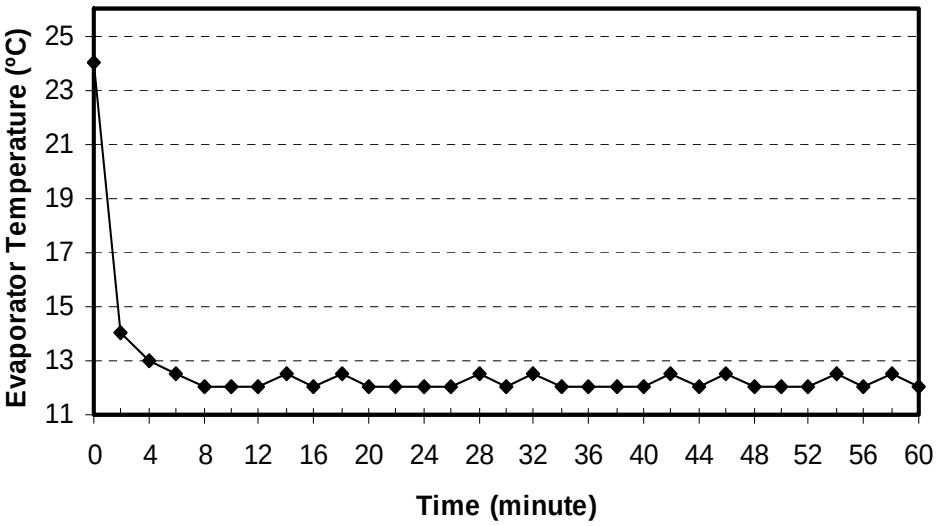

Figure 4.15 Variation of evaporator temperature with time

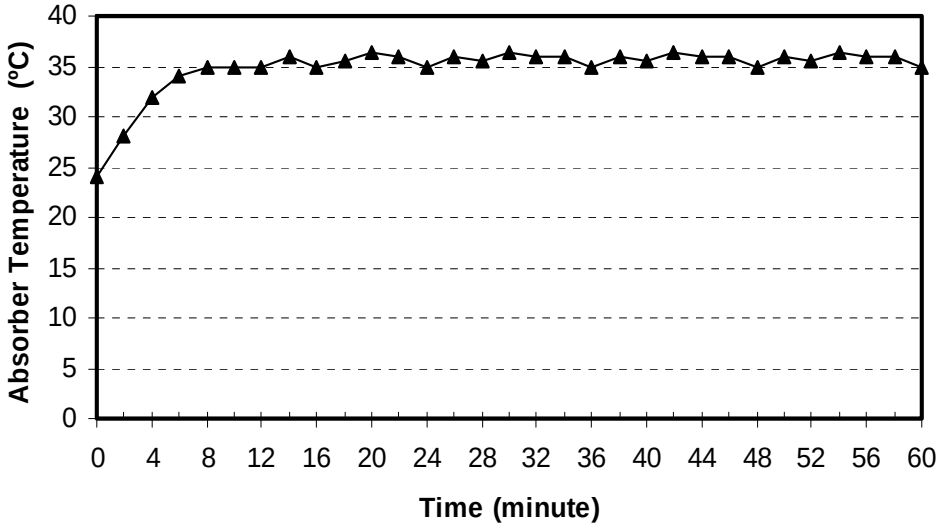

Figure 4.16 Variation of absorber temperature with time

4.2.2 The Experimental Results Of Absorption Refrigeration System Integrated In Combustion Engine

Determining the engine capability to drive the experimental refrigeration system required the study of the power and heat distribution of the engine under various conditions. The first type generator was called 1st type, while the second type generator was called 2nd type.

4.2.2.1 The Effect of the Generators on Performance of the Engine

The effect of generators on the performance parameters of engine for various speeds is shown in Figures 4.17-21. When experimenting with the combined system, particular attention was given to examining the effect on the performance of the IC engine of inserting the generators of refrigeration system into the engine exhaust system. An excessive drop in pressure in the exhaust system could have a detrimental

effect on engine performance. The correlation given below is used to determine the effect of engine back pressure on engine performance [5].

$$W = \frac{\Delta P . \dot{m}}{\rho} \tag{4.1}$$

where W, ΔP, $\dot{m}$ *and* ρ show power loss, the back pressure at the exhaust manifold, mass flow rate of exhaust gas and density of exhaust gas, respectively. The pressure measured in generator inlet increase as amount of pressure loss due to generator. Thereby, the power loss is calculated with respect to the back pressure.

Fuel consumption, exhaust pressure, power loss and engine efficiency are functions of engine speed. As engine speed increases fuel consumption increases as shown in Figure 4.17. The first type generator didn't affect fuel consumption with respect to no generator. But the second type generator effected at the ratio of 8%. Likewise, Figure 4.18 shows that as engine speed increases engine back pressure increases. Similarly, the first type generator did not affect exhaust pressure. But the second type generator rebounded exhaust pressure approximately 12% higher than the first type generator with respect to no generator. Because the second type generator created more head loses due to its construction with respect to no generator and first type generator.

The most important effect of generators on the engine performance is shown in Figure 4.19 as power loss. As the engine speed is increased slightly, the power loss increases slightly. But at high speeds, the power loss increases sharply.

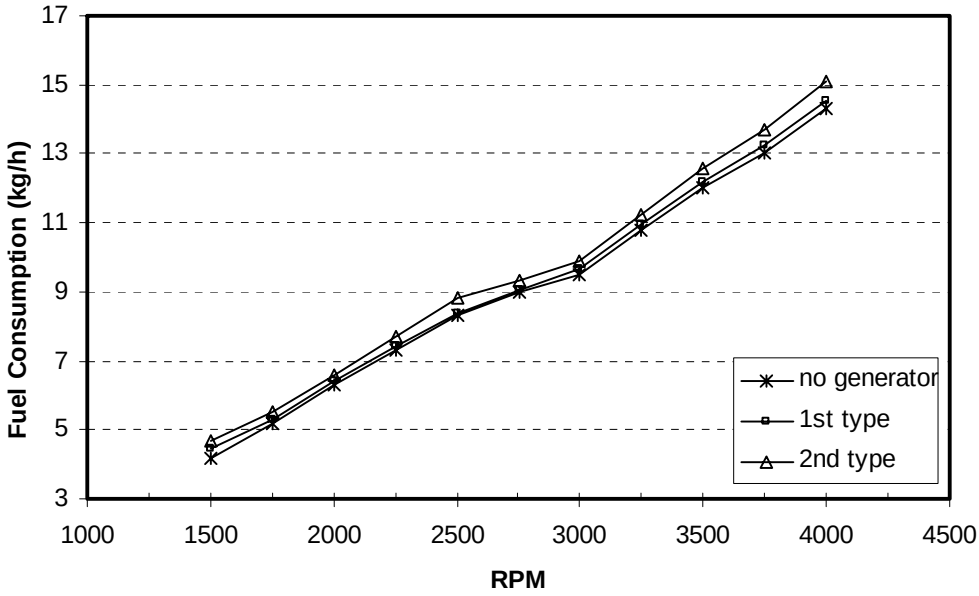

Figure 4.17 Fuel Consumption against speed

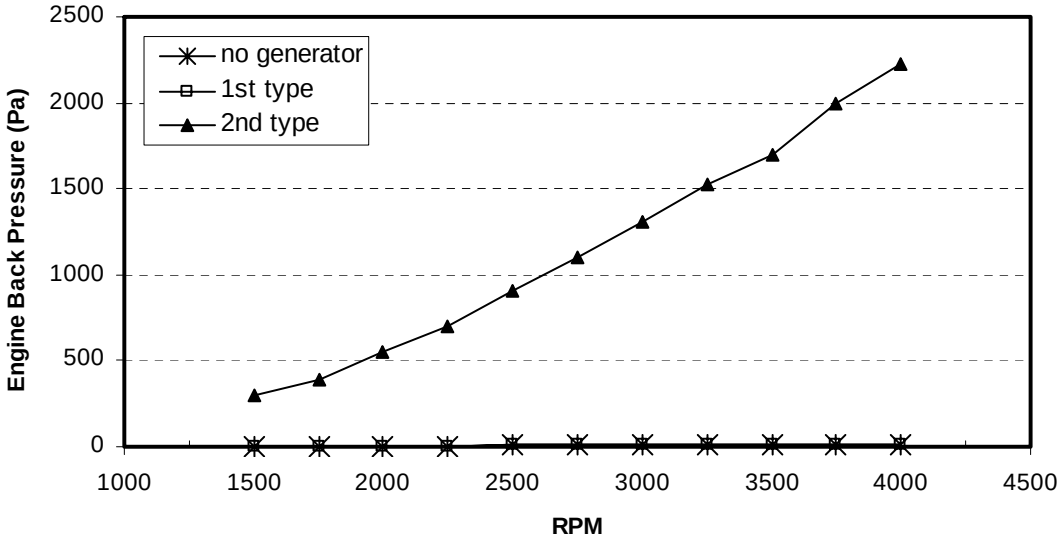

Figure 4.18 Engine back pressure against speed

The increase of power loss affects fuel consumption. So, the higher fuel consumption caused lower engine efficiency. Engine efficiency did not decrease until 2750 rpm and then, as engine speed increases further, the engine efficiency decreases as shown in Figure 4.20. In order to validate the measurements, the results have been compared with the similar experimental data in the literature [5]. Horuz' s study

included an experimental investigation into use of vapour absorption refrigeration (NH_3/Water) systems for road transport vehicles using the waste heat in the exhaust gases of the 6 liter diesel engine as the energy source [5]. Since the engine used in Horuz' study runs efficiently at between 1000 and 2250 rpm, the measurements are carried out in that speed region. In our study measurements are taken between 1500 and 4000 rpm due to use of a gasoline engine. In comparison to Horuz's study, the efficiency of present study increases until the speed of the engine reaches at 2750 rpm, at which the engine runs most efficiently, and then the efficiency starts decreasing as engine speed increases further. The efficiency of designed system shows similar trend to Horuz's system after the speed of 2750 rpm. As mentioned before, the measurements are done in different engine speed region due to engine characteristics such as gasoline and diesel engine.

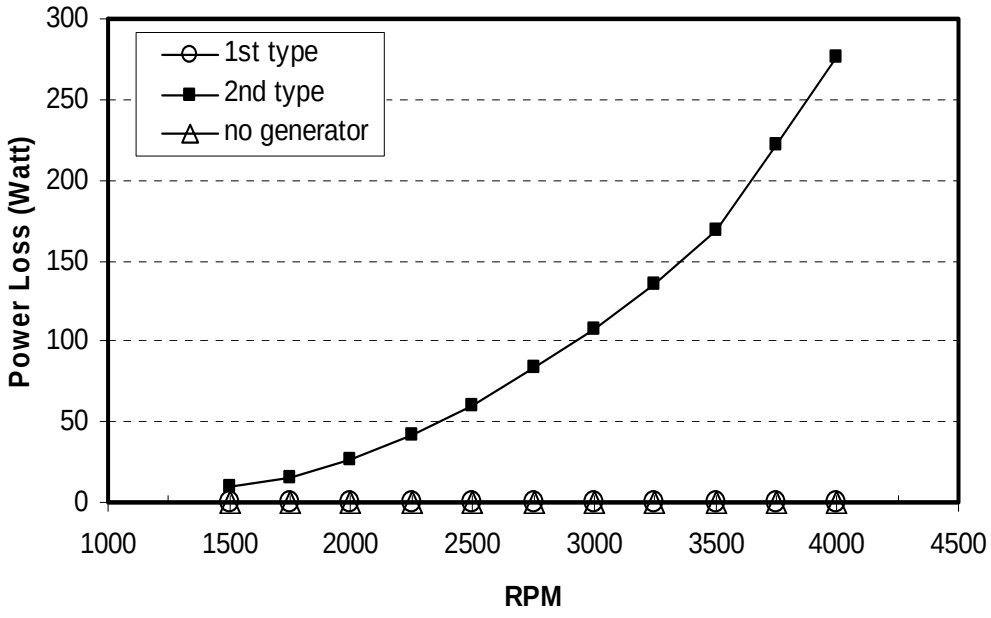

Figure 4.19 Power loss against speed

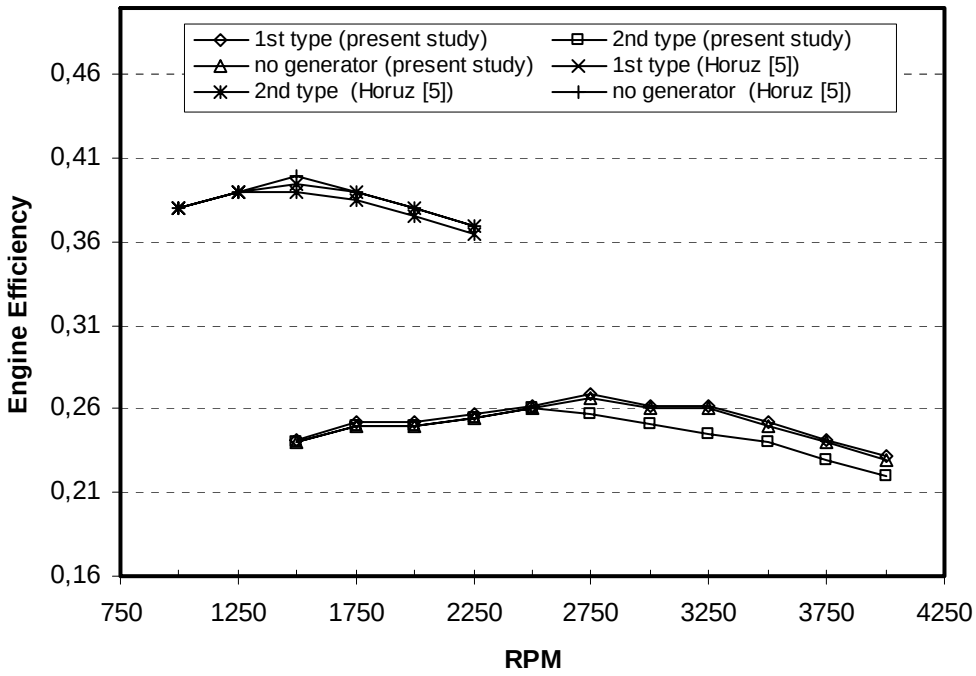

Figure 4.20 Engine efficiency against speed

4.2.2.2 The Effect of the Generators On The Performance Of The Absorption Refrigeration System

The variation of cooling capacity with engine speed is shown Figure 4.21. The results obtained are compared with that of Horuz's results in the Figure 4.22. While the engine speeds were varied between 1500 and 4000, the torqueses were set at 100, 120 and 135 Nm. Since the engine used in Horuz's study runs efficiently at between 1000 and 2250 rpm, the measurements are carried out in that speed region. As engine speed increases cooling capacity increases as shown in Figure 4.23.The cooling capacity of the system used in the present study is lower than that of Horuz's system. This difference, as mentioned before, is due to engine characteristics. Likewise, as seen Figure 4.23, as the engine speed increases, the recovered heat energy also increased. Because, when the engine speed increases, the exhaust gas temperature and flow rate increase. Therefore, generator capacity increases. At the absorption refrigeration system, required heat is approximately 3,5 kW. However, the engine can provide sufficient heat capacity at 2000 rpm. This heat capacity

reaches to approximately 10 kW at minimum. The variation of COP with engine speed is shown in Figure 4.24. When engine speed is increased, the COP increases. The results obtained are also compared with that of Horuz's results. The similar trend is observed.

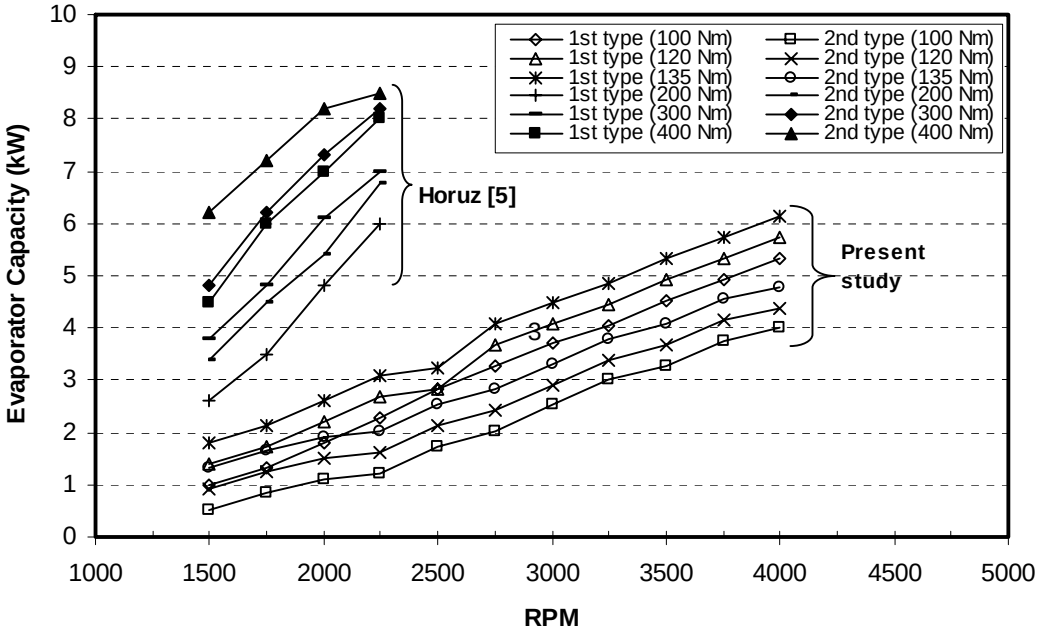

Figure 4.21 Cooling capacity against speed at different torques

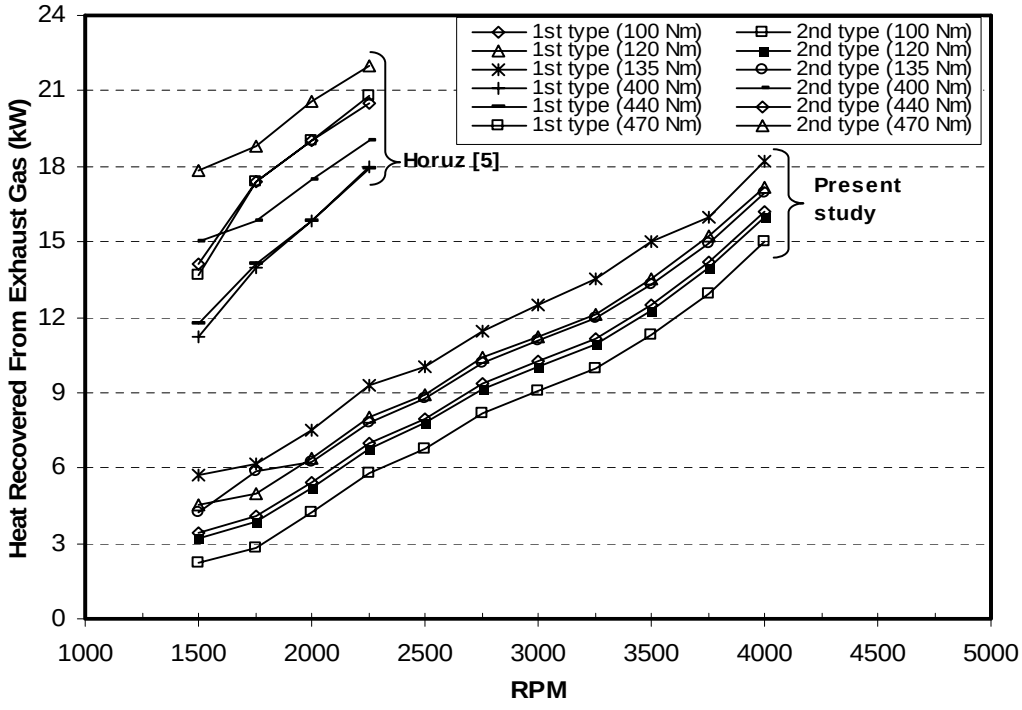

Figure 4.22 Heat recovered from exhaust gases against speed at different torques

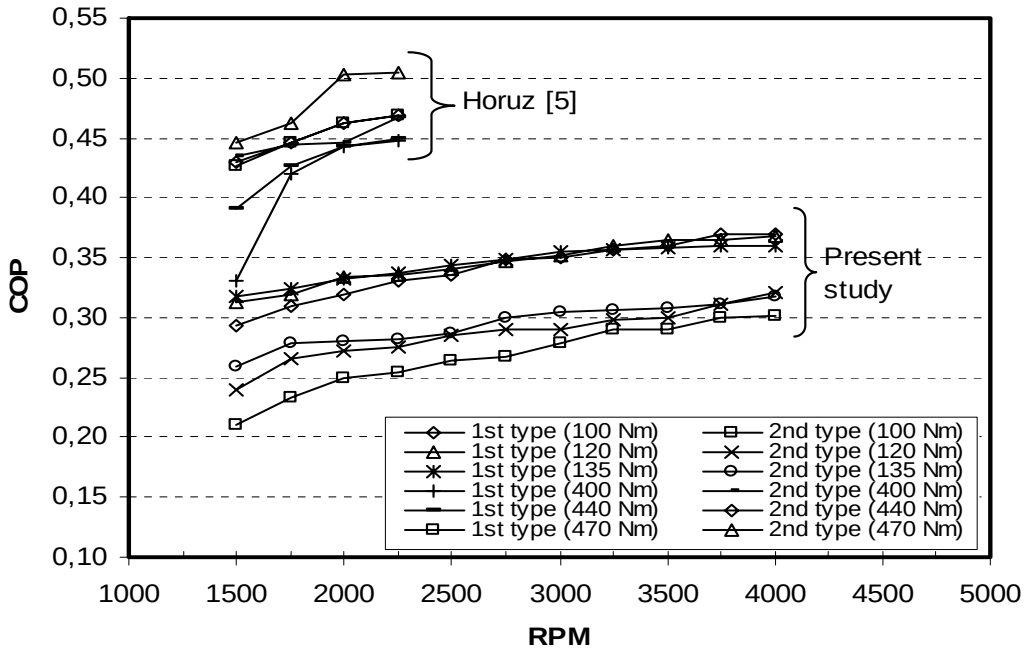

Figure 4.23 COP against speed at different torques

4.3 GENERAL DISCUSSION

When the effect of the generators of absorption refrigeration system on the performance of the IC engine is concerned, Figures compare the fuel consumption, exhaust pressure and power loss against speed. In the first type generator, the engine power loss is about the same as without heat exchanger and hence fuel consumption is about the same. In the second type generator, engine pressure is higher than the first because of restricted flow area. This caused higher fuel consumption and hence, higher power loss and lower engine efficiency.

In respect of absorption refrigeration system, as figures indicate , more heat recovered from the exhaust gas of the IC engine the more heat transferred to the generator and hence this caused an increase on the cooling capacity of the experimental refrigeration system. This is due to the fact that, in the refrigeration system, the cooling capacity is directly proportional to the heat input to the generator.

At this design condition, the required waste heat input to the generator is 3,5 kW. At normal driving conditions, the waste heat available from the exhaust gas would be marginally sufficient, but the waste heat available from the engine exhaust gas is more than sufficient. At idle conditions and slow-moving traffic conditions, conditions which normally tend to overheat the engine cooling system, the cooling capacity will be ample to maintain steady-state conditions and the absorption cooling system will actually help the cooling system rather work than against it (as the conventional compressor driven systems do).

As shown Figure 4.21, at idle conditions the cooling capacity is 2 kW while at under full load conditions the cooling capacity increases to 5 kW. The performance of an absorption refrigeration system that would provide the same cooling capacities (at idle and under full load conditions) with the vapor compression system.

According to these results, the waste heat from the exhaust was between 5 kW and 18 kW from idle to under full load, respectively. Using this range, the effect of the available heat to be used in the generator was evaluated for different engine speeds. The worst case scenario (when the system has the smaller cooling capacity) is at idle when the available waste heat from the exhaust system has the smaller value.

CHAPTER 5

CONCLUSION

The absorption refrigeration system is a feasible alternative to the traditional vapor compression system for automotive case. The absorption refrigeration systems use an environmentally-refrigerants and very little power for operation when compared to traditional vapor compression systems. The reduction in power can be achieved because the system can be operated using the waste heat rejected from the engine coolant system and because no compressor is required.

An experimental investigation was carried out to analyze the absorption refrigeration system in detail and investigate the use of the absorption system utilizing the waste heat in the exhaust gases from the main propulsion unit of a road transport vehicle for refrigerated road transport.

The study included the experimental analysis air-cooled absorption system in detail, the experimental analysis of the availability and recovery of the exhaust waste heat from engine and experimental study of the integrated system performance.

As far as the absorption system is concerned, air-cooled absorption system which uses water as the refrigerant and LiBr as the absorbent was constructed for experiments in the laboratory. The system which had a cooling capacity of approximately 2,5 kW was originally designed and constructed for automobile air-conditioning system.

Experimental results showed that, evaporator's air flow rate increases, the cooling capacity decreases. If the air temperature increases, the cooling capacity decreases. If the condenser's air flow rate increases, cooling capacity increases.

A 1.3 liter internal combustion engine was also analyzed experimentally by carrying out the study of the power and heat distribution under various speed and load conditions. Experimental results proved that the experimental engine was capable of driving the experimental absorption refrigeration system via its waste exhaust heat, if the waste heat in the exhaust gases could be utilized without penalizing engine.

As far as the integrated system is concerned, the experiments were focused on the effect on the performance of the engine and effect on the performance of the absorption refrigeration system.

Introducing the refrigeration system into the exhaust system of the engine caused an increase on the engine back pressure and this caused higher fuel consumption and lower efficiency. The effect can be reduced by designing a generator with a minimum pressure drop.

If a generator is designed with a minimum pressure drop, but a maximum heat transfer efficiency, more cooling effect can be obtained even in the lower engine speed and loads.

When the absorption system is used in vehicles, in order to utilize the waste heat in the exhaust gases without excessive pressure drops in the exhaust systems and hence without excessive reduction in efficiency of the vehicle's engine, different shaped generator can be designed. The corrosion effect of the exhaust gas to the generator material can be reduced by using the materials which can accommodate the exhaust gases, such as galvanized or stainless steel. The solution will overcome the corrosion problem but will increase cost.

Balancing the fluctuations in the cooling capacity due to variation in vehicle speed can be obtained by employing a generator combining heat source, such as gas

burner. Employing a generator combining a gas burner is also an option to carry on cooling while the vehicle is stationary.

The absorption refrigeration system can be mounted to the same location on the vehicle as the conventional system, and for trailer type vehicles can be connected to the vehicle's exhaust pipe by flexible pipe work. In this case, the exhaust pipe work connection engagement and the exhaust gas flow control valve arrangement should be designed. The generator should be as close as the exhaust manifold in order to reduce the heat loses and the pressure drops along the flexible pipe.

Experimental results proved that it was possible to drive a vapour absorption refrigeration system using the exhaust gases from a internal combustion engine. This suggests that such a system could be used in vehicles. However, further consideration is required with respect to the following: the design of a heat exchanger to extract waste heat without excessive pressure drops in the exhaust systems, the effect of increased back pressure on the engine performance, the corrosion effect of the exhaust gases on the heat exchanger material, the fluctuations in the cooling capacity due to variations in vehicle speed, and alternative energy input while vehicle is stationary, the effect of varying ambient conditions on the system performance, and accommodating the system on the vehicle.

CHAPTER 6

SUGGESTIONS FOR FUTURE STUDIES

The experimental set-up designed and constructed is very flexible and it enables for doing in a wide range of experiments with so many system design and operation parameters under control for future research on the manner. Some suggestions for the development of set-up and study concepts are outlined below:

1. The heat exchanger to extract waste heat without excessive pressure drops in the exhaust systems can be designed.

2. To decrease corrosion effect, the convenient materials for generator on the exhaust pipe can be selected.

3. While the vehicle is stationary (idle position) , an alternative energy input can be added.

4. The development/documentation of alternative refrigerant-absorbent pairs can be try.

5. Expediently proving the concept of a coolant waste heat driven cycle using a conventional internal combustion engine paves the way for absorption refrigeration air conditioning systems to become a standard for the contemporary vehicle

6. The system could be powered by a hydrogen-fueled internal combustion engine, a fuel cell, or a hybrid electric system – any power system that produces waste heat.

7. The system could be powered by a hydrogen-fueled internal combustion engine, a fuel cell, or a hybrid electric system – any power system that produces waste heat.

APPENDICES

APPENDIX 1

CALIBRATION OF MEASUREMENT DEVICES

All of measurement devices used in experimental set-up were explained the calibration details in this appendix.

1.1 THERMOCOUPLE CALIBRATION

A controlled temperature must be provided in which the reference junction is maintained at a constant chosen temperature. The reference junction temperature should be controlled to a better accuracy than that expected from the thermocouple calibration. The most commonly used reference temperature is 0 degrees C., but other temperatures may be used if desired.

One of the most common reference junctions is the ice bath. The ice bath is made up of a mixture of melting shaved ice and water. The ice bath is a convenient and inexpensive way to achieve an ice point, it can be reproduced with ease and with exceptional accuracy. Junctions formed between the thermocouple materials and instrument leads can be simply immersed into the slush mixture Quick electrical connection can then be made between thermocouple and instrument leads.

The calibration characteristics of thermocouples are shown Figure A1.1.

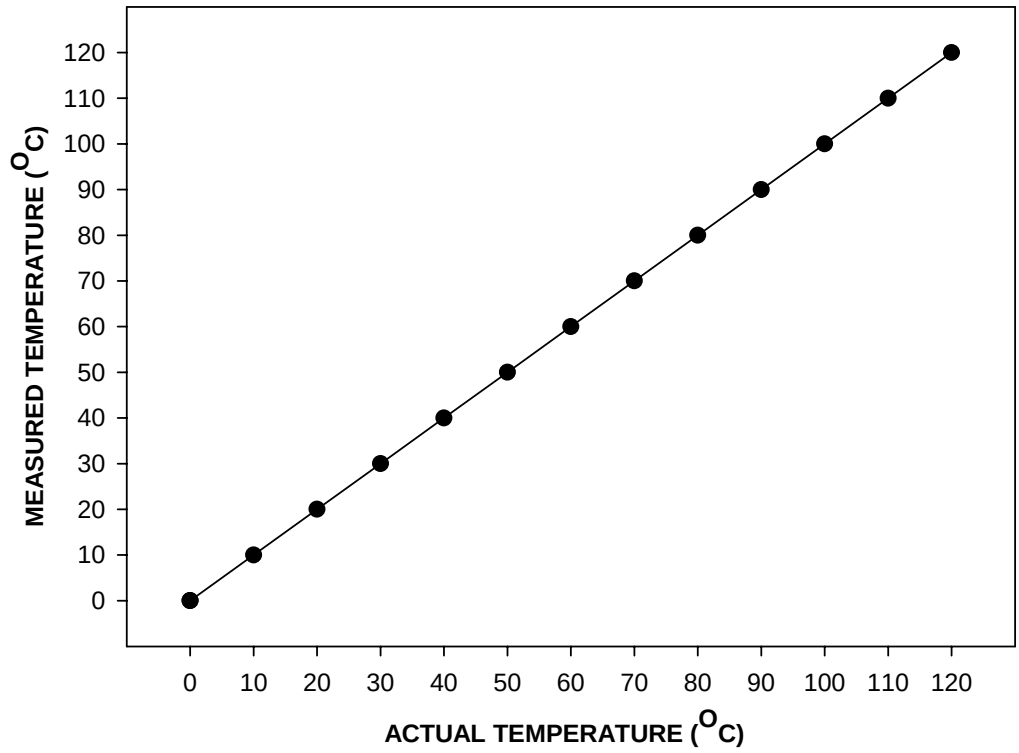

Figure A1.1 Calibration Curve of Thermocouples

1-2 PRESSURE TRANSDUCER CALIBRATION

The dead weight tester was used to calibrate the pressure transducers. The calibration curve for transducers is shown in Figure A1.2.

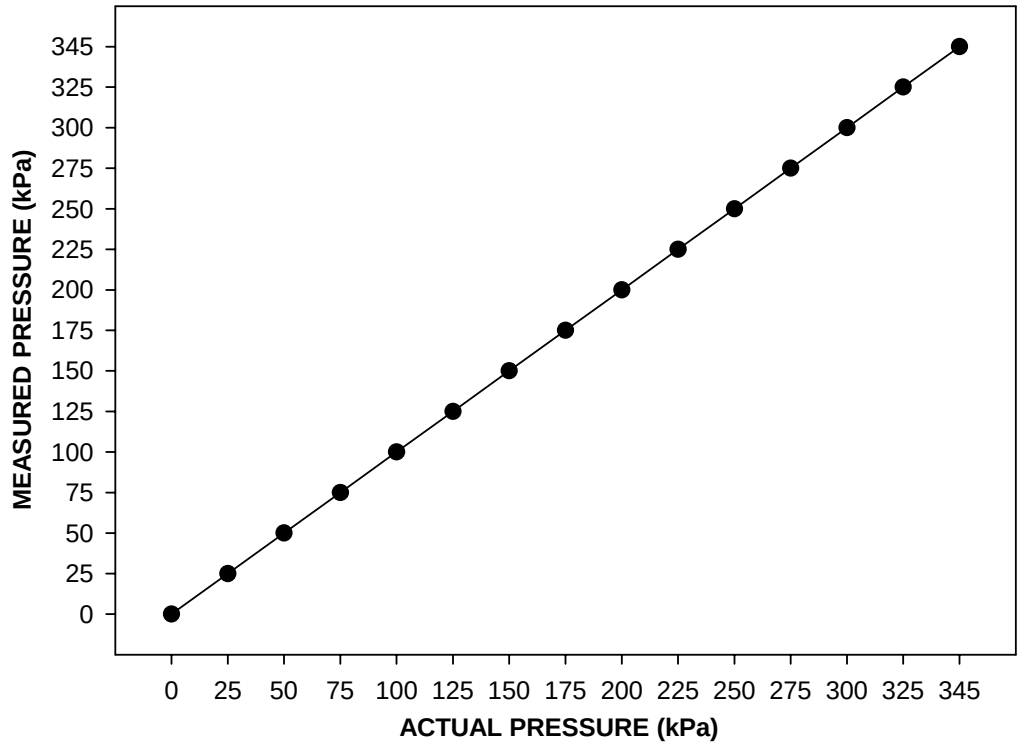

Figure A1.2 Calibration Curve of Pressure Transducer

1.3 TURBINE AND MAGNETIC TYPE FLOWMETER CALIBRATION

The flowmeter is calibrated by weighing the quantity of water that passes the flowmeter during a certain measuring time. Hereto the water is collected in the weighing tank, whereby the mass weight is measured by calibrated scale.

The calibration curves of turbine and magnetic flowmeter are shown in Figure A1.3 and Figure A1.4.

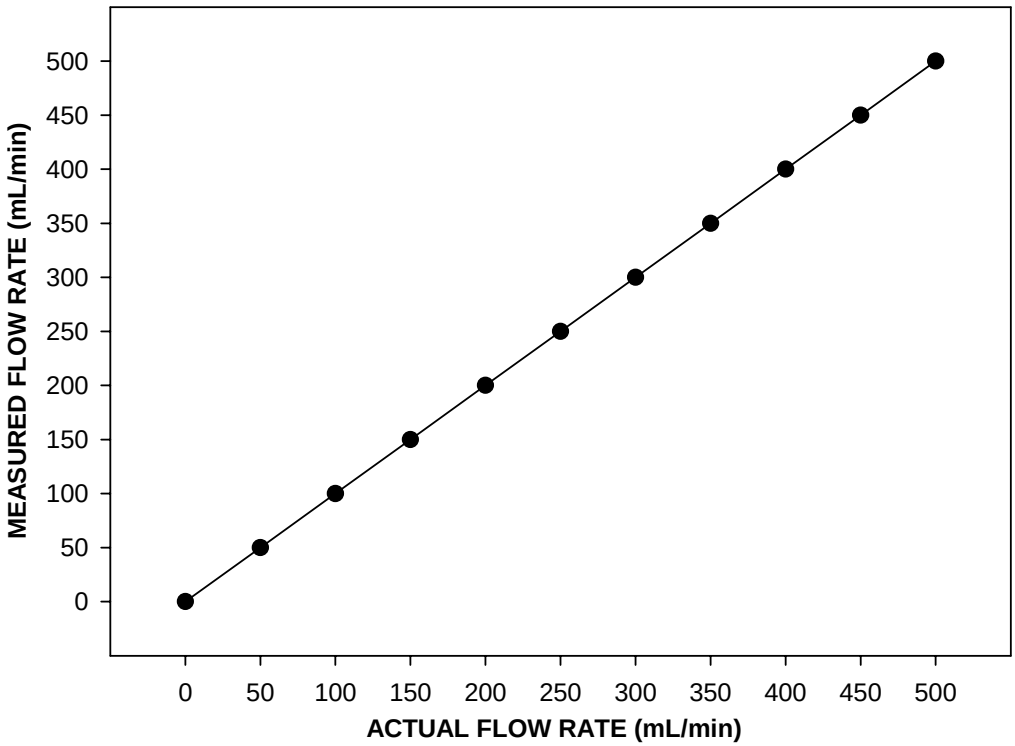

Figure A1.3 Calibration Curve of Turbine Type Flowmeter

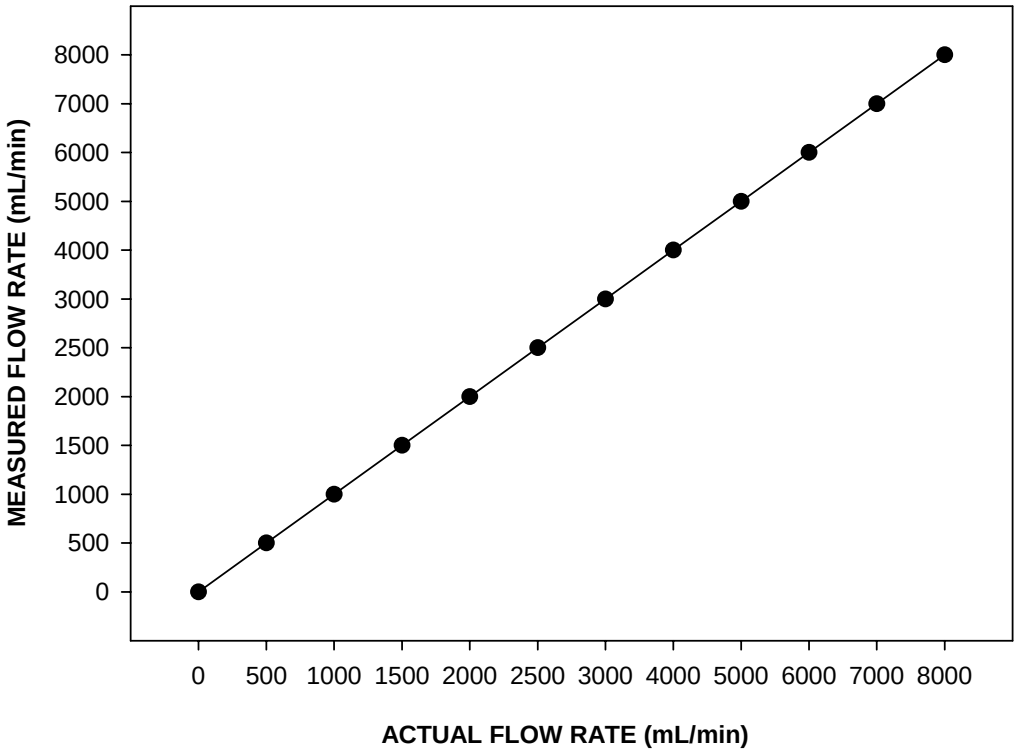

Figure A1.4 Calibration Curve of Magnetic Flowmeter

APPENDIX 2

THE COMPUTER CODES FOR THEORETICAL ANALYSIS OF PROPOSED ABSORPTION SYSTEM AND SIZE ANALAYSIS OF HEAT EXCHANGERS USED IN EXPERIMENTAL SET-UP

The theoretical analysis of proposed absorption system and size calculations of heat exchangers used in experimental set-up were explained the computer codes details in this appendix.

2.1 The theoretical analysis of proposed absorption system

```
".....PREPARED BY ISMAIL HILALI....."
"        "



T[1]=7"°C"
T[2]=85"°C"
T[3]=35"°C"
T[4]=7"°C"
T[5]=37"°C"
T[8]=85"°C"
T[9]-T[6]=20"°C"

"Equilibrium saturated conditions are assumed for states 1,3,5 and 8"
"        "
"***************Cooling Capacity***************"
"        "
Q_evap=2,5"kW"
"        "
" ***************1. Point*****************"
"        "

P[1]=PRESSURE(Steam;T=T[1];x=1)"kPa"
h[1]=ENTHALPY(Steam;T=T[1];x=1)"kJ/kg"
s[1]=ENTROPY(Steam;T=T[1];P=P[1])
x[1]=0
V[1]=VOLUME(Steam;T=T[1];P=P[1])"m^3/kg"
rho[1]=1/V[1]"kg/m^3"
C_p[1]=SPECHEAT(Steam;T=T[1];P=P[1])"kJ/kg.K"
mu[1]=VISCOSITY(Steam;T=T[1];P=P[1])"Pa.s"
k[1]=CONDUCTIVITY(Steam;T=T[1];P=P[1])"W/m.K"

"        "
" ******************2. Point*********************"
"        "

P[2]=P[3]"kPa"
h[2]=ENTHALPY(Steam;T=T[2];P=P[2])"kJ/kg"
s[2]=ENTROPY(Steam;T=T[2];P=P[2])
x[2]=0
V[2]=VOLUME(Steam;T=T[2];P=P[2])"m^3/kg"
rho[2]=1/V[2]"kg/m^3"
C_p[2]=SPECHEAT(Steam;T=T[2];P=P[2])"kJ/kg.K"
mu[2]=VISCOSITY(Steam;T=T[2];P=P[2])"Pa.s"
k[2]=CONDUCTIVITY(Steam;T=T[2];P=P[2])"W/m.K"
```

```
"        "
" ******************3. Point******************"
"        "
P[3]=PRESSURE(Steam;T=T[3];x=0)"kPa"
h[3]=ENTHALPY(Steam;T=T[3];x=0)"kJ/kg"
s[3]=ENTROPY(Steam;T=T[3];x=0)
x[3]=0
V[3]=VOLUME(Steam;T=T[3];x=0)"m^3/kg"
rho[3]=1/V[3]"kg/m^3"
C_p[3]=SPECHEAT(Steam;T=T[3];x=0)"kJ/kg.K"
mu[3]=VISCOSITY(Steam;T=T[3];x=0)"Pa.s"
k[3]=CONDUCTIVITY(Steam;T=T[3];x=0)"W/m.K"

"        "
" *****************4. Point**************************"
"        "
h[4]=h[3]"kJ/kg"
P[4]=P[1]"kPa"
s[4]=s[3]
x[4]=0
V[4]=VOLUME(Steam;T=T[4];x=0)"m^3/kg"
rho[4]=1/V[4]"kg/m^3"
C_p[4]=SPECHEAT(Steam;T=T[4];x=0)"kJ/kg.K"
mu[4]=VISCOSITY(Steam;T=T[4];x=0)"Pa.s"
k[4]=CONDUCTIVITY(Steam;T=T[4];x=0)"W/m.K"

"        "
" ********************5. Point**********************"
"        "
P[5]=P[1]"kPa"
h[5]=H_LIBR('SI' ;T[5];x[5])"kJ/kg"
s[5]=0,26
x[5]=X_LIBR('SI';T[5];P[5])
V[5]=V_LIBR('SI' ;T[5];x[5])/1000"m^3/kg"
rho[5]=1/V[5]"kg/m^3"
k[5]=COND_LIBR('SI' ;T[5];x[5])"W/m.K"
Mu[5]=VISC_LIBR('SI' ;T[5];x[5])"Pa.s"
C_p[5]=(0,0976*x[5]^2 -37,512*x[5] + 3825,4)/1000 "kJ/kg.K"

"        "
" ************************6. Point**********************"
"        "

h[6]=h[5]"kJ/kg"
s[6]=s[5]
T[6]=T[5]"°C"
x[6]=x[5]
P[6]=P[3]"kPa"
V[6]=V_LIBR('SI' ;T[6];x[6])/1000"m^3/kg"
rho[6]=1/V[6]"kg/m^3"
```

```
k[6]=COND_LIBR('SI' ;T[6];x[6])"W/m.K"
Mu[6]=VISC_LIBR('SI' ;T[6];x[6])"Pa.s"
C_p[6]=(0,0976*x[6]^2 -37,512*x[6] + 3825,4)/1000"kJ/kg.K"


"         "
" **********7. Point**********"
"         "

x[7]=x[5]
h[7]=h[6] +(m_dot[8]/m_dot[5])*(h[8]-h[9])
s[7]=0,4
h[7]=H_LIBR('SI' ;T[7];x[7])"kJ/kg"
P[7]=P[6]"kPa"
V[7]=V_LIBR('SI' ;T[7];x[7])/1000"m^3/kg"
rho[7]=1/V[7]"kg/m^3"
k[7]=COND_LIBR('SI' ;T[7];x[7])"W/m.K"
Mu[7]=VISC_LIBR('SI' ;T[7];x[7])"Pa.s"
C_p[7]=(0,0976*x[7]^2 -37,512*x[7] + 3825,4)/1000"kJ/kg.K"

"         "
" **********8. Point**********"
"         "

P[8]=P[3]"kPa"
h[8]=H_LIBR('SI' ;T[8];x[8])"kJ/kg"
s[8]=0,50
x[8]=X_LIBR('SI';T[8];P[8])
V[8]=V_LIBR('SI' ;T[8];x[8])/1000"m^3/kg"
rho[8]=1/V[8]"kg/m^3"
k[8]=COND_LIBR('SI' ;T[8];x[8])"W/m.K"
Mu[8]=VISC_LIBR('SI' ;T[8];x[8])"Pa.s"
C_p[8]=(0,0976*x[8]^2 -37,512*x[8] + 3825,4)/1000"kJ/kg.K"

"         "
" **********9. Point**********"
"         "

P[9]=P[3]"kPa"
x[9]=x[8]
h[9]=H_LIBR('SI' ;T[9];x[9])"kJ/kg"
s[9]=0,38
V[9]=V_LIBR('SI' ;T[9];x[9])/1000"m^3/kg"
rho[9]=1/V[9]"kg/m^3"
k[9]=COND_LIBR('SI' ;T[9];x[9])"W/m.K"
Mu[9]=VISC_LIBR('SI' ;T[9];x[9])"Pa.s"
C_p[9]=(0,0976*x[9]^2 -37,512*x[9] + 3825,4)/1000"kJ/kg.K"

"         "
" **********10. Point**********"
```

```
"        "

h[10]=h[9]"kJ/kg"
s[9]=s[10]
x[10]=x[8]
T[10]=T[9]"°C"
P[10]=P[1]"kPa"
V[10]=V_LIBR('SI' ;T[10];x[10])/1000"m^3/kg"
rho[10]=1/V[10]"kg/m^3"
k[10]=COND_LIBR('SI' ;T[10];x[10])"W/m.K"
Mu[10]=VISC_LIBR('SI' ;T[10];x[10])"Pa.s"
C_p[10]=(0,0976*x[10]^2 -37,512*x[10] + 3825,4)/1000"kJ/kg.K"

"        "
"********************mass flow rates****************"
"        "
Q_evap=m_dot[1] * (h[1]-h[4])"kW"

m_dot[2]=m_dot[1]"kg/s"
m_dot[3]=m_dot[1]"kg/s"
m_dot[4]=m_dot[1]"kg/s"

m_dot[8]=m_dot[1]*(x[1]-x[5])/(x[5]-x[10])"kg/s"

m_dot[9]=m_dot[8]"kg/s"
m_dot[10]=m_dot[8]"kg/s"

m_dot[5]=m_dot[1]+m_dot[8]"kg/s"

m_dot[6]=m_dot[5]"kg/s"
m_dot[7]=m_dot[5]"kg/s"
"        "
"********************Heat capacities****************"
"        "
Q_cond=m_dot[2]*(h[2]-h[3])"kW"
Q_abs=m_dot[1]*h[1]+m_dot[10]*h[10]-m_dot[5]*h[5]"kW"
Q_gen=m_dot[2]*h[2]+m_dot[8]*h[8]-m_dot[7]*h[7]"kW"
Q_shex=m_dot[6]*(h[7]-h[6])"kW"

COP= Q_evap/Q_gen
Balance=Q_cond+Q_abs-Q_gen-Q_evap

w_pomp =V[5]*(P[6]-P[5])*m_dot[5]*1000"W"


"        "
"        "
"        "
"                                    UA-LMTD method                    "
"        "
```

```
"         "
"         "
T[11]=500
T[12]=300
T[13]=22
T[14]=24
T[15]=20
T[16]=22
T[17]=20
T[18]=11

P_atm=101,2
P[11]=P_atm
P[11]=P[12]
P[12]=P[13]
P[13]=P[14]
P[14]=P[15]
P[15]=P[16]
P[16]=P[17]
P[17]=P[18]
Q_gen = UA_gen *LMTD_gen
m_dot[11]=0,042                    "From  engine test"
m_dot[11]=m_dot[12]
h[11]=594,75
h[12]=515,68
s[11]=0,9914
s[12]=1,0985

LMTD_gen = ((T[11]-T[8])-(T[12]-T[2]))/(ln((T[11]-T[8])/(T[12]-T[2])))

"         "
Q_cond = UA_cond *LMTD_cond
LMTD_cond = (T[16]-T[15])/(ln((T[3]-T[15])/(T[3]-T[16])))
Q_cond =m_dot[15]*(h[16]-h[15])
h[16]=ENTHALPY(Air;T=T[16])
s[16]=ENTROPY(Air;T=T[16];P=P_atm)
h[15]=ENTHALPY(Air;T=T[15])
s[15]=ENTROPY(Air;T=T[15];P=P_atm)
m_dot[15]=m_dot[16]
"         "
"         "
Q_evap = UA_evap *LMTD_evap
LMTD_evap = (T[17]-T[18])/(ln((T[17]-T[1])/(T[18]-T[1])))
Q_evap =m_dot[17]*(h[17]-h[18])
h[17]=ENTHALPY(Air;T=T[17])
h[18]=ENTHALPY(Air;T=T[18])
s[17]=ENTROPY(Air;T=T[17];P=P_atm)
s[18]=ENTROPY(Air;T=T[18];P=P_atm)
m_dot[17]=m_dot[18]
```

```
"        "
Q_abs = UA_abs *LMTD_abs

LMTD_abs = ((T[10]-T[14])-(T[5]-T[13]))/(ln((T[10]-T[14])/(T[5]-T[13])))
Q_abs =m_dot[13]*(h[14]-h[13])
h[13]=ENTHALPY(Air;T=T[13])
h[14]=ENTHALPY(Air;T=T[14])
s[13]=ENTROPY(Air;T=T[13];P=P_atm)
s[14]=ENTROPY(Air;T=T[14];P=P_atm)
m_dot[13]=m_dot[14]

"        "
Q_shex = UA_shex *LMTD_shex
LMTD_shex = ((T[8]-T[7])-(T[9]-T[6]))/(ln((T[8]-T[7])/(T[9]-T[6])))



                                                                    "
"                                EXERGY ANALYSIS                    "
"
                                                                    "

T_0=T[15]
h_0=ENTHALPY(Air;T=T_0)
s_0=ENTROPY(Air;T=T_0;P=P_atm)
psi[1]=(h[1]-h_0)-(T_0+273,15)*(s[1]-s_0)
psi[2]=(h[2]-h_0)-(T_0+273,15)*(s[2]-s_0)
psi[3]=(h[3]-h_0)-(T_0+273,15)*(s[3]-s_0)
psi[4]=(h[4]-h_0)-(T_0+273,15)*(s[4]-s_0)
psi[5]=(h[5]-h_0)-(T_0+273,15)*(s[5]-s_0)
psi[6]=(h[6]-h_0)-(T_0+273,15)*(s[6]-s_0)
psi[7]=(h[7]-h_0)-(T_0+273,15)*(s[7]-s_0)
psi[8]=(h[8]-h_0)-(T_0+273,15)*(s[8]-s_0)
psi[9]=(h[9]-h_0)-(T_0+273,15)*(s[9]-s_0)
psi[10]=(h[10]-h_0)-(T_0+273,15)*(s[10]-s_0)
psi[11]=(h[11]-h_0)-(T_0+273,15)*(s[11]-s_0)
psi[12]=(h[12]-h_0)-(T_0+273,15)*(s[12]-s_0)
psi[13]=(h[13]-h_0)-(T_0+273,15)*(s[13]-s_0)
psi[14]=(h[14]-h_0)-(T_0+273,15)*(s[14]-s_0)
psi[15]=(h[15]-h_0)-(T_0+273,15)*(s[15]-s_0)
psi[16]=(h[16]-h_0)-(T_0+273,15)*(s[16]-s_0)
psi[17]=(h[17]-h_0)-(T_0+273,15)*(s[17]-s_0)
psi[18]=(h[18]-h_0)-(T_0+273,15)*(s[18]-s_0)

DeltaPsi_Gen=m_dot[8]*psi[8]+m_dot[2]*psi[2]-m_dot[7]*psi[7]
DeltaPsi_Cond=m_dot[2]*(psi[2]-psi[3])
DeltaPsi_v1=m_dot[3]*(psi[3]-psi[4])
DeltaPsi_v2=m_dot[10]*(psi[10]-psi[9])
DeltaPsi_evap=m_dot[1]*(psi[4]-psi[1])
DeltaPsi_abs=m_dot[1]*psi[1]+m_dot[10]*psi[10]-m_dot[5]*psi[5]
DeltaPsi_shex=m_dot[8]*psi[8]+m_dot[6]*psi[6]-m_dot[7]*psi[7]-m_dot[9]*psi[9]
DeltaPsi_pump=m_dot[5]*(P[6]-P[5])/P[6]
```

2.2 Size calculations of heat exchangers

{ABSORBER ANALYSIS}

D_w = 0,035 {Tube width}
D_ht= 0,0035 {Tube hight}
t = 0,0002 {Fin thickness}
f= 0,018 {Condenser fin depth}
l =0,600 {Fin length}
y_i = 0,350 {Fin hight}
V = 16 {m/s} {Fan Velocity}
A_i =0,035*0,0035 {Flow area}
A_tot=l *y_i {Total Area perpendicular to air flow}
N_pipe= 22 {Total Pipe number}
e=0,0025 {Fin spacing}
A_tot_pipe=1,0164 {Total Pipe surface area}
N_fin=7040
A_tot_fin=7040*,035*,0125*2 {Fin number}
A_tot_surface=A_tot_fin+A_tot_pipe {Total heat transfer area}

D_h=4*(D_w*D_ht)/(2*(D_w+D_ht))
Nus=3,66+(0,0668*Re*Pr[5] *(D_h/l))/ (1+0,04*((D_h/l)*Re*Pr[5])^(2/3))

h_i =Nus*k[5] / D_h

"Flow velocity inside pipe"

U=m_dot[5]*V[5] /(A_i)

Re=U*D_h/(mu[5]*V[5])

" Physical properties of air "

T1= 21 {Degree celcius}
P1=101,2
rho_air=DENSITY(Air;T=T1;P=P1)
mu_air=VISCOSITY(Air;T=T1)
k_air=CONDUCTIVITY(Air;T=T1)
v_air =VOLUME(Air;T=T1;P=P1)
C_p_air=SPECHEAT(Air;T=T1)
Pr=PRANDTL(Air;T=T1)

m_dot_air=rho_air * V*A_tot

"Outside heat transfer coefficient"

Re_o=V*D_h*rho_air/mu_air {fin number/cm=4}

St*Pr^(2/3)=0,003 {From Table}
St*Pr^(2/3)=h_o * Pr^(2/3)/(C_p_air *1000* V*rho_air) {h_o is found}

eta_cond=0,95 {Assume from experimental}

{Overall heat transfer coefficient }

U_overall=(1/(h_o * eta_cond)+1/h_i *A_tot_surface/A_tot_pipe)^(-1)

DeltaT_ln=((T[10]-T_c)-(T[5]-T1))/ln((T[10]-T_c)/(T[5]-T1))

Q_abs=m_dot_air*C_p_air*(T_c -T1)

Q_abs=U_overall*A_1*DeltaT_ln/1000

{CONDENSER ANALYSIS}

D_w = 0,02 {Tube width}
D_ht= 0,0038 {Tube hight}
t = 0,0002 {Fin thickness}
f= 0,018 {Condenser fin depth}
g_i =0,500 {Fin length}
y_i = 0,352 {Fin hight}
V = 16 {m/s} {Fan Velocity}
A_i =0,02*0,0038 {Flow area}
A_tot=g_i *y_i {Total Area perpendicular to air flow}
N_pipe= 27 {Total Pipe number}
e=0,0025 {Fin spacing}
A_tot_pipe=0,6226 {Total Pipe surface area}
N_fin=8600
A_tot_fin=8600*,02*,01*2 {Fin number}
A_tot_surface=A_tot_fin+A_tot_pipe {Total heat transfer area}

{Copper tube and Aluminun fin are chosen for condenser design}

"I. Region"

```
h_f=ENTHALPY(Steam;T=T[3];x=1)

Q_cond_1=m_dot[2]*(h[2]-h_f)

Nus=ff/8*(Re-1000)*Pr_f / (1+12,7*(ff/8)^(1/2)*(Pr_f ^(1/3) -1))

ff=0,316*Re^(-1/4)                                        {friction factor}

h_i_1 =Nus*k_f / D_h

" Physical Properties of T_f=(T_2 +T_3)/2 "

T_f=(T[2]+T[3])/2

V_f=VOLUME(Steam;T=T_f;x=1)
Cp_f=SPECHEAT(Steam;T=T_f;x=1)
mu_f=VISCOSITY(Steam;T=T_f;x=1)
k_f=CONDUCTIVITY(Steam;T=T_f;x=1)
Pr_f=PRANDTL(Steam;T=T_f;x=1)

"Flow velocity inside pipe"

U=m_dot[2]*V_f /(A_i )

D_h=4*(D_w*D_ht)/(2*(D_w+D_ht))

Re=U*D_h/(mu_f*V_f)


" II. Region "

" Physical properties of air at 308 K"

T1= 20                                                    {Degree celcius}
P1=101,2
rho_air=DENSITY(Air;T=T1;P=P1)
mu_air=VISCOSITY(Air;T=T1)
k_air=CONDUCTIVITY(Air;T=T1)
v_air =VOLUME(Air;T=T1;P=P1)
C_p_air=SPECHEAT(Air;T=T1)
Pr=PRANDTL(Air;T=T1)

Q_cond_2=m_dot[2]*(h_f-h[3])

m_dot_air=rho_air * V*A_tot
Q_cond_2=m_dot_air *C_p_air *(T_air_exit1-T1)
Q_cond_2=m_dot_air *C_p_air *(T_air_exit2-T_air_exit1)

rho_L=DENSITY(Steam;T=T[3];x=0)
```

```
rho_g=DENSITY(Steam;T=T[3];x=1)

Alpha_g=1/(1-rho_g/rho_l)^(2/3)
Omega=0,728*Alpha_g

h_i_2=Omega*(k[3]^3*rho_L*(rho_L-rho_g)*9,81*(h_f-
h[3])*1000/mu[3]*D_h*(T[3]-(T1+T_air_exit2)/2))^(1/4)


"Outside heat transfer coefficient"

Re_o=V*D_h*rho_air/mu_air      {fin number/cm=4}

St*Pr^(2/3)=0,003                                          {From Table}
St*Pr^(2/3)=h_o * Pr^(2/3)/(C_p_air *1000* V*rho_air)      {h_o is found}

eta_cond=0,95                                              {Assume from
experimental}

{Overall heat transfer coefficient for I. region}

U_1=(1/(h_o * eta_cond)+1/h_i_1 *A_tot_surface/A_tot_pipe)^(-1)

{Overall heat transfer coefficient for II. region}

U_2=(1/(h_o * eta_cond)+1/h_i_2 *A_tot_surface/A_tot_pipe)^(-1)


DeltaT_ln1=((t[2]-t_air_exit2)-(t[3]-t_air_exit1))/ln((t[2]-t_air_exit2)/(t[3]-
t_air_exit1))

DeltaT_ln2=((t[3]-t1)-(t[3]-t_air_exit1))/ln((t[3]-t1)/(t[3]-t_air_exit1))

Q_cond_1=U_1*A_1*DeltaT_ln1/1000
Q_cond_2=U_2*A_2*DeltaT_ln2/1000

A =A_1+A_2


"         "
{********************EVAPORATOR  ANALYSIS************************}
"         "
D_w  = 0,058                    {Tube width}
D_ht= 0,003                     {Tube hight}
 t = 0,0002                     {Fin thickness}
l =0,168                        {Fin length}
y_i = 0,238                     {Fin hight}
V = 13                          {m/s}                  {Fan Velocity}
A_i =0,058*0,003                {Flow area}
A_tot=l *y_i                    {Total Area perpendicular to air flow}
```

```
N_pipe= 20                          {Total Pipe number}
e=0,010                             {Fin spacing}
A_tot_pipe=(D_w+D_ht)*2*l*N_pipe  {Total Pipe surface area}
N_fin=2130                          {Fin number}
A_tot_fin=N_fin*D_w*e*2         {Total fin area}
A_tot_surface=A_tot_fin+A_tot_pipe                    {Total heat transfer
area}


{Auminum tube and Aluminun fin are chosen for evaporator design}

"         "
"******Inside heat transfer coefficient******"

"         "

D_h=4*(D_w*D_ht)/(2*(D_w+D_ht))

h_i = h_L * (1,136*Co^(-0,9)*(25*Fr)^(,3)+667,2*Bo^(,7)*1,5)"kW/m^2 .K"

h_L =0,023*Re^(0,8)*Pr^(,4)*k_l/D_h                    "kW/m^2 .K"

Re=G*(1-,5)*D_h/mu_l

G=m_dot[2]/A_i

Co=((1-,5)/,5)^(,8)*(rho_g/rho_l)^(,5)

Fr=G^2/(rho_l ^2 *9,81*D_h)

Bo=Q_evap/(G*h_fg*A_tot_pipe)

"         "
"**************Thermophysical properties of steam  at 7 C*************"
"         "

rho_l=DENSITY(Steam;T=T[4];x=0)"kg/m^3"
rho_g=DENSITY(Steam;T=T[4];x=1)"kg/m^3"
k_l=CONDUCTIVITY(Steam;T=T[4];x=0)"W/m.K"
k_g=CONDUCTIVITY(Steam;T=T[4];x=1)"W/m.K"
mu_l=VISCOSITY(Steam;T=T[4];x=0)"Pa.s"
mu_g=VISCOSITY(Steam;T=T[4];x=1)"Pa.s"
h_f=ENTHALPY(Steam;T=T[4];x=0)"kJ/kg.K"
h_g=ENTHALPY(Steam;T=T[4];x=1)"kJ/kg.K"
h_fg=h_g-h_f"kJ/kg.K"
Pr=PRANDTL(Steam;T=T[4];P=P[4])
"         "
"*****Outside heat transfer coeffcient******"
"         "
h_o=h*,555*V^(,101)"kW/m^2 .K"
```

```
"         "
" Physical Properties of T_f "
"         "
T1= 20 "°C"
T2=18
P1=101,2"kPa"
T_f=(T1+T2)/2"°C"

rho_air=DENSITY(Air;T=T1;P=P1)"kg/m^3"
mu_air=VISCOSITY(Air;T=T_f)"Pa.s"
k_air=CONDUCTIVITY(Air;T=T_f)"W/m.K"
v_air =VOLUME(Air;T=T_f;P=P1)"m^3/kg"
Cp_air=SPECHEAT(Air;T=T_f)"kj/kg.K"
Pr_air=PRANDTL(Air;T=T_f)

Re_o=V*D_h*rho_air/mu_air

J_4row=0,0014+0,2618*Re_o ^(-0,4)*(A_tot_surface/A_tot_pipe)^(-0,15)
"         "
"Row' s number(N) is equal to 20"
"         "
N=20
"         "
J_N/J_4row =0,992*(2,24*Re_o ^(-,092)*(N/4)^(-,031))^(,607*(4-N))
"         "
J_N=h*Pr_air ^(2/3)/(rho_air*V*Cp_air*1000)
"         "
eta_evap =0,98
"         "
U=(1/(h_o * eta_evap)+1/h_i *A_tot_surface/A_tot_pipe)^(-1)"kW/m^2 . K"
"         "
T_air_exit =T2     {found experimental from real air-conditioning system of
automobile}
"         "
DeltaT_ln=((T1-T[4])-(t_air_exit -T[4]))/ln((T1-T[4])/(t_air_exit -T[4]))"K"
"         "
Q_evap=U*A*DeltaT_ln/1000 "kW"
```

APPENDIX 3

THE THERMODYNAMIC AND TRANSPORT PROPERTIES OF LiBr/WATER SOLUTION

Thermodynamic and Transport properties of working fluids were collected from various sources.

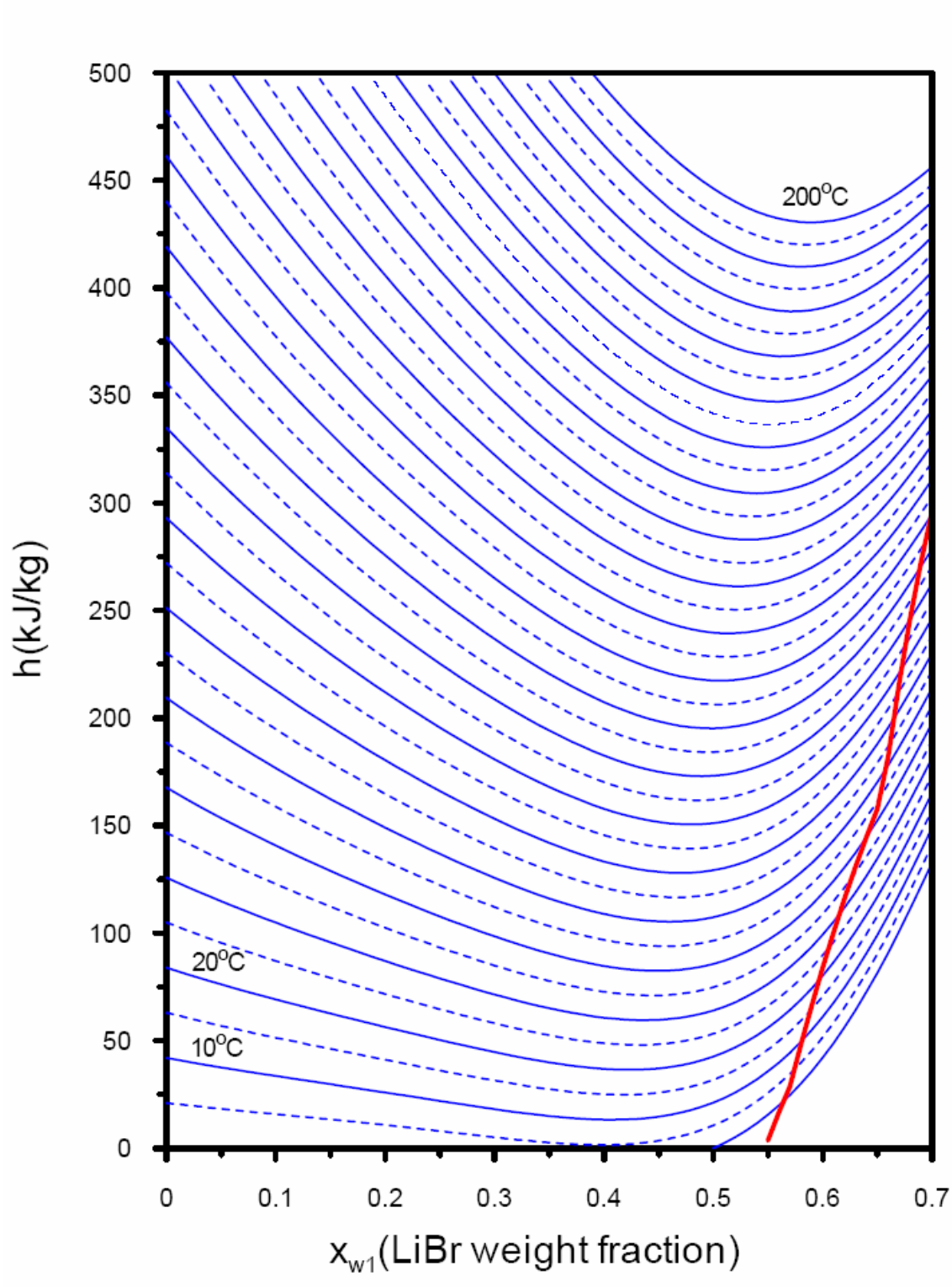

Figure A3.1 Enthalpy-concentration for aqueous LiBr solution

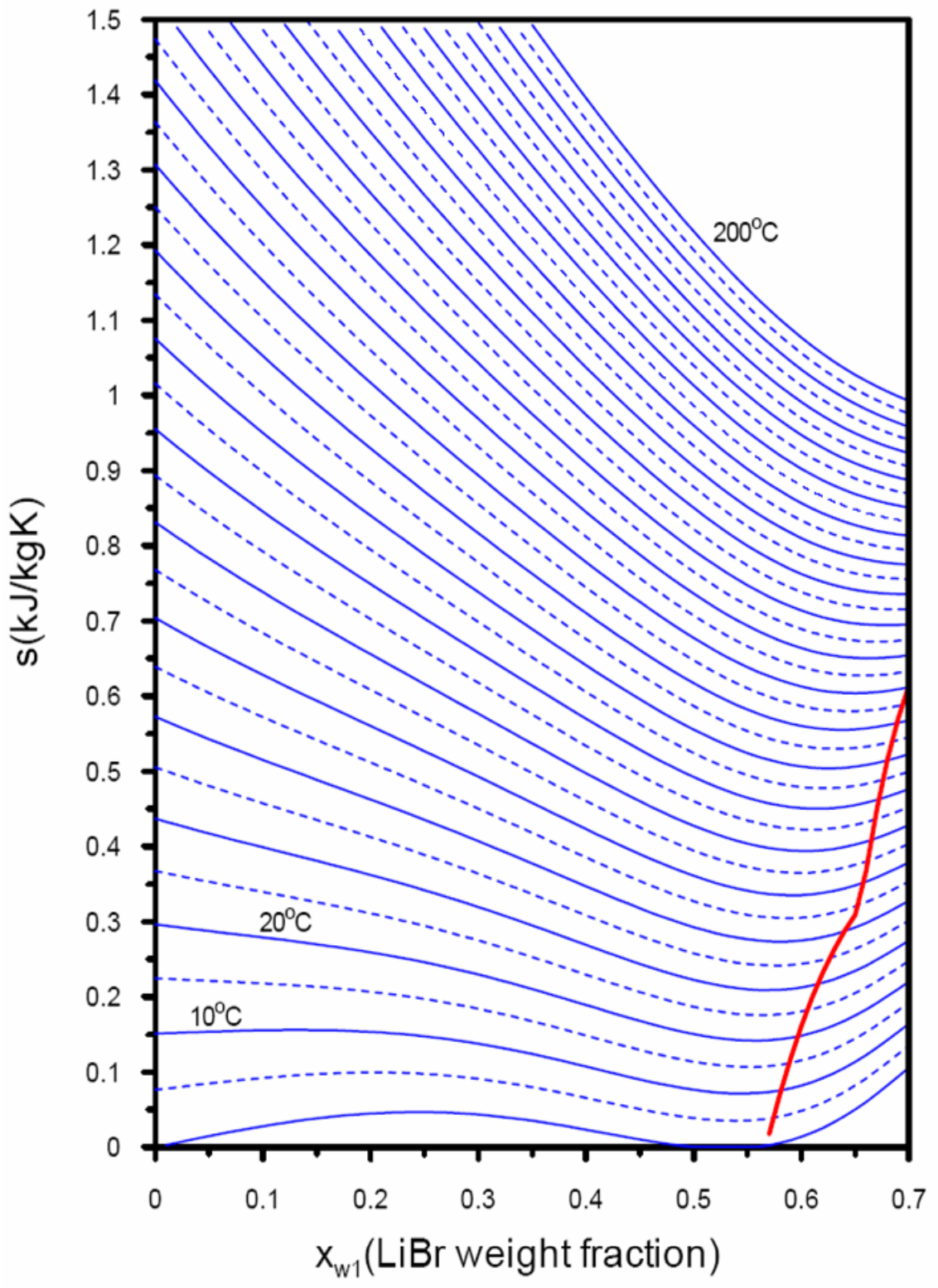

Figure A3.2 Entropy-concentration for aqueous LiBr solution

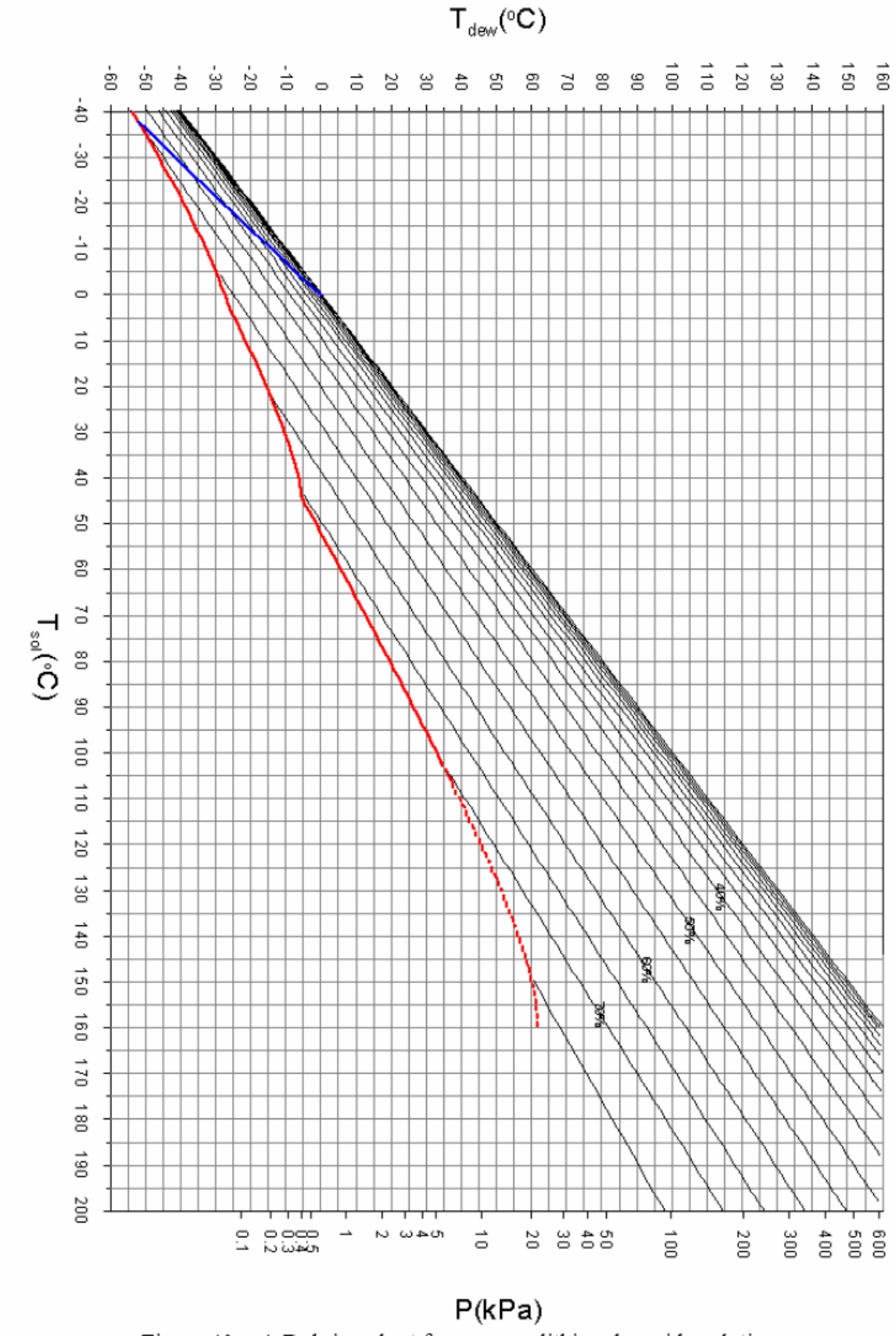

Figure A3.3 The Duhring chart for aqueous LiBr solution

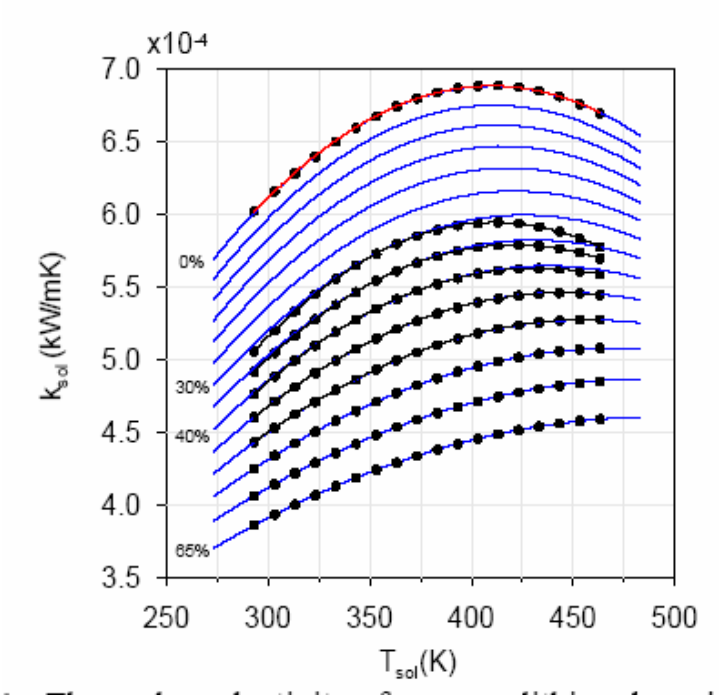

Figure A3.4 Thermal conductivity of aqueous LiBr solution

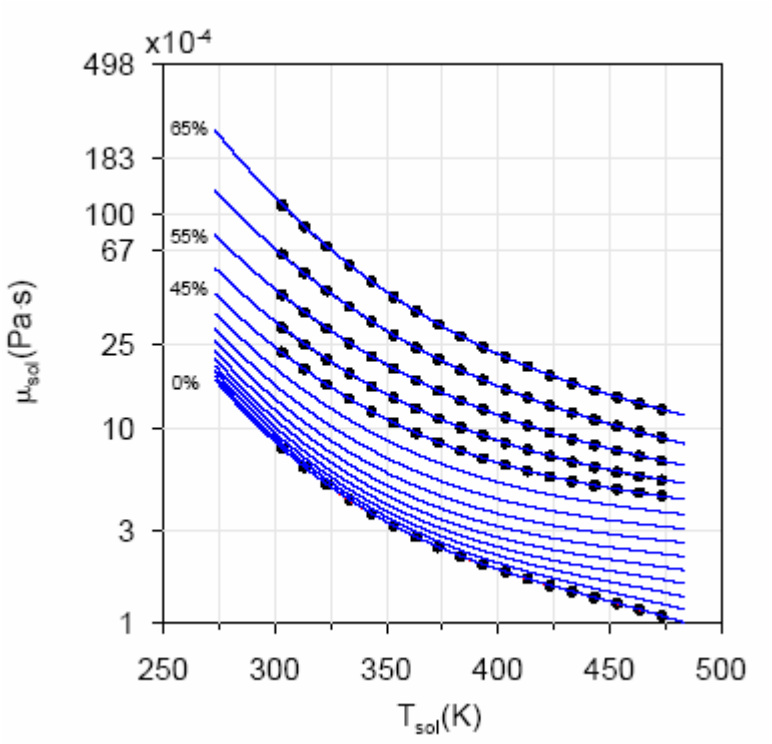

Figure A3.5 Dynamic viscosity of aqueous LiBr solution

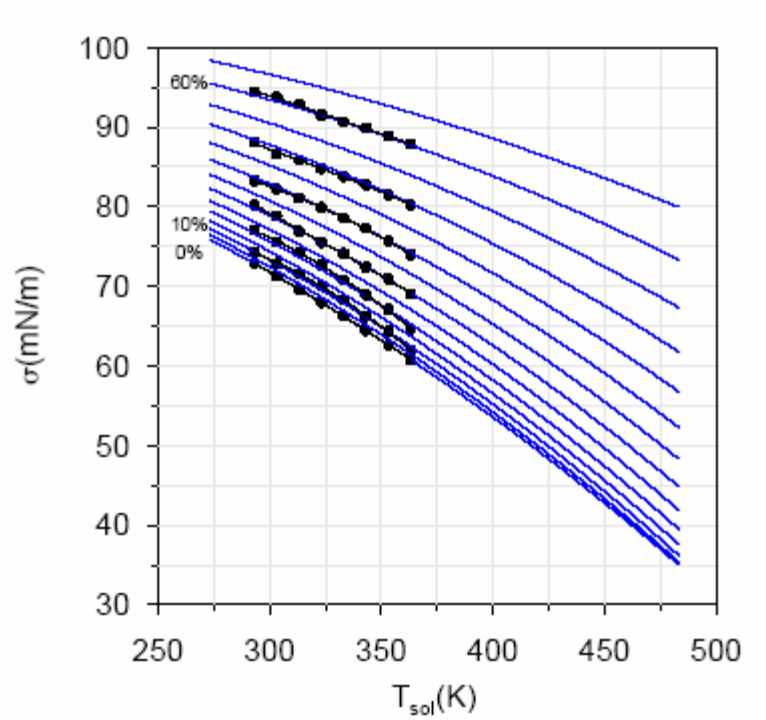

Figure A3.6 Surface tension of aqueous LiBr solution

APPENDIX 4

THE DETAILS OF PARTS OF CONTROL UNIT

Modularity is achieved using plug-and-modules to select the appropriate type and number of I/O points for a specific application. Up to 40 I/O modules allow to 256 I/O points configured in control unit by controller. The modules allow resistance, digital, pulse 0 to 10 or 0 to 5VDC, or 0(4)-20 mA inputs and digital or 0-10VDC outputs (See Figure A4.2).

Each module, including the power supply, clips to DIN rail for flexible mounting options in a custom built enclosure (See Figure A4.3). The controller is contained in the processor module. The processor module uses Flash memory to provide nonvolatile memory for applications. Interconnectivity to the programming interface is provided at the processor level.

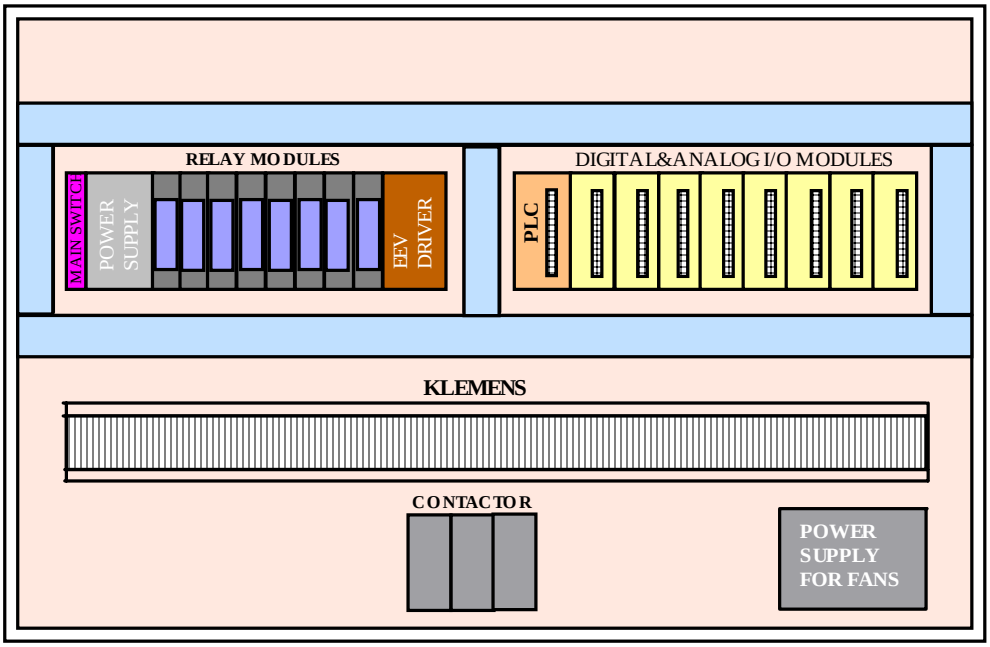

Figure A4.2 Control Panel Drawing

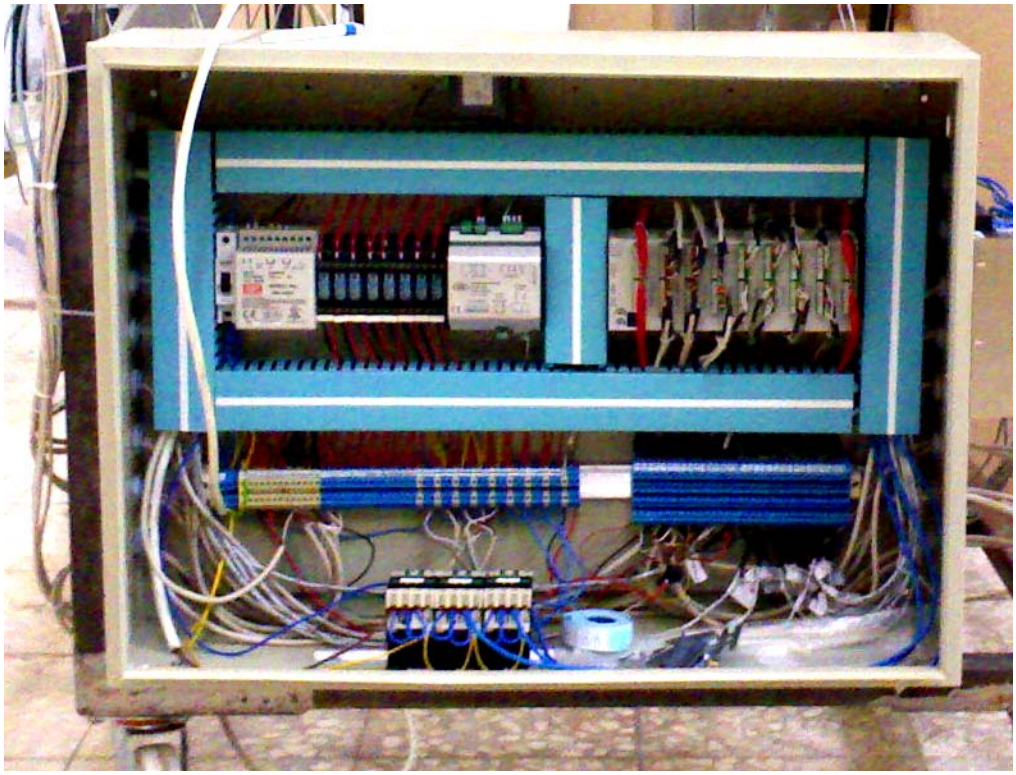

Figure A4.3 Control panel photograph

Microprocessor Module

As seen Figure A4.4, the processor module provides the connectivity to the I/O modules. 24VDC power is received from the power supply and passed along the I/O bus to the I/O modules. The operating panel plugs directly into the processor module using an RJ-11 connector. The network address is set to establish communication to other modules on the network in the software. Transfer speeds of 9.6, 19.2 and 38.4 kboud are set in the software.

- Modbus RTU/ASCII communication
- RS-232, RS-485 communication ports
- Communicate with any controller that supports ASCII protocol
- Built-in RUN/STOP switch on CPU
- Expandable up to 256 I/O points
- 8DI, 4DO on CPU and 8/16 points I/O extension units
- 8 temperature/analog expansion modules can be connected
- RS-485 communication port on analog/temperature extension units
- 13 points 32 bit, single phase 30kHz, double phase 7 kHz high speed counter
- 2 points single axis max 50 kHz, double axis 10 kHz, high speed pulse output

Figure A4.4 Microprocessor module

Input/Output Modules

Three type modules are used in control unit. The first type module is **DVP-06XA** for measurement devices and control valves except thermocouples and EEV (see Figure A4.5). The second type module is DVP-04TC for thermocouples (see Figure A4.6). The third type module is universal driver module for EEV (see Figure A4.7). The controller uses modular components to maximize flexibility. The input and output modules provide the bulk of this flexibility by allowing virtually any mix of input and output channels. Up to 40 modules can be installed for a maximum of 256 I/O points. Typically, the modules accept 4 input points and control 2 output points. The thermocouple modules accept 4 inputs.

The first type modules accepts resistance, pulse, volt-free digital, 0 to 5VDC, 0 to 10VDC and 0 to 20 mA input signal. Jumpers/links are used to set the incoming signal type. The second type thermocouple module accepts J type thermocouple signals. The driver module contains all required algorithms, hardware and software the only requirements are an analog 4-20 mA or 0-10 V signal. Configured to operate as a: Electronic Expansion Valve.

The power supply is an auto-switching unit allowing usage 230 VAC. It provides a regulated 24 VDC to the processor module, which, in turn, supplies the I/O modules. An auxiliary power outlet is included with 230 VAC for Fan and heater.

- 6 Channel
- 4 Analog Input 2 Analog Output
- 12 Bit Analog Resolution
- 0-10 V, ±10 V, 0-20 mA, 4-20 mA, ±20 mA Selectable input type
- ASCII / RTU MODBUS Communication Mode
- 4-20 mA, 0-10 V Selectable Output Type

Figure A4.5 The first type I/O module

- 4 Channel
- J / K Type Thermocouple Input
- J: -200~700 C^o
  K: -100~1000 C^o Temperature Input Range
- ASCII / RTU MODBUS Communication Mode

Figure A4.6 The second type I/O module

- 2 Channel
- 1 Analog Input 1 Analog Output
- 12 Bit Analog Resolution
- 0-10 V, 4-20 mA, Selectable input type
- ASCII / RTU MODBUS Communication Mode

Figure A4.7 The third type I/O module

APPENDIX 5

TEST ENGINE SPECIFICATIONS

The engine chosen as a test engine was a spark ignition engine as shown in Figure A5.1.

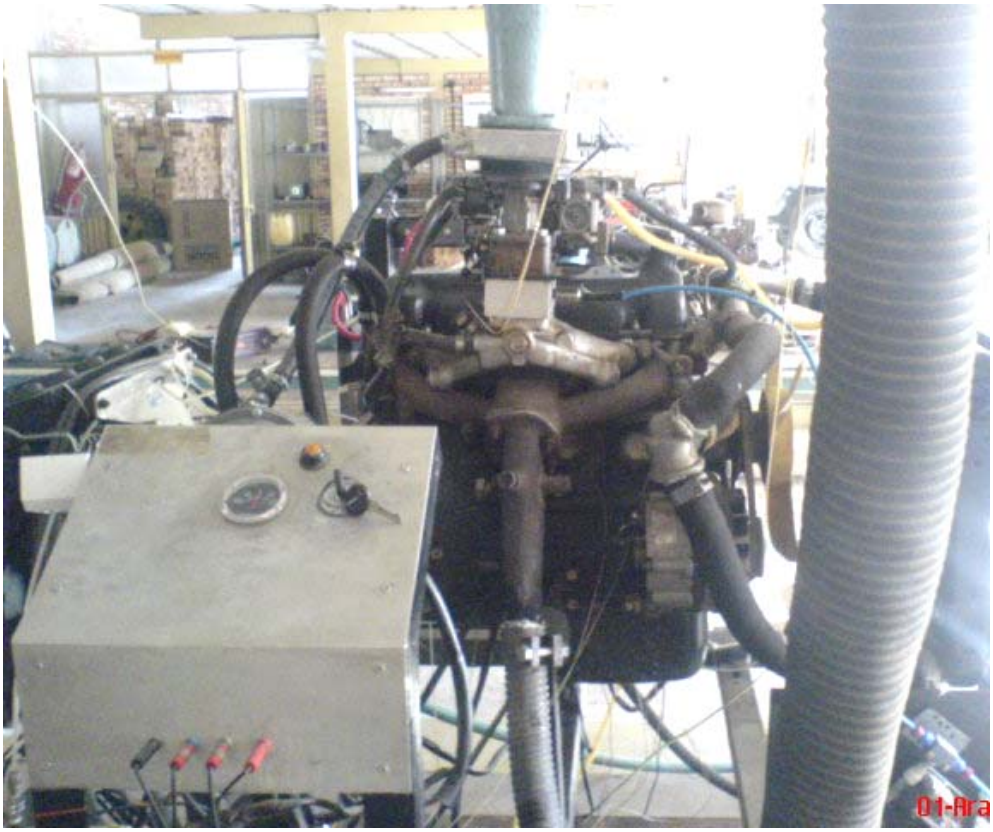

Figure A5.1 Test Engine

Air flow measurement

The air flow was measured with the help of air flow meter as shown in Figure A5.2. The air stream that was drawn into the engine passes through a pulse damping drum and then exits through a flexible hose before arriving to the intake manifold. Moreover, the filter cap filled with oil filters the air that will go into the intake manifold. The flow rate was measured by means of the pressure difference across the nozzle. An inclined manometer was used for the measurement of this pressure difference.

Figure A5.2 Air flow meter

Fuel flow measurement

In order to calculate the fuel flow rate, it is necessary to determine accurately the mass of fuel that is consumed by the engine per unit time under the given operating conditions. To accomplish this, the engine fuel was supplied with fuel from a small tank. The tank rests on a digital scale that was calibrated in grams. This

allows the mass of fuel used by the engine over a given length of time to be measured, so the mass fuel consumption per unit time can be calculated. The entire fuel flow system can be seen in Figure A5.3.

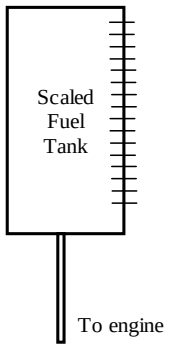

Figure A5.3 The fuel flow measuring system

Measurement of engine speed

Engine speed, rpm, can be measured by an inductive pick-up clamp on ignition secondary cables, by capacitive pick-up on a primary wire or an injector wire, or via a direct connection to a square wave from the engine management system. In this thesis, engine speeds were measured by this method.

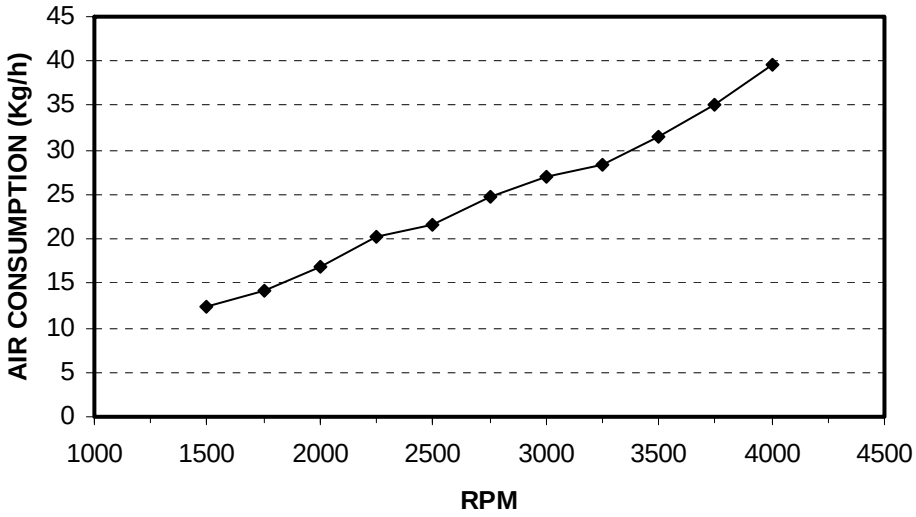

Figure A5.4 Variation of air consumption with engine speed

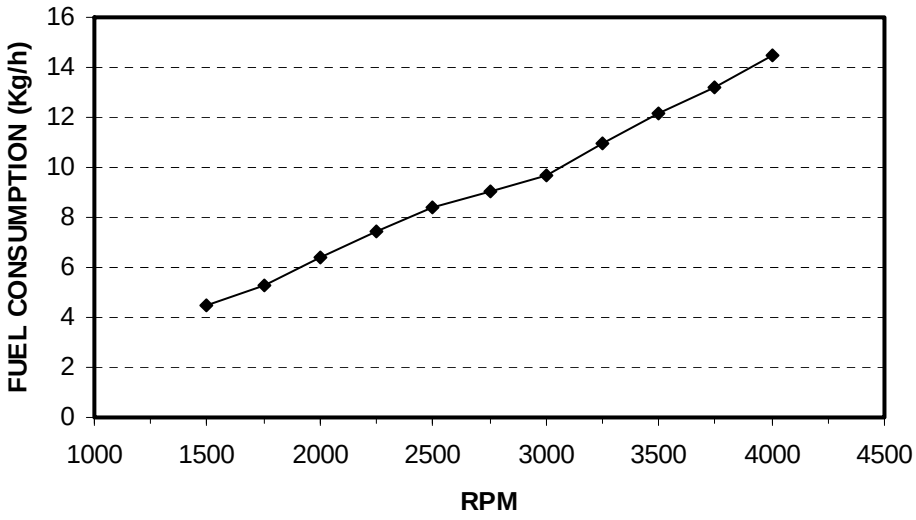

Figure A5.5 Variation of fuel consumption with engine speed

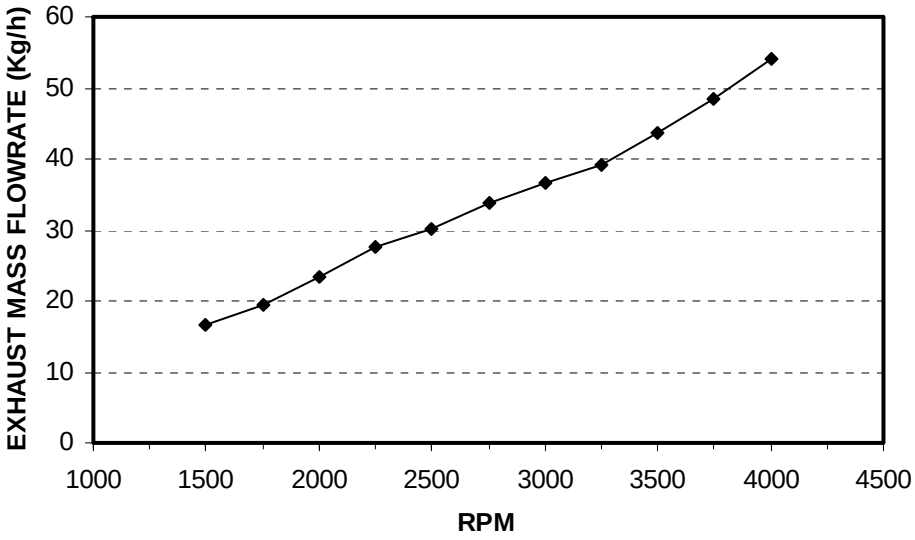

Figure A5.6 Variation of exhaust mass flow rate with engine speed

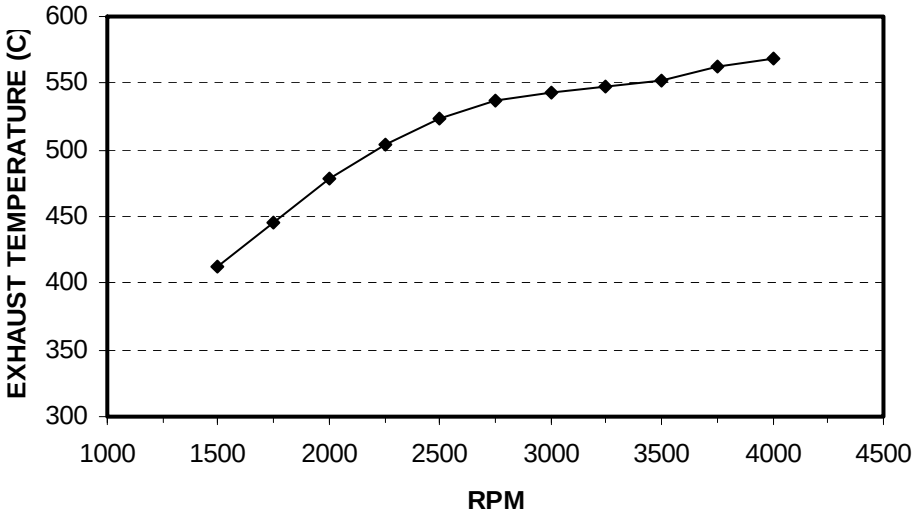

Figure A5.7 Variation of exhaust temperature with engine speed

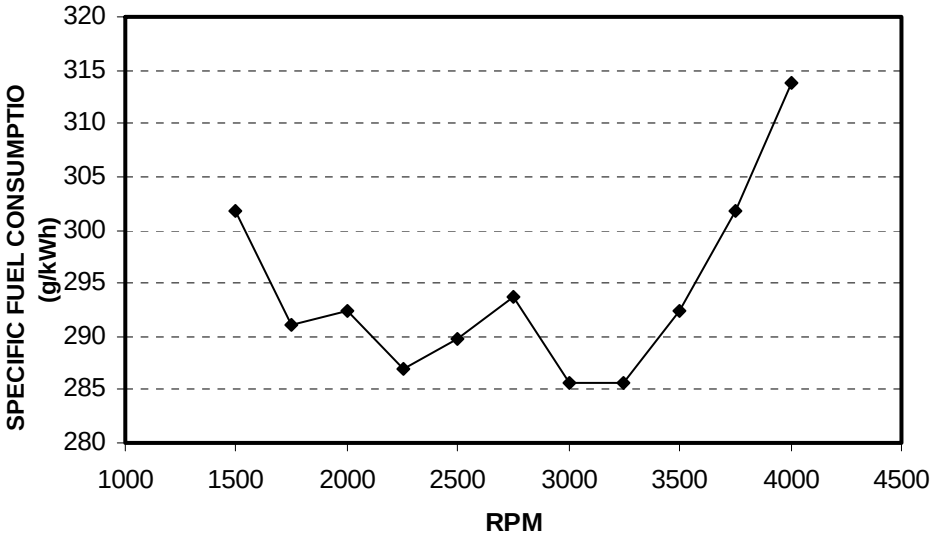

Figure A5.8 Variation of SFC with engine speed

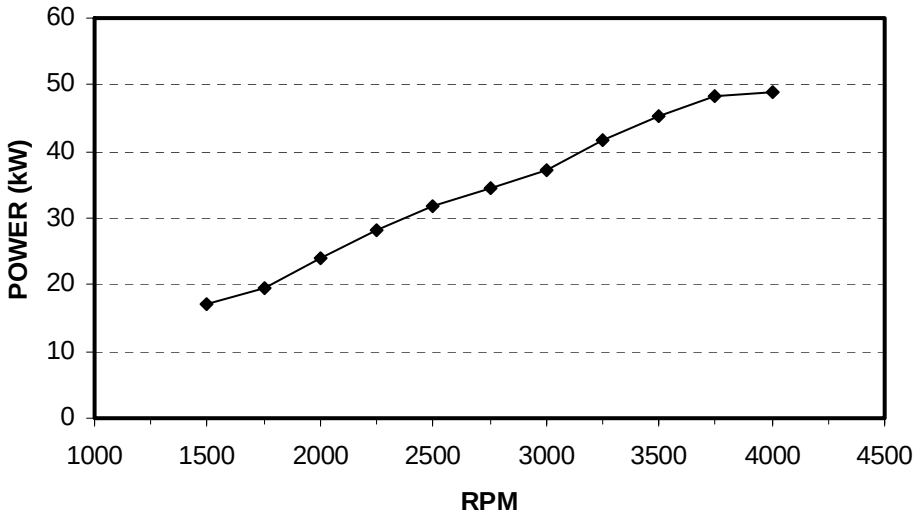

Figure A5.9 Variation of power with engine speed

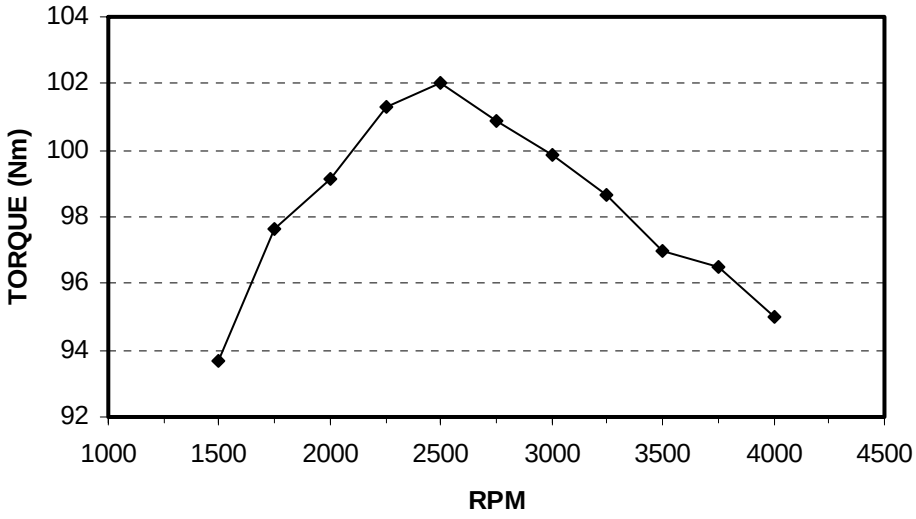

Figure A5.10 Variation of torque with engine speed

REFERENCES

1. Casals, X.G. (2006). Solar Absorption Cooling in Spain: Perspectives and Outcomes from the Simulation of Recent Installations, *Renewable Energy,* 31, 1371-1389

2. Zogg, R.A., Feng, M. Y. (2005). Guide to Developing Air-Cooled LiBr Absorption for Combined Heat and Power Applications, *Distributed Energy Program Report,* U.S. Department of Energy, 1-50

3. Horuz, I., Callender, T.M.S. (2004). Experimental Investigation of a Vapor Absorption Refrigeration System, *Journal of Refrigeration,* 27, 10-16.

4. Horuz, I. (1999). Vapour Absorption Refrigeration in Road Transport Vehicles, *Journal of Energy Engineering*, 125, 48-58

5. Horuz, I. (1994). An Experimental Study of the Use of Vapour Absorption Refrigeration in Road Transport Vehicles, PhD Thesis, University of Strathclyde.

6. Keating, C.L. (1954). Absorption Refrigeration System for Mobile Application, *U.S. Patent No. 2,667,040*.

7. McNamara, T.J. (1972). Absorption Refrigeration and Air Conditioning System, *U.S. Patent No. 3,661,200*.

8. Akerman, J.R. (1971). Automotive Air Conditioning Systems with Absorption Refrigeration, *Automotive Engineering Congress, Society of Automotive Engineers,* SAE Paper No: 710037

9. Vincent Mei, P.E. (1979). A Truck Exhaust Gas Operated Absorption Refrigeration Systems, *ASHRAE Transactions,* 85, 66-76

10. Koehler, J., Tegethoff, W.J. (1997). Absorption Refrigeration System for Mobile Applications Utilizing Exhaust Gases, *Heat and Mass Transfer*, 32, 333-340

11. Salim, M. (2001) *Simulation of Automotive LiBr/H2O Absorption A/C Machine*, ASME IMECE2001/AES-23620.

12. Alva, L., González, J. (2002). Simulation of an Air-cooled Solar-assisted Absorption Air Conditioning System*. ASHRAE Transactions*, 124, 54-64

13. Florides, G.A., Kalogirou, S.A., Tassou, S.A. (2003). Design and construction of a LiBr-Water absorption machine, *Energy Conversion & Management* , Article in press

14. Garrabrant, M.A. (2003). Proof-of-Concept Design and Experimental Validation of a Waste Heat Driven Absorption Transport Refrigerator, *ASHRAE Transactions,* 109, 401-411.

15. Izquierdo, M., Venegas, M., et al. (2004) Crystallization as a limit to develop solar air- cooled LiBr-H2O absorption systems using low-grade heat. *Solar Energy Materials and Solar Cells*, 81.

16. Stoecker, W.F., Jones, J. W. (1994) Refrigeration *& Air conditioning*, McGRAW-Hill, 2nd ed.

17. Dossat, R.J. (1991). *Principles of Refrigeration*, Prentice Hall, Englewood Cliffs, 3rd ed.

18. Çengel, Y.A., Boles, M.A. (1989). *Thermodynamics: An Engineering Approach*, New York, NY, McGraw-Hill Book Company.

19. Tozer, R., James, R.W. (1998). Heat Powered Refrigeration Cycles, *Applied Thermal Engineering,* 18, 733-743.

20. Rıffat, S.B., James, S. (1998). Computer Simulation and Experimental Analysis of Working Fluids for Absorption Cycles, *Journal of the Institute of Energy,* 71, 158-162.

21. Kaita, Y., (2001). Thermodynamic Properties Of Lithium Bromide-Water Solutions At High Temperatures, *International Journal of Refrigeration*, 24, 374-390

22. Saravan, R., Maiya, M.P. (1998). Thermodynamic Comparison Of Water Based Working Fluid Combinations For A Vapor Absorption Refrigeration System, *Applied Thermal Engineering*, 18, 553-568

23. Horuz, I. (1998). A Comparison Between Ammonia-Water And Water-Lithium Bromide Solutions in Vapor Absorption Refrigeration Systems, *International Communications in Heat and Mass Transfer*, 25, 711-721

24. Herold, K. and Moran, M. (1987) Thermodynamic Properties of LiBr/H2O Solutions, *ASHRAE Transactions*, 1, 35-48.

25. McNeely, L.A. (1979) Thermodynamic Properties of Aqueous Solutions of Lithium Bromide, *ASHRAE Transactions*, 85, 413-434.

26. Srikhirin, P., Aphornratana, S. (2001). A Review Of Absorption Refrigeration Technologies, *Renewable & Sustainable Energy Reviews*, 5, 343-372

27. Sun, Da-Wen, (1997). Thermodynamic Design Data And Optimum Design Maps For Absorption Refrigeration Systems, *Applied Thermal Engineering*, 17, 211-221

28. Kaynakli, O., Kilic, M. (2007). Theoretical Study on the Effect of Operating Conditions on Performance of Absorption Refrigeration System, *Energy Conversion & Management* , 48, 599-607

29. Joudi, K.A., Lafta, A.H. (2001). Simulation of a Simple Absorption Refrigeration System, *Energy Conversion & Management* , 42, 1575-1605

30. Abrahamsson, K. and Jernqvist, A. (1994). Modeling and Simulation of Absorption Heat Cycles. *ASME IAHP conference proceedings, 31, 12-19*

31. Abrahamsson, K. and Jernqvist, A. (1994). Modelling and Simulation of Absorption Heat Cycles. *ASME IAHP conference proceedings*, .31.

32. Klein, S.A, (2006). EES (Engineering Equation Solver), F-Chart Software.

33. Mostavavi, M., Agnew, B. (1996). Thermodynamic Analysis of Combined Diesel Engine and Absorption Refrigeration Unit-Naturally Aspirated Engine with Precooling, *Applied Thermal Engineering,* 17, 593-599

34. Mostavavi, M., Agnew, B. (1998). Thermodynamic Analysis of Combined Open-Cycle-Twin-Shaft Gas Turbine and Exhaust Gas Operated Absorption Refrigeration Unit, *Applied Thermal Engineering,* 18, 847-856

35. NG, K.C., CHUA, H.T., Han, Q. (1999). Thermodynamic Modeling of Absorption Chiller and Comparison with Experiments, *Heat Transfer Engineering,* 20, 42-51

36. Mroz, T.M. (2006). Thermodynamic And Economic Performance Of The Libr-H_2O Single Stage Absorption Water Chiller, *Applied Thermal Engineering,* 26, 2103-2109

37. Abrahamsson, K., Jernqvist, A. and Aly, G.(1994) Thermodynamic Analysis of Absorption Heat Cycles. ASME IAHP conference proceedings, AES-Vol.31.

38. Incropera, F.P., Dewitt, P. (1990). *Fundamentals of Heat and Mass Transfer,* John Wiley and Sons, Florida.

39. Castro, J., Leal, L., Pozo, P., Perez-Segarra, C.D., Oliet, C. (2002). Development and Performance of an Air-Cooled Water/LiBr Absorption Cooling Machine. *International Forum on Renewable Energies FIER'2002 Proceedings.* Morocco, 59-65

40. Chuang, C.C., Sue, D.C., Lin, Y.T.(2003). Simulation and Performance Analysis of Lithium Bromide/Water for Absorption Heat Transformer Cycle Systems. *Transactions of American Society of Heating, Refrigeration and Air-Conditioning Engineers.* Vol. 4733, 409-416

41. Agnew, B., Talbi, M. (2000). Exergy Analysis: An Absorption Refrigerator Using Lithium Bromide and Water as the Working Fluids, *Applied Thermal Engineering,* 20, 619-630.

42. Carmody, S. and Shelton, S. (1994) Direct Second Law Analysis of Advanced Absorption Cycles Utilizing an Ideal Solution Model. ASME IAHP conference proceedings, AES-Vol.31.

43. Agnew, B., Alikitiwi, A., Anderson, A.A., Fisher, E.H. (2002). A finite time analysis of combined Carnot driving and cooling cycles optimized for maximum refrigeration effect with applications to absorption refrigeration systems. *Exergy , An international Journal.* 186-191

44. Izquierdo, M., Vega, M. (2000). Entropy Generated and Exergy Destroyed in Lithium Bromide Thermal Compressors Driven by the Exhaust Gases of an Engine, *Journal of Energy Research,* 24, 1123-1140.

45. Reisler, A. Perez., Gonzalez, Jorge E. (2004). Design and Construction of Air-Cooled Absorption Machine for Solar Energy Applications, *Proceedings of ISEC, 1-7.*

46. Levy, A., Jelienk, M., Borde, I. (2002). Numerical Study on the Design Parameters Ejector for Absorption Systems, *Applied Energy,* 72, 467-478.

47. Kim, D.S., Ferreira, C.A. (2003). Solar Absorption Cooling, Final Report, Delft University of Technology, Netherlands

48. Grossman, G. (2002) Advanced modular simulation of open absorption systems. *Keynote Lecture, Proceedings, the 7th International Sorption Heat Pump Conference*.

49. Grossman, G. (1994) Modular and Flexible Simulation of Advanced Absorption Systems*, ASME IAHP conference proceedings*, AES-Vol.31.

50. Homma, R., Nishiyama, N. and Wakimizu, H. (1994) Simulation and Experimental Research of Single-effect Absorption Refrigerators Driven by Waster Hot Water*. ASME IAHP conference proceedings*, AES-Vol.31.

51. Jeong, S., Kang, B., Lee, C. and Karng, S. (1994) Computer Simulation on Dynamic Behavior of a Hot Water Driven Absorption Chiller*. ASME IAHP conference proceedings*, AES-Vol.31.

52. Holman, J.P. (1989). *Experimental Method for Engineers, 5th ed. McGraw-Hill, Inc;p41*

53. Beckwith, T. Marangoni, R., Lienhard, J. (1993) *Mechanical Measurements*. Fifth Edition. Addison-Wesley Publishing Company, New York.

54. Kline, S., McClintock, F. *Describing Uncertainties in Single-Sample Experiments. Mechanical Engineering. 1*959

55. Vinaspre, M., Bourouis, M. Coronas, A. (2004). Monitoring and Analysis of an Absorption Air-Conditioning System, *Energy and Buildings,* 20, 121-131.

56. Ferraro, V., Kaliakatsos, D. (2006). Project and .Experimental Testing of the Control System of an Air Conditioning Plant, *Energy and Buildings,* 38, 554-561.

57. *Heywood, John B. (1988). Internal Combustion Engine Fundamentals,* New York, NY, McGraw-Hill Book Company.

58. Boatto, P., Boccaletti, C., Cerri, G., Malvicino, C. (2000). Internal Combustion Engine Waste Heat Potential For An Automotive Absorption System Of Air Conditioning Part 1: Tests On The Exhaust System Of A Spark-Ignition Engine, *Proceedings of the I MECH E Part D Journal of Automobile Engineering,* 214, 979-982

59. Deng, S.M., Ma, W.B. (1999). Experimental Studies on the Characteristics of an Absorber Using LiBr/Water Solution as Working Fluid, *Journal of Refrigeration,* 22, 293-301.

60. Tsuda, H., Perez, H. (2001). An Experimental Study of a Vibrating Screen as means of Absorption Enhancement, *Heat and Mass Transfer,* 44, 4087-4094.

61. Greiter, I., Wagner, A., Weiss, V. and Alefeld, G. (1994) Experimental Investigation of Heat and Mass Transfer in a Horizontal-tube Falling-film Absorber with Aqueous Solutions. *ASME IAHP conference proceedings*, AES-Vol.31.

62. Agnew, B., Talbi, M., Mostafavi, M. (1999). Combined Power and Cooling, an Analysis of the Combined Diesel-absorption Cycle, *Applied Thermal Engineering,* 19, 1097-1105.

63. Agnew, B., Talbi, M. (2002). Energy Recovery Form Diesel Engine Exhaust Gases for Performance Enhancement and Air Conditioning, *Applied Thermal Engineering,* 22, 693-702.

64. Yoon, Jung-In, Choi, K., Moon, C. (2003). A Study On The Advanced Performance Of An Absorption Heater/Chiller With A Solution Preheater Using Waste Gas, *Applied Thermal Engineering*, 23, 757-767

65. Wu, S., Eames, I. W. (1998). A Novel Absorption-Recompression Refrigeration Cycle. *Applied Thermal Engineering,* 18, 1149-1157.

66. Atmaca, I., Yiğit, A., Kiliç, M. (2002) The Effect of Input Temperatures on the Absorber Paramaters. 29, 1177-1186.

67. Kairouani, L., Nehdi, E. (2006). Cooling Performance and Energy Saving of a Compression Absorption Refrigeration System Assisted by Geothermal Energy, *Applied Thermal Engineering*, 26, 288-294.

68. Frances, V.M.S., Ojer, J.M. (2003). Validation of Model For the Absorption Process of H_2O by LiBr in a Horizontal Tube Bundle, *Heat and Mass Transfer,* 46, 3299-3312.

69. Fu, D.G., Poncia, G., Lu, Z. (2006) Implementation of an Object-oriented Dynamic modeling Library for Absorption Refrigeration Systems, *Applied Thermal Engineering,* 26, 217-225.

70. Rivera, W., R.omero, R.J., Cardoso, M.J. (2002). Theoretical and Experimental Comparison of the Performance of a Single-Stage Heat Transformer Operating with Water/LiBr and Water/Carrol, *Journal of Energy Research,* 26, 747-762.

71. Sabir, H.M., Eames, I.W. (1997). Theoretical Comparison Between Lithium Bromide/Water Vapour Resorption and Absorption Cycles, *Applied Energy,* 18, 683–692.

72. Asdrubali, F., Grignaffini, S. (2005). Experimental Evaluation of the Performances of a LiBr-Water Absorption Refrigerator under different Service Conditions, *Journal of Refrigeration,* 28, 489–497.

73. Agnew, B., Talbi, M., Mostavavi, M. (1999). Combined Power and Cooling an Analysis of the Combined Diesel-Absorption Cycle*, Applied Thermal Engineering,* 19, 1097-1105

74. Silviera, Jose L., Walter, A.C., Luengo, A.C. (1996). A Case Study Of Compact Cogeneration Using Various Fuels, FUEL, 76, 447-751

75. Misra, R.D., Sahoo, P.K., Gupta, A. (2003). Thermoeconomic Optimization of A Single Effect Water-LiBr Vapor Absorption Refrigeration System*, International Journal of Refrigeration*, 26, 158-169

76. Park, C.W., Jeong, J.H., Kang, Y.T. (2004). Energy Consumption Characteristics of an Absorption Chiller during the Partial Load Operation, *International Journal of Refrigeration*, 27, 9488-954

77. Kim, D.S., Ferreira, C.A. (2005). A Gibbs Energy Equation for LiBr Aqueous Solutions, *International Journal of Refrigeration*, 28, 1-11

78. Kakaç, S. (1970). *Boilers, Evaporators and Condensers*, John Wiley and Sons, Florida.

79. Romero, R. J. et al. (2006). Monomethylamine-Water Vapour Absorption Refrigeration System, *Applied Thermal Engineering,* 25, 867-876

80. Saravanan, R., Maiya, M.P. (2003). Experimental Analysis Of A Bubble Pump Operated H_2O-Libr Vapour Absorption Cooler, *Applied Thermal Engineering,* 23, 2383-2397

81. Boccaletti, C., Martellucci, L. (2001). Study of An Air Conditioning System for a Small Hybrid Vehicle Based on the Absorption Principle, *SAE Paper No 3808,* 1–11

82. Boatto, P., Boccaletti, C., Cerri, G., Malvicino, C. (2000). Internal Combustion Engine Waste Heat Potential For An Automotive Absorption

System Of Air Conditioning Part 2: The Automotive Absorption System, *Proceedings of the I MECH E Part D Journal of Automobile Engineering,* 214, 983-989

83. Bassols, J., Schneider, R. et al. (1994). First Operation Results of a Gas-fired 250kW Absorption Heat Pump with Plate-Fin Heat Exchangers. *ASME IAHP conference proceedings*, AES-Vol.31.

84. Garimella, S. and Christensen, R. (1994) Gas-fired Absorption Systems for Space Conditioning in Recreational Vehicles. *ASME IAHP conference proceedings*, AES-Vol.31.

85. Gee, T.A., Cao, J., Mathias, J.A., Christensen, R. N. (2001) Experimental Testing and Modeling of a Dual-Fired LiBr-H2O Absorption Chiller, *ASHRAE Transactions*, V. 107.

86. Greiter, I., Schweigler, C., Alefeld, G. and Scharfe, J. (1994) A 500 kW Absorption Heat Pump for Heating at Two Temperature Levels. *ASME IAHP conference proceedings*, AES-Vol.31. 1994

87. Hellmann, H. and Ziegler, F.(1999) Simple Absorption Heat Pump Modules for System Simulation Programs. *ASHRAE Transactions* V.105.

88. Tongu, S., Makino, Y., Ohnishi, K. and Nakatsugawa, S. (1994). Practical Operating of Small-sized Air-cooled Double-effect Absorption Chiller-heater by using LiBr and Aqueous. *ASME IAHP conference proceedings*, AES-Vol.31.

89. Arzoz, D., Rodriguez, P., Izquierdo, M. (2005). Experimental Study on the Adiabatic Absorption of Water Vapor into LiBr-Water Solutions, *Applied Thermal Engineering,* 25, 797-811.

90. Ghassemi, B.(1987). Theoretical Study of Absorption Refrigeration for Vehicle Application, XVII. International Congress of Refrigeration, Vol. D

91. Martinez, P.J., Pinazo, J.M. (2002). A Method for Design Analysis of Absorption Machine, *International Journal of Refrigeration*, 25, 634-639

CURRICULUM VITAE

PERSONAL INFORMATION

Surname, Name: HİLALİ, Ismail
Nationality: Turkish (TC)
Date and Place of Birth: 13 June 1972, Şanlıurfa
Marital Status: Married
Phone: +90 532 3736992
Fax: +90
e-mail: ihilali@gmail.com

EDUCATION

Degree	Institution	Year of Graduation
MS	Harran University	1995
BS	Fırat University	1993
High School		

WORK EXPERIENCE

Year	Place	Enrollment
2003- Present		
199x-200x		

FOREIGN LANGUAGES

English

PUBLICATIONS

1.

HOBBIES